



HAL
open science

Biophysical Regulation of Epithelial Apoptosis

Victoire Cachoux

► **To cite this version:**

Victoire Cachoux. Biophysical Regulation of Epithelial Apoptosis. Cellular Biology. Université Paris sciences et lettres, 2022. English. NNT : 2022UPSLS023 . tel-04842200

HAL Id: tel-04842200

<https://theses.hal.science/tel-04842200v1>

Submitted on 17 Dec 2024

HAL is a multi-disciplinary open access archive for the deposit and dissemination of scientific research documents, whether they are published or not. The documents may come from teaching and research institutions in France or abroad, or from public or private research centers.

L'archive ouverte pluridisciplinaire **HAL**, est destinée au dépôt et à la diffusion de documents scientifiques de niveau recherche, publiés ou non, émanant des établissements d'enseignement et de recherche français ou étrangers, des laboratoires publics ou privés.



THÈSE DE DOCTORAT
DE L'UNIVERSITÉ PSL

Préparée à l'Institut Curie

Biophysical Regulation of Epithelial Apoptosis

Régulation Biophysique de l'Apoptose Epitheliale

Soutenue par

Victoire Cachoux

Le 06/07/2022

École doctorale n°515

Complexité du Vivant

Spécialité

Bio-informatique et Biologie du développement

Composition du jury :

Jean-François JOANNY Professeur, Collège de France	<i>Président</i>
Edouard HANNEZO Assistant Professor, IST Austria	<i>Rapporteur</i>
Yanlan MAO Associate Professor, UCL	<i>Rapportrice</i>
Magali SUZANNE Directrice de Recherche, CBI Toulouse	<i>Examinatrice</i>
Yohanns BELLAÏCHE Directeur de recherche, Institut Curie	<i>Directeur de thèse</i>
Boris GUIRAO Chargé de recherche, Institut Curie	<i>Co-encadrant de thèse</i>

Biophysical Regulation of Epithelial Apoptosis

Victoire Cachoux

06/07/2022



À Marie-Françoise Cachoux.

Therefore I would ask you to write all kinds of books, hesitating at no subject however trivial or however vast. By hook or by crook, I hope that you will possess yourselves of money enough to travel and to idle, to contemplate the future or the past of the world, to dream over books and loiter at street corners and let the line of thought dip deep into the stream.

Virginia Woolf – *A Room of One's Own* (1929)

Acknowledgements

As I am putting a final dot to my PhD manuscript, I would first like to express my deepest gratitude to the people who made it possible for me to hold into my hands a document I am proud of. I sincerely thank Yohanns Bellaïche, Boris Guirao and François Graner for their corrections and suggestions. Thanks to Lale Alpar for creating a wonderful alternative cover that will make me want to regularly come back to this manuscript. Thanks to Richard Cachoux, Gwen-Jirō Clochard and the Institut Henri Poincaré for nurturing pleasant environments where most of the writing was done (and to Lorette Noiret for suggesting the Institut!). I wish to thank the reviewers, Dr. Edouard Hannezo and Dr. Yanlan Mao, as well as the jury members, Pr. Jean-François Joanny and Dr. Magali Suzanne, for accepting to review my work and to sit on my jury. It is an honour to be evaluated by scientists whose work I so admire, and whose comments will, no doubt, greatly improve my project.

This work would never have been possible without a wonderful team of co-supervisors, who took me in as an intern in 2016 and welcomed me back 2 years later to work on an exciting project about cell death. I want to express my deepest gratitude to Yohanns and Boris for their co-mentoring. Yohanns, thank you for your continuous commitment to improving how we work as a team; for your communicative enthusiasm when doing science, and your cautiousness and integrity when talking about it; and for making me feel validated despite my minimal knowledge of biology. Boris, thank you for the continuous trust and autonomy you gave me; for your ever-sagely critical thinking which taught me to stop hopping from one task to the next; and for your infinite kindness. I hope you will get that HDR now!

I came to research for the science, and stayed for the people. The Bellaïche team is a terrific place to do ambitious science and to be inspired by the people doing it. Many thanks to Maria Balakireva for her experimental work, which fed my hunger for quantitative analysis, and for her patience with me. I would also like to thank Floris Bosveld for his work on the 3D, wealth of ideas, and for the constant supply of Dutch

liquorice; Mélanie Gracia for her experiments of pupa compression and her expertise on apoptosis; Stéphane Rigaud for his exquisite knowledge of image analysis, and for his friendship dear to me; Isabelle Gaugué, for the ERK-KTR reporter, and for being a model of how rigorous work and fun go well together; Aude Maugarny-Calès, Lale Alpar and Lorette Noiret, for being not only an endless source of inspiration as amazing and successful women scientists but also the best Wine & Crochet group. Not a Bellaïche team member *stricto sensu*, I am especially grateful to François Graner for his suggestions, interest in my work and guidance: 私に感謝しています. All the team members, past and present, have built a great environment that survived the pandemic and have provided many inputs on my work over these past 4 years: Inês Cristo, Florencia di Pietro, Amina Joudat, Cyril Kana-Tepakbong, Adrien Leroy, Jesús López-Gay, Olga Markova, Stéphane Pelletier, Lucas Sancéré, Eric Van Leen, Aurélien Villedieu, Zhimin Wang, Satoshi Yamashita as well as Lucie Daveau who worked with me as an intern, thank you all!

More generally, I am grateful to the BDD members for the quality of the interactions in our department. Special thanks to the imaging platform for their expertise, to Bénédicte Leveillé Nizerolle at the fly food facility, and to the administrative team, Isabelle Basson, Virginie Bourgeois and Déborah Merlini, whose work allowed me to focus on the science and not so much on the administrative hurdles that come with doing a PhD in France. Of course, the President of the BDD reflects its qualities: I wish to extend my gratitude to Pierre Léopold for our scientific discussions, for his support, and for his management which must not have been easy during a global pandemic. On a more personal note, I could not continue without sincerely thanking Özge Özguç and Manon Josserand for their friendship which made me feel at home at Curie.

This PhD is the latest step of a decade of thrilling science discussions and encounters with people who inspired me to go further. I thank Claudine Husson for making me fall in love with mathematics, and Roger Mansuy and Yves Duval for teaching me all I know about this discipline. I am forever grateful to Dr. Alexandre Kabla for making me grow as a scientist. Many thanks to him, as well as Dr Magali Suzanne and Dr. Auguste Genovesio, for sitting on my PhD committee.

Je souhaite exprimer toute ma gratitude à ma famille. Leur soutien et leur confiance me portent à chaque pas. À commencer par mes parents, Lætitia et Guillaume, à qui je dois des années vraiment heureuses et qui ont toujours encouragé ma curiosité. Maman, merci infiniment pour ton soutien sans faille, et merci à mon

beau-père Jacques-Olivier de nous accompagner à tes côtés. Merci de tout cœur à Diane et Gautier, à la fois ma fratrie et mes meilleurs amis ; il n'existe pas plus fière grande sœur que moi devant tout ce que vous avez accompli. Je remercie ma famille à Paris que je suis très heureuse d'avoir retrouvée pendant cette période de doctorat. Bénédicte Vezon, Nicolas, Camille, Pauline et Rose Cachoux, ma marraine et mon filleul Odile et Augustin ainsi que Patrice et Clément Roche, Vincent, Florence, Alice et Claire Girard ; je vous remercie pour votre façon de constamment voir en moi celle que je pourrais devenir. Loin des yeux mais jamais loin du cœur, merci à mes grands-parents qui ont créé un cocon bienveillant dans lequel je file me ressourcer dès que j'en ai la possibilité. Christian et Marie-Jo Vezon, Richard Cachoux, vous me rappelez chaque jour l'importance de la famille comme Mamie Françoise le faisait.

Pour terminer, j'aimerais remercier la famille de cœur qui m'a soutenue pendant ces quatre années de doctorat : Charlene Telhier, Pauline Pasquier, Amina Bouri, Cybèle Vigneron, Marine Cornille et Paul Verdier, Julien de Botton et Justine Lanore, Margot Lyautey, Marie Eon, Elodie Hu-Yang, Victoire Kühn, Violette Vinel, Aniss Ziad, Emilie Mayer, Shérazade Gadhoudi et Diane Payrard, ainsi que ma dream-team Low Carbon France, Anouk Lucas et Emma Urbain. Vous m'apprenez tous les jours à être une meilleure amie, avec ambition, bienveillance et beaucoup de joie. M'être entourée de personnes comme vous est une de mes plus grandes fiertés. La liste ne serait bien sûr pas complète sans Gwen-Jirō, qui a été à mes côtés pour célébrer les hauts et traverser les bas de nos deux doctorats. Merci infiniment pour ces 8 années ; avec Baya et toi, 未来が楽しみだ！

Abstract

Apoptosis is a form of programmed cell death which plays a key role in shaping multicellular organisms during development, in adult tissue homeostasis, as well as in pathological conditions such as cancer. While the molecular pathways triggering apoptosis have been extensively studied, the role of biophysical factors in driving cell death is far less understood. In particular, cell size and geometry impact a variety of cell processes, yet their possible interplay with apoptotic pathways remains unknown. Using the developing dorsal thorax (or notum) of the *Drosophila* as a model, I developed during my PhD advanced quantitative analyses of time-lapse microscopy data that, combined with the powerful genetic tools available in *Drosophila*, aimed at uncovering the biophysical mechanisms regulating apoptosis. First, I investigated the early characteristics of apoptotic cells and discovered two predictive geometrical features of these cells: small absolute and relative apical areas. Second, I studied in detail these two geometrical parameters and showed that their actions were linked to distinct genetic pathways, which I identified. By doing so, I also uncovered a novel coupling between cell proliferation and cell death in the control of tissue development. Overall, this work provides a new perspective to the understanding of epithelial apoptosis by identifying geometrical parameters that play an early role in the regulation of cell survival.

Résumé

L'apoptose est une forme de mort cellulaire programmée qui joue un rôle clé lors de la morphogenèse (acquisition de formes et structures pendant le développement), dans l'homéostasie des tissus adultes, ainsi que dans certaines maladies telles que les cancers. Alors que les signaux moléculaires responsables du déclenchement de l'apoptose ont été l'objet de multiples recherches, le rôle de facteurs biophysiques dans le contrôle de la mort cellulaire reste peu connu. Durant ma thèse qui avait pour modèle d'étude le thorax dorsal (ou notum) de la puppe de drosophile, j'ai développé des techniques d'analyse quantitative de données vidéo-microscopiques qui, combinées à l'utilisation d'outils génétiques de pointe, visaient à comprendre la régulation biophysique de l'apoptose. Tout d'abord, j'ai cherché à décrire les caractéristiques précoces des futures cellules apoptotiques et ai découvert deux caractéristiques géométriques prédictives de ces cellules : des petites aires apicales absolue et relative. Ensuite, j'ai étudié en détail ces deux facteurs géométriques et ai montré que leurs actions dans le contrôle de la mort faisaient intervenir deux voies de signalisation génétiques différentes, voies que j'ai identifiées. Ce faisant, j'ai également découvert une connexion inédite entre prolifération et mort cellulaire dans le contrôle du développement tissulaire. En conclusion, mon travail apporte un éclairage nouveau à notre compréhension de l'apoptose épithéliale en identifiant des facteurs géométriques impliqués de façon très précoce dans la régulation de la mort cellulaire.

Contents

Contents	xv
List of Figures	xvii
List of Supplementary Figures	xviii
List of Abbreviations	xix
1 Introduction	1
1.1 Determinants and roles of cell geometry	2
1.1.1 A great diversity of geometries	2
1.1.2 Regulation of cell geometry	3
1.1.3 Scaling laws in multicellular organisms	7
1.1.4 Effects of cell geometry	13
1.1.5 Dysregulation of cell geometry in diseases	17
1.2 Cell geometry in epithelial morphogenesis	18
1.2.1 Characteristics of epithelia	19
1.2.2 Epithelial planar architecture at the cell scale	20
1.2.3 The single-cell mechanics of epithelial morphogenesis	22
1.2.4 An example: geometric regulation of cell division	29
1.3 The mechanics of apoptosis	33
1.3.1 A short history of apoptosis discovery	34
1.3.2 Apoptotic signalling pathways	35
1.3.3 Apoptosis in the mechanical regulation of morphogenesis	38
1.3.4 Biophysical modulation of apoptosis	41
1.4 Aims and outline of the thesis	46
2 Apical cell area controls apoptosis in developing epithelium	49

2.1	Contributions	49
2.2	Results	50
3	Early 3D Geometry in the Posterior Notum	89
3.1	Introduction	89
3.2	Contributions	90
3.3	3D segmentation of the posterior notum	90
	3.3.1 Segmentation method	90
	3.3.2 Results	92
3.4	Study of 3D cell shapes	93
	3.4.1 Geometric features of interest	93
	3.4.2 Notum cells under the apical surface	96
3.5	Characteristics of cells with apoptosis-related geometries	98
	3.5.1 Cells with small apical areas	98
	3.5.2 Cells with small relative apical areas	99
3.6	Discussion	104
4	Conclusion and Discussion	109
4.1	Biophysical regulation of apoptosis in the notum apical plane	110
	4.1.1 Control of apoptosis by size factors	110
	4.1.2 Generality of research findings	111
	4.1.3 Molecular signalling: the role of Hippo and Notch	112
	4.1.4 Coupling of cell division and cell death	114
	4.1.5 A process of geometric cell competition?	115
4.2	Gaining deeper insight: the role of 3D geometry	115
	4.2.1 Results	115
	4.2.2 Possible regulations of apoptosis by 3D cell shape	116
	4.2.3 Future work: going 4D	117
4.3	The role of apoptosis regulation	117
	References	121

List of Figures

1.1	Diversity of sizes and shapes of human cells	3
1.2	Regulation and effects of cell geometry	8
1.3	Experimental observations of an intrinsic regulation of organ size	11
1.4	Characteristics of epithelial tissues	20
1.5	Elementary single-cell behaviours	23
1.6	Principles of stress inference in 2D tissues	25
1.7	Cell geometry dynamics driving tissue morphogenesis	30
1.8	Apoptotic signalling pathways	37
1.9	Apoptosis in the mechanical regulation of morphogenesis	42
1.10	Compaction-induced apoptosis	44
2.1	Spatiotemporal patterns of apoptosis in the <i>Drosophila</i> notum	53
2.2	Relative timings of tissue compaction and apoptosis	55
2.3	Apoptotic cells display early specific geometric features	57
2.4	Prediction of the distribution of apoptoses using absolute and relative apical areas	60
2.5	Uniaxial mechanical compression of developing pupae	62
2.6	Coupling between proliferation and apoptosis in the developing notum	64
2.7	Cell area modulates apoptosis through Hippo/Yki activity	66
2.8	Loss of Tor function modulates cell size heterogeneity and apoptosis of surrounding wt cells	69
2.9	Cell relative apical area regulates apoptosis through Notch activity	71
3.1	3D segmentation method	91
3.2	Segmented posterior notum	92
3.3	Some relevant cell geometric features in 3D	94
3.4	Pairwise scatter plots of cell geometric features	95
3.5	Cell tilt angle versus in-plane extension	96

3.6	Maps of cell height, length and orientation	97
3.7	Maps of cell apical area, volume and tubularity	100
3.8	Pairwise scatter plots of cell relative geometric features	101
3.9	Probability distributions of $\mathcal{R}(T)$ and $\mathcal{R}(V)$ for cells with extreme relative areas	103
3.10	Probability distributions of $\mathcal{R}(h)$, $\mathcal{R}(l)$, $\mathcal{R}(zAV)$, $\mathcal{R}(l/h)$ and $\mathcal{R}(\theta)$ for cells with extreme relative areas	105
3.11	Relative volume and tubularity of cells with small relative areas	106

List of Supplementary Figures

2.1	Spatial distribution of apoptosis in the notum	82
2.2	Expression of <i>miRHG</i> only has a mild impact cell apical size	83
2.3	Map of cell apical areas in the tissue	84
2.4	Apical area of cells: impact of growth and proliferation	85
2.5	Validation of a new live sensor for ERK	86
2.6	Inhibition of <i>azot</i> and absence of impact on apoptosis	87
2.7	ERK activity and neighbor stretching during apoptosis	88

List of Abbreviations

2D	Two-dimensional
3D	Three-dimensional
ATP	Adenosine triphosphate
Azot	Ahuizotl
CIP	Contact inhibition of proliferation
CPM	Cellular Potts model
CycE	Cyclin E
DIAP	<i>Drosophila</i> inhibitor of apoptosis
Dilp8	<i>Drosophila</i> insulin-like peptide 8
DNA	Desoxyribonucleic acid
ECM	Extra-cellular matrix
ERK	Extracellular signal-regulated kinase
FA	Focal adhesion
hAPF	Hours after pupa formation
HeLa	Henrietta Lacks
hMSC	Human mesenchymal stem cell
IGF	Insulin growth factor

IIS	Insulin/insulin-like growth factor signalling
MAPK	Mitogen-activated protein kinase
MDCK	Madin-Darby canine kidney
NFκB	Nuclear factor kappa B
PCP	Planar cell polarity
PDMS	Polydimethylsiloxane
RHG	Reaper, Hid and Grim
RNA	Ribonucleic acid
ROCK	Rho-associated protein kinase
Scrb	Scribble
TCJ	Tri-cellular junction
TOR	Target of rapamycin
Trbl	Tribbles
TSC	Tuberous sclerosis complex
YAP	Yes-associated protein
Yki	Yorkie

Chapter 1

Introduction

Contents

1.1	Determinants and roles of cell geometry	2
1.1.1	A great diversity of geometries	2
1.1.2	Regulation of cell geometry	3
1.1.3	Scaling laws in multicellular organisms	7
1.1.4	Effects of cell geometry	13
1.1.5	Dysregulation of cell geometry in diseases	17
1.2	Cell geometry in epithelial morphogenesis	18
1.2.1	Characteristics of epithelia	19
1.2.2	Epithelial planar architecture at the cell scale	20
1.2.3	The single-cell mechanics of epithelial morphogenesis	22
1.2.4	An example: geometric regulation of cell division	29
1.3	The mechanics of apoptosis	33
1.3.1	A short history of apoptosis discovery	34
1.3.2	Apoptotic signalling pathways	35
1.3.3	Apoptosis in the mechanical regulation of morphogenesis	38
1.3.4	Biophysical modulation of apoptosis	41
1.4	Aims and outline of the thesis	46

1.1 Determinants and roles of cell geometry

1.1.1 A great diversity of geometries

When studying cells in a tissue, one of their first features that can be observed is their geometry, or the combination of their shape and their size. In multicellular animal organisms, cells vary greatly in their geometry between different tissues and cell types (**Figure 1.1**). At the same time, within a tissue, both the shape and size of cells typically display a striking regularity. In fact, a large heterogeneity in cell morphologies is a hallmark of pathological conditions such as cancer (as we will see in Section 1.1.5). Thus, geometry is a precisely regulated characteristic of animal cells in the formation of multicellular organisms with appropriate body, organ and cell sizes (developed in Section 1.1.3). Moreover, cell morphology is dynamic and responds to variations in both internal and external cues (see Section 1.1.2).

The variety of cell morphologies mirrors the variety of functions that cells perform in the body. Each cell type has evolved a shape and size that is appropriate to its function.

A first example is the mammalian spermatozoon, or sperm cell. The main function of the sperm cell is to reach the oocyte and fuse with it to form a zygote. To perform this role, the spermatozoon needs to swim over relatively large distances. The morphology of the sperm cell illustrates and allows its high motility: by far the longest part of the cell is an appendage, the flagellum, capable of oscillatory motions that propel the cell ([Gaffney et al. 2011](#)). The flagellum typically measures $50\ \mu\text{m}$ and is appended to a $5\ \mu\text{m}$ -long head that contains the genetic material delivered to the oocyte.

Another highly elongated cell type is the neuron. Neurons are the building blocks of the nervous tissues that form the neural systems of most animals. A neuron consists of a compact soma from which thin and branched filaments extrude ([Stevens 1979](#)). These filaments are typically of two types: the dendrites, and a single axon. They allow the neuron to reach out to other nerve cells and to transmit electro-chemical signals. Most neurons have a polarized structure, receiving signals to the dendrites and sending them from the axon. The longest neurons in the human body are found in the sciatic nerve which connects the foot toes to the base of the spinal cord: their axons are approximately one meter-long.

In contrast, epithelial cells generally have more compact geometries that allow them to form tight space tessellations. This is appropriate to the function of ep-

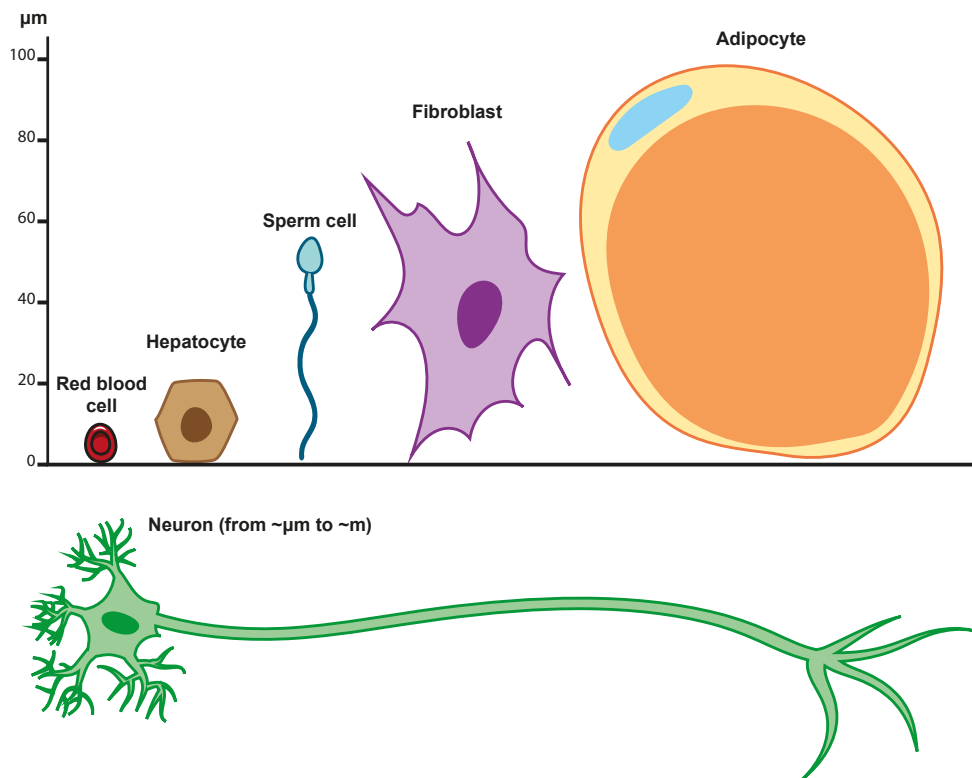


Figure 1.1 *Diversity of sizes and shapes of cells. Cells are drawn to their typical size in the human body. Inspired by (Ginzberg et al. 2015).*

ithelial tissues, which act as continuous and protective barriers in the organism (see Section 1.2.1). For instance, epithelial cells can be cuboidal, as in the human intestinal epithelium; in this tissue, cells also show apical membrane extensions called microvilli which facilitate nutrient absorption (Madara et al. 1987). In curved epithelia such as the *Drosophila* salivary gland, they may adopt scutoid shapes to stabilise three-dimensional packing (Gómez-Gálvez et al. 2018).

In addition to supporting cell function, cell geometry influences a wide range of cell behaviours as we will describe in Section 1.1.4, showing the need for a precise regulation of cell shape and size throughout their lives.

1.1.2 Regulation of cell geometry

Cell geometry is robustly set within a given cell type, and yet is flexible to changing conditions, as illustrated by the ability of some cells to grow dramatically. For instance, physical exercise stimulates the hypertrophy of adult muscle cells, or my-

ocytes. Thus, to understand how cells establish and maintain their geometry, we need to answer (i) how cells adopt a given geometry, and (ii) how cells sense their shape and size. The latter question is out of the scope of our introduction and has already been addressed in several excellent reviews (such as [Ginzberg et al. 2015](#) and [Haupt and Minc 2018](#)). In this section, we will focus on the first question and describe the factors that elicit changes in cell shape and size.

1.1.2.1 Environmental and molecular factors

First, cell size is impacted by changes in the environmental conditions, in particular in terms of nutrient availability. A classical paper by [Fantes and Nurse](#) showed that in the fission yeast *S. pombe*, cell size at division is controlled by the nutritive quality of the environment, with nitrogen-rich media promoting the development of large yeast cells while nitrogen-poor media host small yeast cells ([Fantes and Nurse 1977](#)). In mammalian cells, nutrient deprivation also blocks cell growth and cell cycle progression ([Pardee 1974](#)).

Second, molecular information contributes to the regulation of cell geometry: over the years, a number of signalling pathways involved in the control of cell growth have been identified.

The best characterized growth-regulatory pathway is the TOR (Target of rapamycin) pathway, whose activity is dynamically modulated by the nutritive quality of the environment. Amino acid deprivation deactivates TOR which reduces cell size, while amino acid addition triggers TOR signalling which drives cell growth, thereby providing a molecular basis for the regulation of cell size by nutritional factors ([Rohde et al. 2001](#); [D.-H. Kim et al. 2002](#); [E. Kim et al. 2008](#)). TOR is a highly conserved pathway. In *Drosophila* ([Oldham et al. 2000](#); [Zhang et al. 2000](#)) as well as in *in vitro* cultures of mammalian fibroblasts ([Fingar et al. 2002](#)), cells in which TOR is inhibited are greatly reduced in size. TOR is negatively regulated by TSC1 and TSC2 ([Gao et al. 2002](#); [Inoki et al. 2002](#); [Tee et al. 2002](#)), whose inhibition in *Drosophila* results in a dramatic increase of cell size ([Tapon et al. 2001](#); [Potter et al. 2001](#)). The insulin growth factor (IGF) acts upstream of TOR and controls the inhibition of TSC1/TSC2 via two signalling cascades: the PI3K/AKT one, and the Ras/Raf/MEK/ERK one (reviewed in [Laplante and Sabatini 2012](#)). TOR controls cell growth by regulating the biosynthesis of proteins and membrane lipids ([Düvel et al. 2010](#)); moreover, activation of TOR downregulates autophagy ([J. Kim et al. 2011](#)).

Other pathways act as crucial regulators of cell growth. We will describe one additional example, which is the transcription factor Myc. Activation of Myc increases cell size in a variety of systems by enhancing protein synthesis (Schuhmacher et al. 1999; Iritani and Eisenman 1999; Johnston et al. 1999) and ribosomal RNA biogenesis (Grewal et al. 2005). Conversely, loss of Myc reduces cell size (Johnston et al. 1999).

1.1.2.2 Mechanical factors

Third, cell shape and size result from internal and external inputs of mechanical nature. This last point has been brought to light by the prolific and exciting research fields of cell mechanosensitivity, which studies how cells probe their mechanical environment, and soft matter physics, whose lessons shed light on how cells adapt their behaviour in response.

Mechanical inputs shaping the cell come at various scales. At the intracellular scale, cell shape is controlled by the cytoskeleton, a dynamic network of interlinking proteins whose spatial reorganisation generates forces that enable the cell to migrate and deform (D. A. Fletcher and Mullins 2010; Boal 2012). The cytoskeleton comprises three types of protein fibers: the intermediate filaments, the microtubules and the actin filaments. Each of these fibers have different rigidity and stability and fulfill different roles in the cell. In particular, the polarised actin filaments interact with Myosin, a molecular motor, to form acto-myosin networks capable of contractile forces. The ability of acto-myosin filaments to transiently and locally deform a cell is illustrated in the migration of epithelial cells, which move by projecting and contracting actin-based protrusions called lamellipodia (Ridley 2011). Moreover, acto-myosin networks are responsible for global cell shape changes. For instance, the apical constriction of epithelial cells is a geometric deformation that drives large-scale tissue remodelling (as detailed in Section 1.2.3.3); apical constriction is driven by apical acto-myosin networks through a variety of behaviours, such as cortical flows, fibers formation, and acto-myosin pulses coupled to ratchet mechanisms (reviewed in Martin and Goldstein 2014). In addition to shape dynamics, the typical "static" morphology of a cell is also heavily regulated by the cytoskeleton. Cell cortical tension is controlled by the cell cortex, a thin and irregular surface-level meshwork of actin filaments which determines cell surface mechanics (reviewed in Clark et al. 2014). Actin and Myosin can also assemble into ordered and thick contractile bundles called stress fibers which maintain cell shape under stress (Kumar

et al. 2006) and are crucial to limit the elongation of large cells in the *Drosophila* dorsal thorax, or notum (López-Gay *et al.* 2020). Acto-myosin assembly can be coordinated over multiple cells to regulate tissue shape: mechanical stretch of a developing tissue triggers the enrichment of Myosin at the junctions parallel to the axis of stress to form multicellular linear cables, which are necessary to limit the deformation of cells (Duda *et al.* 2019).

Cytoskeletal components also probe the local mechanical environment of the cell via their interaction with adhesion complexes. Through this mechanism, cell geometry responds to physical interactions with the cell's surroundings. In multicellular organisms, the extracellular matrix (ECM) is often a key component of the environment of cells. The mechanical properties of the ECM impact cell migration and cell shape in many different cell types cultured *in vitro* (Roca-Cusachs, Sunyer, *et al.* 2013; Rens and Merks 2020). Moreover, recent *in vivo* studies revealed how modulation of the mechanical cell environment by the ECM promotes cell shape changes during development. During the elongation of the *Drosophila* wing, cells undergo a columnar-to-cuboidal shape change that drives tissue expansion. This cell deformation requires the degradation of the ECM which otherwise constrains cells into columnar shapes (Diaz-de-la-Loza *et al.* 2018). The interaction between cells and the ECM is often two-way, with cells secreting or degrading proteins that actively change the mechanical properties of the ECM. For instance, follicular cells are responsible for the stiffening of the ECM during the development of the *Drosophila* ovarian follicle. The maturing follicles undergo a series of transformations including rotation, antero-posterior migration and elongation. During follicle rotation, follicular cells secrete oriented fibrils that contribute to the anisotropic stiffening of the extracellular membrane and subsequent egg elongation (Chlasta *et al.* 2017). Moreover, a gradient of ECM stiffness drives the deformation of follicular cells from cuboidal shapes to either squamous (flatter) or columnar shapes; cell flattening requires interactions with a softer membrane, as is indicated by the absence of flattening upon mutation of integrins or focal adhesion kinases (two proteins involved in the binding to the extracellular substrate) (Chlasta *et al.* 2017). The ECM is not the only source of mechanical signals impacting cell shape and size: cells have the ability to adapt to a variety of physical inputs from their environment, such as flow-derived stresses. In mammalian kidneys, the cells lining the tubules are ciliated. Polycystic kidney disease is associated with large cells exhibiting defective primary cilia. Strikingly, the cilium functions as a mechanosensor whose bending under urine flow activates

Lkb1, a tumor suppressor present in the cilium and at its base (Boehlke et al. 2010). Lkb1 negatively regulates the TOR pathway which is responsible for maintaining a small cell size. In polycystic kidney disease, the cell cilia do not perform well their mechanosensing function, leading to high TOR activity and cell overgrowth. This example demonstrates the capacity of cells to probe and respond to a myriad of mechanical inputs.

Finally, at the tissue scale, a global pattern of extrinsic forces promotes large deformations associated to cell shape changes. During *Drosophila* mesoderm invagination, tissue tension is anisotropic with a predominant orientation along the antero-posterior axis. The cells also exhibit isotropic apical flows of acto-myosin; yet, the combination of this isotropic cell contractility with an anisotropic global stress leads to the oriented constriction of cells and tissue elongation (Martin, Gelbart, et al. 2010). A similar antero-posterior tensile force, this time caused by the invagination of the mesoderm, is responsible for the passive elongation of cells during *Drosophila* germ-band extension (Butler et al. 2009).

In this section, we described the many sources of information which participate in the regulation of cell geometry. A summary is given in **Figure 1.2A**.

1.1.3 Scaling laws in multicellular organisms

It is absolutely striking that animals within given species can be of variable sizes, and yet retain well-preserved proportions of their limbs and different body parts. Starvation during development can cause *Drosophila* to be as small as 35 μg (in dry weight) compared to the normal average weight of 290 μg , and yet these tiny animals have normal body proportions and look just like the miniaturised version of a typical fly (Beadle et al. 1938). The scaling of biological structures and their components has puzzled and amazed biologists for decades (D. W. Thompson 1917). Here, we will discuss how the size of the building block of life, the cell, scales with that of intracellular structures and organs to build appropriate-sized multicellular organisms.

1.1.3.1 Intracellular scaling

One of the most studied organelle in terms of scaling is the nucleus. It has been known for over a century that in general, nuclear volume scales with cell volume, and

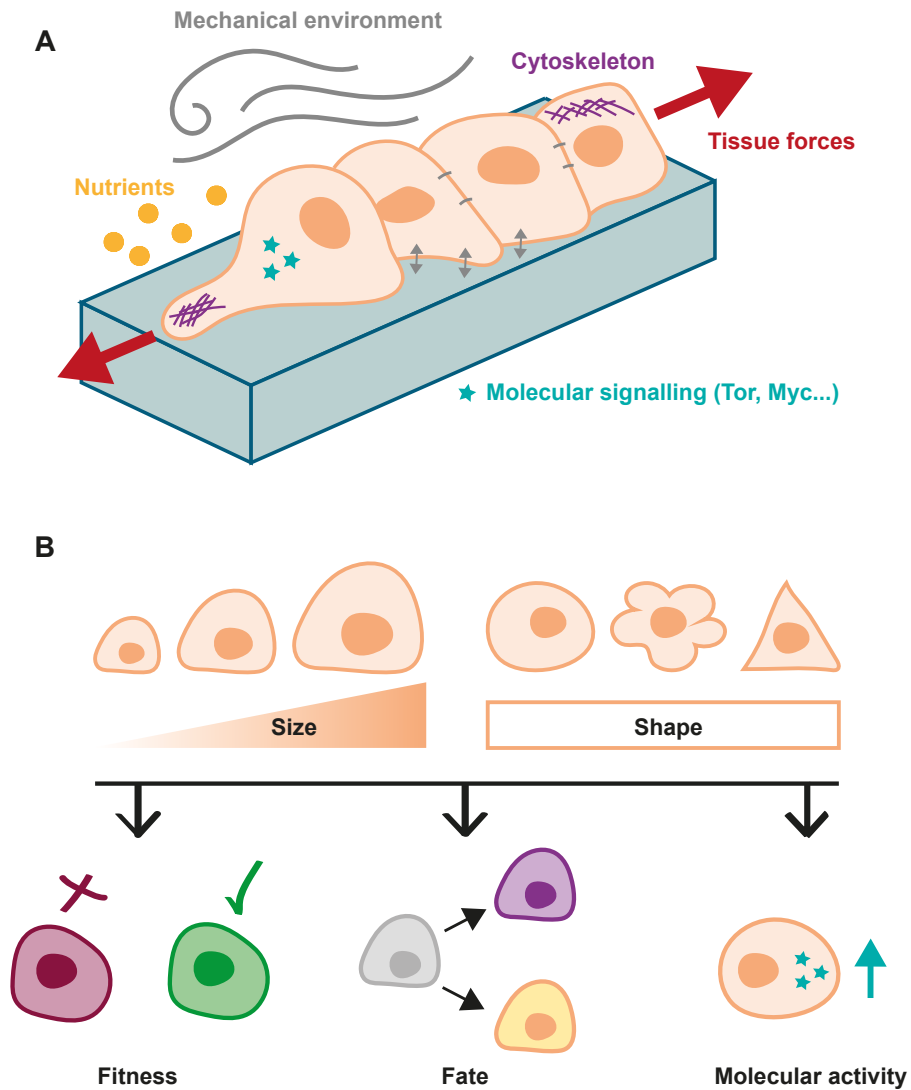


Figure 1.2 *Regulation and effects of cell geometry. (A) Graphical abstract of Section 1.1.2: cell geometry is modulated by a variety of molecular, environmental and mechanical factors. (B) Graphical abstract of Section 1.1.4: cell geometry impacts cell's fitness, fate and molecular activity.*

more precisely, with cytoplasm volume (Conklin 1912; Wilson 1925). In accordance with this idea, the nucleus of a small erythrocyte expands upon transplantation into a bigger HeLa cell (Harris 1967). Moreover, *Xenopus laevis* embryonic nuclei exposed to different volumes of cytoplasm in microfluidic channels (Hara and Merten 2015) or microfluidic droplets (P. Chen et al. 2019) adjust their size accordingly. However, the mechanism by which this scaling is ensured remains unknown: while (Hara and Merten 2015) found that nucleus expansion was controlled by the molecular motor Dynein which moves along microtubules, (P. Chen et al. 2019) verified that nuclei growth is not blocked in the absence of microtubules in microfluidic droplets and they identified nucleoplasmin as a scaling regulator.

Does the nuclear DNA content scales with nuclear size and cell size? In many plants, the volume of the nucleus does indeed correlate with the amount of DNA it contains (Baetcke et al. 1967). Furthermore, a way to create drastically bigger cells is to increase their ploidy, or the number of sets of chromosomes in their nucleus. This condition is termed polyploidy and it causes cells to be bigger proportionally to the increase in their DNA content (Fankhauser 1945; Fankhauser et al. 1955; Hermaniuk et al. 2017). Polyploidy can be a natural strategy of organisms in normal conditions to generate large cells, such as in mammalian livers. Observations in the tailtip of developing salamanders showed a clear scaling between the nuclear volume and the cell's ploidy (Fankhauser 1945), suggesting that DNA quantity may regulate the nuclear size. However, later experimental manipulations of the DNA content in *Xenopus* saw relatively small effects on the size of the nucleus which contradict this idea (Levy and Heald 2010). Regarding mitotic chromosomes, their length scales with cell size in *Caenorhabditis elegans* as well as in the late developing *Xenopus*, from the blastula-to-neurula stage (Kieserman and Heald 2011; Ladouceur et al. 2015).

Little is known about the general scaling rules of morphologically complex organelles, such as the Golgi apparatus and the endoplasmic reticulum. The size of these organelles is typically difficult to define and to measure. Further investigation will be needed to understand how their size might be set to ensure their proper functioning (Chan and Marshall 2010; Wesley et al. 2020).

Cell size relates to fitness and metabolism (detailed later in Section 1.1.4). Consequently, the appropriate scaling of a cell's intracellular contents could be a necessary condition for its proper functioning. At the organismal level, the metabolic rate approximately follows a $\frac{3}{4}$ -power law with respect to the body mass as stated by

the famous Kleiber's law (Kleiber 1932). At the cellular level though, the number of mitochondria is proportional to cell size but the mitochondrial membrane potential is not, defining an "optimal" cell size associated with increased proliferation (Miettinen and Björklund 2016). One could imagine that the proliferative power of cells depends on the scaling of intracellular organelles associated to the division process. Indeed, doubling the cytoplasmic volume of mouse oocytes (by performing electrofusion with enucleated oocytes) delays chromosome alignment and increases chromosome segregation errors (Kyogoku and Kitajima 2017). Thus, intracellular scaling affects the efficiency of division. However (and perhaps fortunately), there is no one proper size for animal cells to function properly, but rather a range of good sizes, which allows for flexibility to environmental conditions and biological variability: as shown by the same study cited above, mouse oocytes whose volume was halved using micropipette aspiration exhibit less division errors than control ones, indicating that the normal size of a cell is not necessarily the "fittest" (Kyogoku and Kitajima 2017).

1.1.3.2 Scaling with organ size and body size

Does an organ know its intrinsic size? In the 20th century, major experimental works intended to answer this question using grafting techniques. Building on the work initiated by (Harrison 1924), Twitty and Schwind carried out limb transplantations between two salamanders with different growth rates and showed that the grafted limb grows similarly to the normal control limb in the donor species (Twitty and Schwind 1931) (**Figure 1.3A**). In *Drosophila*, when imaginal wing discs are transplanted into the abdominal cavities of adult flies, they grow and end up being the normal size they would be expected to reach at the time of pupariation (Bryant and Levinson 1985) (**Figure 1.3B**). These experiments indicate the existence of organ-intrinsic cues that carry on an autonomous developmental programme.

The final size of a multicellular organ mainly depends on two factors: cell sizes, and cell number. As a result, proliferation, cell loss and cell growth crucially contribute to the proper development and scaling of the organ. Interestingly, manipulating only one of these three parameters during development is often not enough to disturb the organ size, as was shown in the *Drosophila* wing disc. In this tissue, enhancing proliferation (by overexpression of Cyclin E or Cdc25) increases cell number, while inhibiting proliferation (by loss of dE2F or overexpression of RBF) results in fewer cells; and yet, in all these mutant conditions, the final tissue size is

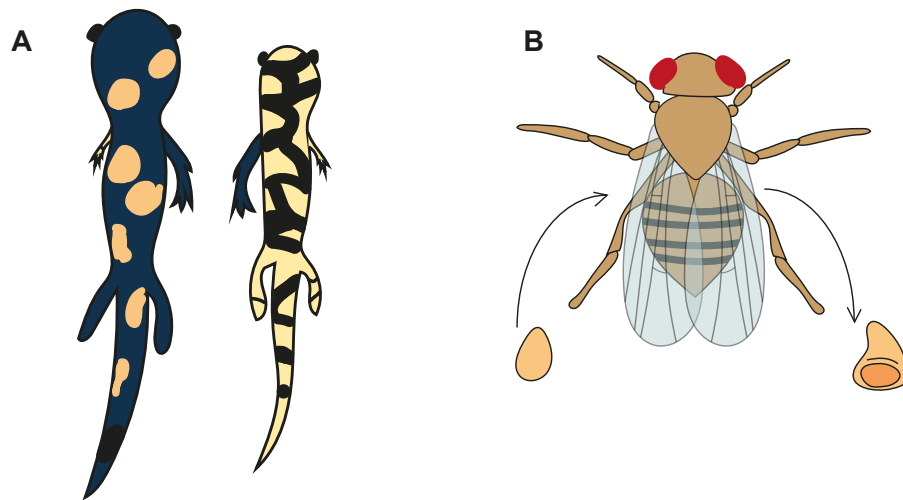


Figure 1.3 *Experimental observations of an intrinsic regulation of organ size. (A) Limb transplantation between two salamanders (*Amblystoma punctatum*, left, and *A. tigrinum*, right) whose transplanted limb ends up the same size as the donor limb. Experiment by (Twitty and Schwind 1931), illustration inspired by (Harrison 1924). (B) Transplantation and subsequent normal growth of an imaginal wing disc in the abdominal cavity of an adult fly. Experiment by (Bryant and Levinson 1985).*

unaffected as the modification of cell number is compensated for by a change of cell size (Neufeld et al. 1998). Instead of changing the proliferation rate, Martín and Morata used a different strategy and experimentally manipulated the proliferation speed with heterozygous mutations of the *minute* gene. By doing so, mosaic compartments of relatively fast- or slow-proliferating cells can form in the wing disc. Each compartment grows at its own rate, but also arrests growth autonomously, and the adult wing ends up being a proper size and shape (Martín and Morata 2006). Also, when cell size is manipulated by inducing polyploidy in newts, the resulting organism is composed of larger but fewer cells and its body is not enlarged (Fankhauser 1945; Fankhauser et al. 1955). These results could suggest that the organism actively compensates for the perturbation by modifying cell size, cell number, or developmental time in order to reach a normal size. One way would be for the cell division and death rates to depend on mechanical constraints. Differential rates of cell growth, which trigger local build-up of pressure, would then be compensated for by proliferation or cell death, leading to the stabilisation of a uniform growth rate in a homogeneous tissue or the elimination of slow-growing clones in a mosaic tissue (Shraiman 2005; Section 1.3.4). Alternatively, the crucial parameter for

regulation could be the total cell mass (Conlon and Raff 1999), which seems to be kept constant by the experimental perturbations described above. Compensating mechanisms would stem from this control of mass. Interestingly, the mouse embryo provides a direct example of such a control of total cell mass. After a few days of gestation, embryos which are formed by the fusion of two 8-cell eggs have the same foetal weight as unfused embryos developed in similar conditions, indicating that the increase of cell material by fusion is followed by an adjustment of the embryonic growth rate (Bowman and McLaren 1970; Buehr and McLaren 1974).

The mechanisms behind the regulation of embryonic mass, cell size or cell number to form a well proportioned adult remain unclear. What is nonetheless known is the relative contributions of cell size and cell number in forming differently sized animals. Changes in cell number more often account for changes in body size, with bigger animals usually having more cells and smaller animals having less cells (Conlon and Raff 1999). Thus, controlling cell size might be easier (or more important) in a well functioning organism than setting a fixed number of cells. Still, cell size and number can be simultaneously perturbed without adjustment, resulting in aberrant growth or tissue shrinkage. For instance, cancerous tumours are highly proliferative tissues whose cells display widely variable morphologies (see Section 1.1.5). Mutations of the insulin/insulin-like growth factor signalling (IIS) pathway constitute another example. Studies in the *Drosophila* uncovered a crucial role for the IIS pathway in regulating body size. It also controls ageing, longevity and nutrient use in both flies and mammals, as well as the production of the hormone ecdysone which regulates developmental timing in insects. Mutants for *chico*, a core component of the IIS pathway that encodes a fly insulin receptor substrate, have both less and smaller cells than normal animals (Böhni et al. 1999). Moreover, inhibition of the PI3K-AKT pathway downstream of Chico, or of the *Drosophila* TOR which is a target of PI3K-AKT, results in the same phenotypes of undergrown flies with small, less proliferative cells (Weinkove et al. 1999; Zhang et al. 2000).

The development of humans, flies or mice occurs following an axis of symmetry so that the left and right sides of the organism have similar proportions. This raises the question of the mechanisms promoting a robust inter-organ coordination and alleviating the effects of possible developmental noise. A recent study identified Dilp8, an insulin-like peptide, as an important effector of inter-organ coordination in developing flies. When growth is impaired in the wing pouch, a size reduction is observed in other tissues originating from the wing disc, such as the hinge and

notum, but also in tissues formed by different imaginal discs, such as the primordial eye. These intra- and inter-organ reductions of growth require the non-autonomous activity of Dilp8 which could act by modulating ecdysone production (Boulan et al. 2019).

1.1.4 Effects of cell geometry

We saw in Section 1.1.1 that the size and shape of cells relate to their functions in the organism. Cell geometry also influences several cell behaviours, as we will describe in this section. A summary is given in **Figure 1.2B**.

1.1.4.1 Role in metabolism and fitness

Cell size is dysregulated in a variety of diseases, as well as during ageing (detailed in Section 1.1.5). This observation raises the question of a possible link between cell size and cell fitness, defined as the ability of a cell to perform its functions.

In human as well as *Drosophila* cell lines, although the number of mitochondria scales with cell size, their membrane potential (a factor which relates to the mitochondrial ability to produce ATP) and the protein synthesis rate are maximal at an intermediate cell size (Miettinen and Björklund 2016). This suggests the existence of an optimal cell size at which cellular fitness, mitochondrial functionality and protein synthesis would be maximal.

What happens when cells largely exceed this optimal size? It should be noted that *in vivo*, cells are most likely not at their maximal size since an increased activity of growth-regulatory pathways can enhance their growth. Another factor which has a drastic impact on cell size is cell ploidy. Compared with their diploid counterparts, polyploid tadpoles with three sets of chromosomes have a lower standard metabolic rate (the amount of energy needed per unit of time), indicating a lower metabolism and fitness (Hermaniuk et al. 2017). However, polyploidy does not affect grown frogs which live in terrestrial habitats unlike water-bred tadpoles, suggesting that the influence of cell size on organism fitness might be environment-dependent.

To generate large cells without changing their DNA content, Neurohr et al. used a different technique: they arrested yeast cells in G1 over several hours, which caused cells to increase their volume up to 4-fold compared to control cells. In overgrown yeast cells, RNA and protein biosynthesis is impaired and stops scaling with cell size, which causes cytoplasm dilution and slowed-down cell division (Neurohr et al.

2019). The resulting giant cells share hallmarks of senescence with old yeast cells. Interestingly, human fibroblasts that have been induced to undergo senescence but whose growth is prevented have a normal proliferative potential, in agreement with previous works (Demidenko and Blagosklonny 2008). Thus, cytoplasmic molecular crowding could contribute to the physiological and functional changes associated with cell senescence.

By which mechanisms could cell size correlate with cell fitness? The topic was developed a few years ago in a review by Miettinen, Caldez, et al., who suggested several possible and great explanations: for example, excessive sizes could affect the structural integrity of the cell constituents, such as the cytoskeleton or the membrane. Alternatively, intracellular distances could become rate-limiting for chemical reactions, or the decrease of the surface-to-volume ratio could slow down metabolic processes (Miettinen, Caldez, et al. 2017).

1.1.4.2 Role in fate specification

The modulation of cell differentiation by geometric information was primarily studied in human mesenchymal stem cells (hMSCs). To differentiate properly, these cells require to be seeded at certain densities, indicating a possible role for cell morphology as a regulator of fate commitment (Pittenger et al. 1999). And indeed, such a role was observed 20 years ago: using micropatterned substrates to control cell spreading, McBeath et al. showed that hMSC shape controls their fate. Flattened and spread cells differentiate almost exclusively into osteoblasts, while round hMSCs adhering on small surfaces become adipocytes (McBeath et al. 2004). Cell shape-driven differentiation requires the modulation of the RhoA-ROCK pathway, involved in the reorganisation of the cytoskeleton. Interestingly, a later study revealed that differences in fate commitment between spread and unspread cells are not driven by changes in the projected cell area, but by associated changes in their contractility (Kilian et al. 2010). At equivalent surface areas, micropatterned shapes that enhances acto-myosin contractility promote an osteoblast fate, and this effect can be halted by the inhibition of F-actin polymerisation, Myosin activity or ROCK activity.

The studies we described here took advantage of the tools provided by micro-engineering techniques to investigate the regulation of stem cell differentiation. Further work will be needed to relate their discoveries, made *in vitro* on two-dimensional (2D) surfaces, to the physiological role of geometric cues in the regulation of cell

differentiation in complex three-dimensional (3D) environments.

1.1.4.3 Role in molecular signalling

Molecular signalling regulates cell geometry through the action of growth regulatory pathways, as described earlier in Section 1.1.2. Conversely, geometric and other mechanical inputs feed back into the cell's chemical activity, a process known as mechanotransduction.

The mechanotransducing pathways have gained a lot of attention in the past few decades, and their actions in a variety of systems have been described in excellent reviews ([Iskratsch et al. 2014](#); [Brás-Pereira and Moreno 2018](#); or [Farge 2011](#) in the context of development). Moreover, we already encountered a few examples of mechanosensitive proteins, such as Lkb1 whose activity is modulated by the flow-sensing cilium ([Boehlke et al. 2010](#)), or the RhoA/ROCK pathway involved in hMSCs differentiation ([McBeath et al. 2004](#)). In this sub-section, we will provide an overview of the diversity of mechanotransducing mechanisms, and detail the situations where their activity specifically links with cell geometry.

The plasma membrane is the primary locus of direct interactions between the cell and its environment, and as such, it is natural that it hosts a number of mechanosensing structures. Among them are mechanosensitive ion channels: these (often very selective) gateways allow ions to travel across the membrane, which generates both electrical and chemical signals. A number of mechanosensitive ion channel proteins have been identified, such as the tension-sensitive Piezo1 whose discovery was awarded the Nobel Prize of Physiology or Medicine in 2021 ([Coste et al. 2010](#)).

The nature of membrane mechanosensing structures differs depending on whether they mediate cell-cell or cell-matrix connection. The neurons of the peripheral nervous system provide an example of heterotypic cell-cell interactions driving mechanotransduction. Schwann cells produce layers of myelin wrapped around the axons of these neurons to improve signal conduction. However, the myelination process is axon size-dependent, both in its initiation (with a trigger threshold at 1 μm of axonal diameter) and in its intensity (as the myelin sheath thickness scales with axon diameter). Neuregulin-1 (NRG1) type III controls the thickness of the myelin sheath in a dose-dependent manner: larger axons present more membrane-bound NRG1 to the surrounding Schwann cells, thereby allowing a measurement of axon size that elicits a proportional response ([Michailov et al. 2004](#)).

At the cell-ECM interface, focal adhesions (FAs) are crucial to the mechanosens-

ing activity of the cell. They involve transmembrane receptors named integrins and promote force propagation through the cytoskeleton (Martino et al. 2018). The localisation of FAs at the cell-ECM interface and their interplay with the cytoskeleton would logically make them a perfect tool to measure cell spreading. In a seminal work using micropatterning techniques to manipulate cell shape, it was shown that the spreading of single endothelial cells governs their survival, with unspread cells being more likely to die (C. S. Chen et al. 1997). Cell adhesion to different integrin ligands changes their sensitivity to spreading, indicating that the modulation of cell survival is fine-tuned by FA proteins. However, this modulation is independent on FAs density as cell-ECM contact area (which the authors uncoupled from cell area) does not impact survival.

In hMSCs cultures, the assembly of FAs is controlled by the transcription co-activator YAP (Yes-associated protein), a well-known mechanotransducer (Nardone et al. 2017). The phosphorylated form of YAP (as well as of its *Drosophila* homologue, Yorkie or Yki) is located in the cell cytoplasm; upon activation, it enters the cell nucleus and modulates gene expression (Kuge et al. 1997). In particular, its downstream targets control cell proliferation, differentiation and death. In *Drosophila* for instance, Yki acts upstream of Cyclin E and DIAP1, as well as of the microRNA *bantam* whose expression is both necessary and sufficient to cause the phenotypic pattern of Yki-induced overproliferation (Nolo et al. 2006, B. J. Thompson and Cohen 2006). YAP/Yki is a major downstream target of the Hippo pathway that plays a key role in the control of organ and body growths (reviewed in Tumaneng et al. 2012). Yki activity is negatively regulated by the gene *hippo*, whose inactivation results in increased proliferation and tissue growth in various tissues including the *Drosophila* eye (Harvey et al. 2003; Udan et al. 2003; Pantalacci et al. 2003). Strikingly, the Hippo pathway "sense" cell size and scales its activity accordingly. *In vitro*, the spreading area of micropatterned hMSCs scales with YAP activity, measured as the ratio of nuclear to cytoplasmic YAP (Nardone et al. 2017, in accordance with previous works Dupont et al. 2011). In a similar manner as in (C. S. Chen et al. 1997), the authors also verified that the cell-ECM contact area does not impact YAP localisation. The size-sensitivity of Hippo/Yki was recently observed *in vivo*: during the development of the *Drosophila* dorsal thorax, the posterior central region elongates under tensile stress and this elongation is accompanied by the formation of apical acto-myosin stress fibers. Stress fibers cluster components of the Hippo pathway; because the number of fibers scales with

cell apical area, the activity of downstream targets of Hippo such as Bantam is also proportional with cell apical size (López-Gay et al. 2020). As a result, Hippo activity translates absolute cell size into chemical signalling.

Intuitively, in tissues where cells adhere and communicate closely with each other (such as epithelia whose characteristics are described in Section 1.2.1), cell relative sizes should impact their surface of contact, the bounding of transmembrane elements, and the amplitude of the resulting intercellular signalling. Indeed, some signalling pathways have been shown to scale with relative cell size in epithelial tissues. *In vitro*, the activity of Notch in neighbouring pairs of cells correlates with their contact area (modelled in Khait et al. 2016); accordingly, in the confluent chick basilar papilla, Notch signalling scales with the relative sizes of cells (Shaya et al. 2017). A consequence of relative size-dependent signalling is that molecular activity should be disrupted by aberrant tissue topology. In the *Drosophila* wing epithelium, the propagation of planar cell polarity (PCP) signalling is impaired in clones of irregular cell areas (Ma et al. 2008). Interestingly, components of the PCP pathway also regulate the regular hexagonal packing of the wing (Classen et al. 2005), suggesting that a possible feedback mechanism co-regulates relative cell areas and PCP signalling. A recent non-peer reviewed work proposed the existence of a similar feedback between morphogen signalling and apical cell size. *In silico* analyses predicted that smaller cell areas improve the variability of morphogen gradients and the resulting positional accuracy (Adelmann et al. 2022): In their discussion, the authors note that some morphogens cause a reduction of the cell cross-sectional area, perhaps as a mechanism to control signalling noise.

1.1.5 Dysregulation of cell geometry in diseases

The mechanisms that control cell shape and size in multicellular organisms are complex, dynamic and diverse. Dysregulation of these controls, in particular the ones related to cell size, is associated with pathological conditions.

As early as the 19th century, pleomorphism (a high variability in cell size and shape) was recognised as a marker of malignant tumour cells. This observation contributed to the establishment of the field of cytopathology, which diagnoses diseases from the study of single free cells in fluids (Diamantis et al. 2013). Mutations of the main growth-regulatory pathways, such as the PI3K/AKT/TOR pathway or Myc, are known to drive tumourigenesis. This led to the development of therapeutic strategies using mTOR inhibitors against cancer. Size pleomorphism could

contribute to cancer propagation by promoting tumour dispersal in epithelial tissues (Ramanathan et al. 2019).

For certain cell types, such as neurons, abnormal sizes may impair their functions. In 1955, Fankhauser et al. generated polyploid newts with three sets of chromosomes instead of the normal two sets. Polyploid newts have similar-sized brains with fewer and larger neurons. This condition is associated with cognitive problems and poor performances in learning tests (Fankhauser et al. 1955), although the study did not allow to differentiate between the roles of the number and size of neurons. 40 years later, researchers compared the brain size, neuron size and brain morphological complexity (assessed with observations of the separation of brain layers and migration of neurons) between 22 species of salamanders and 17 species of frogs (Roth et al. 1994). They found a clear negative correlation between neuron size and brain complexity; moreover, this correlation was independent of the total brain size in frogs, suggesting the absence of significant influence of the number of neurons (while in salamanders, brain size does correlate with complexity). In humans, tuberous sclerosis is a rare pathological condition associated with the mutation of the TSC1/TSC2 complex and consequently, the over-activation of the TOR pathway. Tuberous sclerosis can cause non-cancerous brain tumours due to the occurrence of giant brain cells, and is associated with developmental disorders such as epilepsy, learning disabilities or autism spectrum disorders (Prather and de Vries 2004; Crino 2011).

Finally, ageing could increase the risk of deregulated cell growth. For instance, ventricular cardiac hypertrophy is a cardiac disease which is more prevalent in older people and which consists in the thickening of the wall of a cardiac ventricle (more commonly the left one). This thickening results from the hypertrophy of cardiac myocytes which can be caused by abnormal activity of IGF or TOR (reviewed in North and Sinclair 2012).

1.2 Cell geometry in epithelial morphogenesis

In the previous sub-chapter, we showed how geometry is a highly regulated characteristic of cells which influences their functioning and behaviour in the organism. It is particularly clear in the context of tissue morphogenesis, the development of complex structures and shapes that emerge from the coordination of single cell behaviours. In this sub-chapter, we describe the morphogenesis of epithelial tissues from the cell's eye view, with a focus on the impact of cell geometry.

1.2.1 Characteristics of epithelia

Epithelial tissues are continuous and protective layers of cells that line organs, vessels, cavities and other body structures. They form barriers that protect the tissues beneath: for instance, the skin is the largest organ of the human body and its outermost layer is an epithelial sheet called the epidermis that protects the organism from infections and aggressions. Epithelia are selective barriers that can perform the absorption or diffusion of molecules and drive directional flows between the inner and outer surfaces. An example is the epithelial sheet lining the intestine which can absorb nutrients from the digestive tracts and release them in the blood.

To ensure the high cohesiveness and integrity necessary for their role as barriers, epithelia are characterised by interconnected cells, with little intercellular space. Cell cohesiveness emerges from the formation of specialised protein complexes that mediate intercellular adhesion. These complexes exist in various forms that differ between species; for example, *Drosophila* epithelial cells are held together through the establishment of adherens junctions and septate junctions (**Figure 1.4A**). Adhesive complexes are linked to the cytoskeleton, providing a mechanism for mechanotransduction and mechanical coupling between neighbouring cells ([Liang et al. 2015](#)).

Moreover, as epithelial cells typically line the outer surfaces of organs or cavities, different sections of the cell membrane face different inner or outer environments. This is reflected in the establishment of a clear apico-basal cell polarity with functionally and molecularly distinct apical, basal and lateral membrane domains (see [Riga et al. 2020](#) for a recent review). Interestingly, the apical and basal sides of cells generally align together at a local scale, which allow us to define apical and basal tissue planes.

There exist several types of epithelial architecture that differ by their thickness (simple, stratified) and cell morphology (squamous, cuboidal, columnar, pseudostratified) (**Figure 1.4B-C**). Simple epithelia are one cell-layer thick, while stratified epithelia consist of several layers of cells. Squamous cells have a larger width than height and appear quite flat, the opposite of columnar cells which are taller than they are wide; cuboidal cells represent an intermediate between squamous and columnar as their width and height are roughly similar. Pseudostratified epithelia contain spindle-shaped cells whose nuclei intercalate at different heights in the tissue.

Epithelial tissues are extensively remodelled during development in order for the complex three-dimensional shapes of viable organs to emerge. We describe in

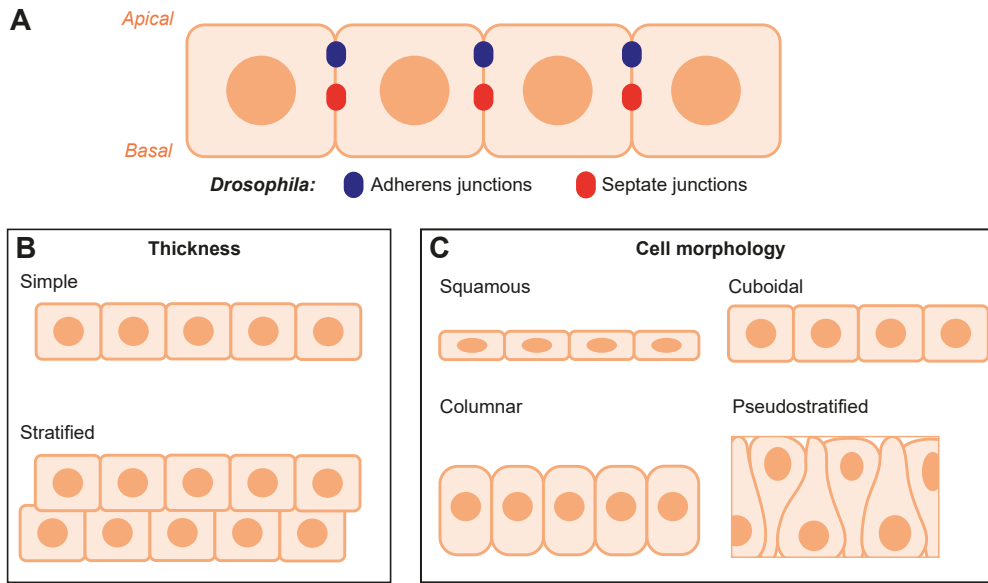


Figure 1.4 *Characteristics of epithelial tissues: (A) intercellular adhesion and apico-basal polarity, (B-C) types of epithelial architectures differing by their thickness (B) and typical cell morphology (C). Lateral view.*

section 1.2.3.3 how the regulation of cell geometry ensures the good execution of morphogenetic processes in epithelia.

1.2.2 Epithelial planar architecture at the cell scale

One way to look at simple epithelia is to model them as planar networks of adjacent 2D cell apical surfaces (apexes) by focusing on the apical plane. Then, the total surface of the epithelial sheet is simply a function of cell apical size and cell number, the latter resulting from the processes of cell loss and cell proliferation.

These three parameters, cell size, cell division and cell extrusion, are interconnected. On the one hand, when cell growth is limited, in-plane division halves cell apical area; on the other hand, cell area impacts cell division, as we show in Section 1.2.4. Over-inducing cell removal in an epithelium (by tissue damage, or cell death blockage) can promote the proliferation of the remaining cells, a process coined "compensatory proliferation" and reviewed in (Fan and Bergmann 2008). Conversely, proliferation can contribute to the modulation of apoptosis, a form of programmed cell death, as we show in Chapter 2 of this thesis. Cell extrusion affects local cell sizes by pulling on the neighbouring cells (Kuipers et al. 2014; Monier et al. 2015; Valon et al. 2021) and promoting rearrangements, which remodel intercellular

junctions (Tsuboi et al. 2018). Cell size, in turn, controls epithelial apoptosis: this result is one of the key findings of my PhD work and is developed in Chapter 2.

The shape of a simple epithelium involves another parameter, the cellular topology. A planar epithelial architecture can generally be described as a packing of polygonal cells. Cell topology describes the connectivity between these polygons by focusing on the neighbour relationships. Intuitively, exchanging two neighbours without modifying their shapes changes the topology of the tissue. Conversely, when stretching a solid sheet of cells whose connections cannot be modified, the size of cells changes but the topology is unaffected.

The tools provided by topology as a branch of mathematics have contributed to major advances to our understanding of epithelial packing. For example, in an epithelial plane with many cells where each vertex is formed by the junction of three cells (tricellular junctions, as is often the case in epithelia), Euler’s formula predicts that the average number of neighbours of each cell \bar{n} is equal to 6. The number of neighbours of any individual cell may vary over time, and may be more or less than 6; but at each time, the average number of cell neighbours over the tissue is equal to 6. In close accordance with this theoretical prediction, hexagons are the predominant polygonal cell shape in many animal epithelia (see for example Gibson et al. 2006 for quantifications in the *Drosophila* wing disc, *Hydra* epidermis and *Xenopus* tail epidermis).

The topological packing of epithelial cells in a plane correlates with their size distribution. Almost a century ago, Frederic T. Lewis studied the epithelial architecture and cell packing in a variety of tissues (Lewis 1928). His observations led him to suggest a law that establishes a linear relationship between the number of neighbours or sides of a cell, n , and its average resting area, A :

$$A = \frac{A_0}{4N} (n - 2), \quad (1.1)$$

where A_0 is the total area of the tissue and N the number of cells. Interestingly, in a regular epithelium with cells of similar resting sizes, this relationship becomes:

$$A = \frac{A \times N}{4N} (n - 2) = \frac{A}{4} (n - 2), \quad (1.2)$$

which automatically implies that $n = 6$ and that the equilibrium configuration is a hexagonal packing. Lewis’s law was justified mathematically as corresponding to the most probable distribution (or, in terms of information theory, the distribution

that maximises entropy) in a packing of confluent cells that verify Euler’s formula (Rivier and Lissowski 1982).

More recently, nurturing exchanges with the field of foam physics instead predicted that the number of sides of a cells could depend linearly on the square root of cell area (or equivalently, on cell radius) (Durand et al. 2014). In his pioneering book, *On Growth and Form*, D’Arcy W. Thompson had already made the inspiring observation that living cell layers seem to follow physical laws that could render meaningful the use of analogies with other physical systems, such as 2D foams (D. W. Thompson 1917; for an excellent review of the work of Thompson and its influence, see Graner and Rivelin 2017). In bubble foams, statistical mechanics models can derive relationships between cell geometry and topology such as the following equation that links n and the square root of A (Durand et al. 2014):

$$\bar{n}(A) \simeq 3 \left(1 + \frac{\sqrt{A}}{\mu(\sqrt{A})} \right), \quad (1.3)$$

where $\bar{n}(A)$ is the average number of sides for cells of area A and $\mu(\sqrt{A})$ is the mean square root of cell area. This relationship and other predictions from the same model show very good agreement with experimental foams over a wide range of dispersities.

Finally, the single cell behaviours that drive epithelial morphogenesis (and that we will describe in Section 1.2.3.1 below) obviously impact tissue topology and packing. Cell proliferation is an example of a cell behaviour that changes geometric patterns by forming new cell-cell junctions. Using a mathematical model of proliferating epithelium, Gibson et al. showed that the geometric changes induced by proliferation can drive the convergence of tissue topology towards an equilibrium distribution of polygons (with a mode at hexagons) that is close to experimental values (Gibson et al. 2006).

1.2.3 The single-cell mechanics of epithelial morphogenesis

1.2.3.1 Bridging cell behaviours and tissue deformations

In the previous section, we saw how the architecture of a planar epithelium emerges from the characteristics (topology, size, number) of its building blocks, the epithelial cells. Similarly, the morphogenetic movements and deformations of a developing epithelium can be described in terms of the coordinated behaviours of its many

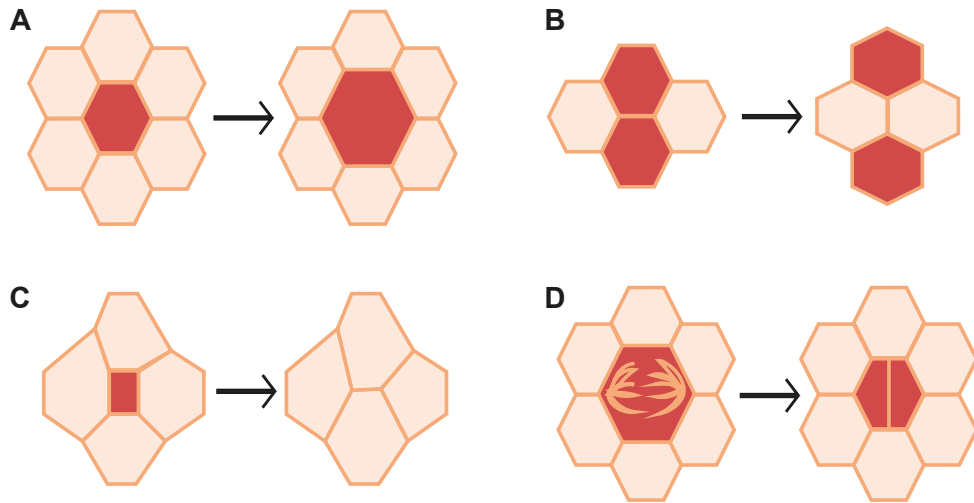


Figure 1.5 *Elementary single-cell behaviours in an epithelial tissue. (A) Cell size and shape changes, (B) rearrangement, (C) cell extrusion and (D) cell division. Apical view.*

cells. At a fixed cell number, tissue dynamics can be seen as the sum of two main cell processes: cell rearrangements, which correspond to topological changes, and cell size and shape changes (Blanchard et al. 2009). In the general case, one should add cell division and cell extrusion, amounting to four the number of key single-cell behaviours that shape an epithelial tissue (Figure 1.5).

Bridging the dynamics of whole tissues and of these four cell processes has proven a very fruitful approach to understand quantitatively how cell behaviours drive morphogenesis, and how they impact each other. This cell-scale description of tissue deformations can be combined with mechanical or genetic perturbative techniques to characterise the mechanisms controlling tissue development. In the *Drosophila* pupa, this approach has been applied to several tissues, such as the wing (Etournay et al. 2015; Guirao et al. 2015) and the notum (Bosveld, Bonnet, et al. 2012; Guirao et al. 2015), as well as the germ-band extension (X. Wang et al. 2020). For instance, the quantitative analysis of notum morphogenesis showed that the Fat/Dachsous PCP pathway is responsible for an anisotropic increase in tissue tension which promotes oriented cell rearrangements; these rearrangements drive local tissue contraction, and finally, global morphogenetic movements (Bosveld, Bonnet, et al. 2012).

Cell size and shape changes are one of the four main cell behaviours that contribute to shaping epithelia. We will describe examples of morphogenetic movements regulated by this cell process in a following part (Section 1.2.3.3). Geometric changes can occur at a large scale during epithelial morphogenesis, as is the case in

the *Drosophila* pupal wing. During development, the wing epithelium transitions from an initially disordered cell array to an extremely regular hexagonal packing. This regular topology emerges from the extensive remodelling of cell-cell contacts through shape changes and rearrangements. This process is regulated by components of the PCP pathways and by the physical properties of cells, such as line tension and contractility (Classen et al. 2005; Farhadifar et al. 2007).

1.2.3.2 Cell geometry and mechanical properties

As physical objects, living cells are shaped by internal and external mechanical forces, some of which we described in Section 1.1.2. As a result, cell geometry relates to local mechanics, and changes of cell geometry are associated with variations in the mechanical state of cells. For instance, the local curvature of a cell surface is influenced by its cytoskeletal dynamics, contractility and surface tension. Another example is the cell stiffness: in single endothelial cells, this mechanical parameter correlates with the projected area (Roca-Cusachs, Alcaraz, et al. 2008; Stroka and Aranda-Espinoza 2011). This relationship is also observed in confluent MDCK cells, where the local stiffness non-linearly increases with cell apical size (Nehls et al. 2019).

In confluent epithelial tissues, cells tightly adhere to each other. As such, they are mechanically coupled, allowing for force transmission. Thus, the mechanical environment of a cell encompasses cell-cell physical interactions. This holds true as well in confluent bubble foams, meaning that once again and as suggested by D’Arcy Thompson’s work (D. W. Thompson 1917), we can apply tools from foam physics to study how the packing of a living tissue relates to its local mechanical constraints.

Foams at a mechanical equilibrium minimise their total surface energy, and this constraint impacts their geometric packing. Plateau’s laws describe the configuration of two-dimensional bubble foams (Plateau 1873).

The first law is also called the Young-Laplace equation and relates the curvature of the wall between two bubbles to the pressure difference between these bubbles. This law implies that the curvature is constant across the wall: in the two-dimensional apical plane, each wall is an arc of a circle (or a straight line if both cells have the same internal pressure). Similarly, the curvature between two living cells is determined by (and can inform us on) the pressure difference between these two cells.

The second law describes the junctions between bubbles. It states that bubbles meet by three. Moreover, since bubbles in a foam have the same wall tension, they

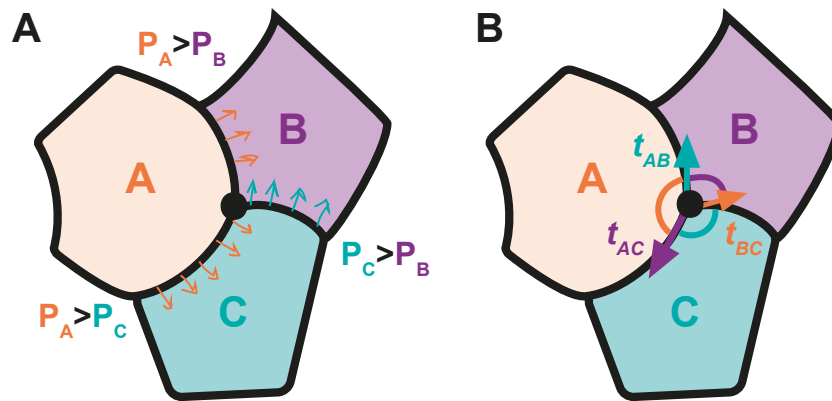


Figure 1.6 *Principles of stress inference in 2D tissues. (A) Each cell (A, B or C, apical view) has a homogeneous pressure whose relative value is calculated using the curvature of cell-cell interfaces. (B) Each junction has a tension whose relative value is inferred from the angles at vertices. Inspired by (Roffay et al. 2021).*

form equal angles at 120° in the plane. In living tissues, wall tension is determined by the cell physical properties and adhesion with its neighbours and is not uniform in space or time. This means that angles can deviate from the Plateau's law, and such deviations can be understood in terms of tension differences. Moreover, cell vertices can join more than three cells.

The method of stress inference, reviewed in (Roffay et al. 2021), builds on these correlations between cell shape and cell mechanics to infer mechanical patterns in confluent epithelia. Stress inference calculates the relative pressures and line tensions in an epithelial tissue using measurements of the line curvatures between cells and angles at vertices (**Figure 1.6**). As a technique, it has the advantage of being non-invasive and quite fast, provided that an accurate segmentation of the cell contours can be obtained. It has been used to analyse the development of many epithelial tissues, including the *Drosophila* wing and notum (Ishihara and Sugimura 2012; Guirao et al. 2015).

The correlation between the geometric packing of an epithelium and its mechanical state has been harnessed to develop theoretical models of living tissues, whose aim is to bridge single-cell dynamics and emergent tissue behaviour. In these models, the cell geometric features are linked to mechanical forces, which are balanced in an equilibrium state, or to a surface energy, which we typically assume the tissue has an intrinsic tendency to minimise via cell movements and deformations. Let us

develop one class of multiscale theoretical models, the Cellular Potts Model (CPM) (Graner and Glazier 1992). The CPM is a lattice model, with each point of the lattice being associated to one cell. The transition probabilities between two states of the lattice depend on a Hamiltonian, which specifies the energy of the system. Each cell contributes to this energy function which the tissue aims to minimise. The Hamiltonian is divided into two terms: a surface energy H_S , and a elastic volume energy H_V , so that the total energy of the system is

$$H = H_S + H_V \quad (1.4)$$

The surface energy term integrates the adhesion and cortical tension of a cell. In the description of the Hamiltonian, we use notations from the paper which establishes the CPM (Graner and Glazier 1992). For two neighbouring points M and M' of the 2D lattice, which belong to cells σ_M and $\sigma_{M'}$ respectively, their contribution to H_S is equal to

$$H_{S,(M,M')} = J(\tau(\sigma_M), \tau(\sigma_{M'})) [1 - \delta_{\sigma_M, \sigma_{M'}}] \quad (1.5)$$

where τ is the cell type, which can take several values when considering cell sorting, and J is the energy associated with the pairing. $[1 - \delta_{\sigma_M, \sigma_{M'}}]$ is a term that simply means that the surface energy only considers pairs of adjacent points from different cells. J can be different for distinct cell types, which can allow for the implementation of stronger adhesion between cells of the same type for example. J is an energy per unit of the membrane: for each cell, the total surface energy will increase with the cell perimeter.

For a given cell σ , the elastic volume energy is given by

$$H_{V,\sigma} = \lambda (a(\sigma) - A_{\tau(\sigma)})^2 \quad (1.6)$$

where $a(\sigma)$ is the area of the cell, $A_{\tau(\sigma)}$ is the preferred area of cells of the same type, and λ is a elasticity parameter representing the cost of deviating from one's preferred area. This elastic volume energy is linked to the surface of the cell and is minimised when a cell is its preferred size. In addition to these two energy terms, the CPM can incorporate additional mathematical constraints to model a specific cell behaviour: for example, a cell motile force (Kabla 2012; Doxzen et al. 2013), or cell growth and division (Izaguirre et al. 2004).

As we can see, the geometric packing of the modelled tissue is crucial to the calculation of the energy function that controls the behaviour of the CPM. The

CPM has proven extremely useful to model collective cell behaviours and to elucidate the mechanisms driving epithelial dynamics in many different systems, such as the skeletal development of the avian limb bud (Izaguirre et al. 2004), the emergence of *in vitro* collective migration (Kabla 2012; Doxzen et al. 2013), or the dynamics of rearrangements in the pupal *Drosophila* wing (Bardet et al. 2013).

Although we described the 2D implementation of the CPM, the theory can easily be extended in 3D. Vertex models are another class of models that link the geometry of cells to the mechanical state of a tissue and which can describe 3D tissue dynamics. They were first introduced to study soap films (Weaire and Kermode 1983) and have since been extended to the study of living tissues where cells are tightly packed, such as epithelia (Okuda et al. 2015; Messal et al. 2019; Yang et al. 2021). As the name suggests, a vertex model implements the displacements of cell vertices subject to forces. Cells are modelled as polygons delineated by straight edges or interfaces associated to these vertices.

In 3D, the differential of the work exerted on a vertex v is given by:

$$\delta W_v = \sum_{\sigma} \lambda (V(\sigma) - V_0) \delta V(\sigma) + \sum_k T_k \delta A_k, \quad (1.7)$$

where σ labels the cells connected to vertex v and k the cell interfaces joining at v . λ is a elasticity parameter and T_k a surface tension on interface k . $V(\sigma)$ is the volume of cell σ , whose preferred volume is V_0 , and A_k is the surface area of interface k . Here again, the geometric features of cells are at the core of the tissue behaviour predicted by a vertex model.

Three-dimensional vertex models have been successfully applied to the study of epithelia (Okuda et al. 2015) and have provided important insights into the mechanisms driving complex 3D morphogenetic events. Recently for instance, they have helped to uncover how the geometry of tubular epithelia impacts the formation of tumours (Messal et al. 2019), and how tissue mechanical properties drive intestinal crypt morphogenesis, which is successfully recapitulated in organoids (Yang et al. 2021).

1.2.3.3 Cell geometry dynamics driving tissue morphogenesis

During development, cells can change their morphology under the influence of internal or external factors. As we described in the previous section, cell deformations are associated to changes in their mechanical states. Because adherent cells are me-

chanically coupled, this mechanical information is propagated and shapes the tissue. In this section, we describe how cell geometry changes can drive the large-scale remodelling of a tissue.

A major example of such a geometry change is apical constriction, the reduction in size of the apical surface of a cell. Apical constriction in a cell, if not accompanied by a similar basal constriction, causes a reduction of the local apical-to-basal surface ratio. Coordination of this 3D cell deformation over multiple cells is associated with a modification of local tissue curvature which has been shown to promote morphogenetic processes such as inward bending invagination in many systems (reviewed in [Martin and Goldstein 2014](#)) (**Figure 1.7A**). An example is the fly mesoderm invagination, a biological process driven by apical constrictions which illustrates the crucial role of mechanical cell coupling in the emergence of large-scale bending from cell shape changes. During mesoderm invagination, apical constriction in the ventral blastoderm is associated with the remodelling of intercellular adherens junctions, which move from sub-apical to apical positions ([Kölsch et al. 2007](#)). Adherens junctions also bridge cellular actomyosin fibers into a supracellular actomyosin network which contributes to cell shape changes ([Martin, Gelbart, et al. 2010](#)). Disruption of adherens junctions impairs epithelial integrity and tissue morphogenesis, thereby illustrating how cell-cell junctions integrate cell deformations into global tissue movements. In addition to tissue invagination, apical constriction over a defined region can also drive the formation of tissue folds. An example is the *Drosophila* leg epithelium, of which we give a more detailed description in Section 1.3.3. In this cylinder-shaped tissue, local pulling forces induced by apoptosis are transmitted to the neighbouring cells which elongate and constrict their apices. These apical constrictions are repeated over multiple cells, and this repetition changes local tissue curvature and causes the formation of the leg folds ([Monier et al. 2015](#)).

In addition to size reduction, coordinated cell growth can also contribute to the proper acquisition of shape of developing organs. Although not an epithelium *stricto sensu*, the plant epidermis consists of a layer of tightly packed cells which fulfills the same protective role as an animal outer epithelium. The outer epidermis of the sepal of *Arabidopsis thaliana* is composed of giant polyploid cells, whose average length is 360 μm , surrounded by small 10 μm -long cells. The giant cells regulate the bending of the sepal: inhibiting the giant cell identity results in the formation of sepals that roll inwards, while increasing the occurrence of giant cells causes sepals to roll outwards ([Roeder, Chickarmane, et al. 2010](#); [Roeder, Cunha, et al. 2012](#)). Thus,

the geometric patterning in the plant epidermis controls tissue curvature (**Figure 1.7B**). Heterogeneous growth rates within a tissue can be enough to induce tissue buckling, as was shown in the *Drosophila* wing disc by an elegant work combining *in silico* finite element modelling and experimental measurements. In this tissue, the non-uniform spatio-temporal pattern of growth is sufficient for the initiation of folds, and crucial for their correct positioning; changes of mechanical properties and constraints are then required for the progression of fold morphogenesis (Tozluoğlu et al. 2019).

Morphogenesis is often a very complex sequence of events that requires the coordination of cell geometry dynamics with other cell processes, such as rearrangements, cell loss and proliferation. The *Drosophila* germ-band extension consists in the antero-posterior elongation and dorso-ventral narrowing of the germ-band during gastrulation. Polarised rearrangements and antero-posterior cell elongation are two processes that both contribute to the germ-band extension (**Figure 1.7C**). The extension rate is biphasic, with an initial fast phase followed by a slower phase. Breaking down tissue morphogenesis into the contributions of cell elongation and intercalation shows that during the initial rapid phase, about a third of total tissue extension is driven by cell shape changes. Moreover, in mutants where intercalation is impaired (such as mutants for the gene *krüppel*), the initial extension is preserved by a compensating increase of cell shape changes (Butler et al. 2009). In the posterior germ-band, extension also involves oriented proliferation in addition to rearrangements and geometry changes (da Silva and Vincent 2007).

1.2.4 An example: geometric regulation of cell division

In the previous sections, we saw that changes in the geometry of cells impact the local mechanics of the tissue and, through mechanochemical coupling, can drive global morphogenetic events such as invagination, bending, or extension. Cell deformations can also regulate other cell behaviours that, in turn, control morphogenesis; in particular, the regulation of cell division by cell geometry has been extensively studied and is the focus of this section.

1.2.4.1 Cell shape and the regulation of cleavage orientation

In a dividing cell, the axis of orientation of the mitotic spindle defines the cleavage plane and the positions of the offspring cells. As such, division orientation con-

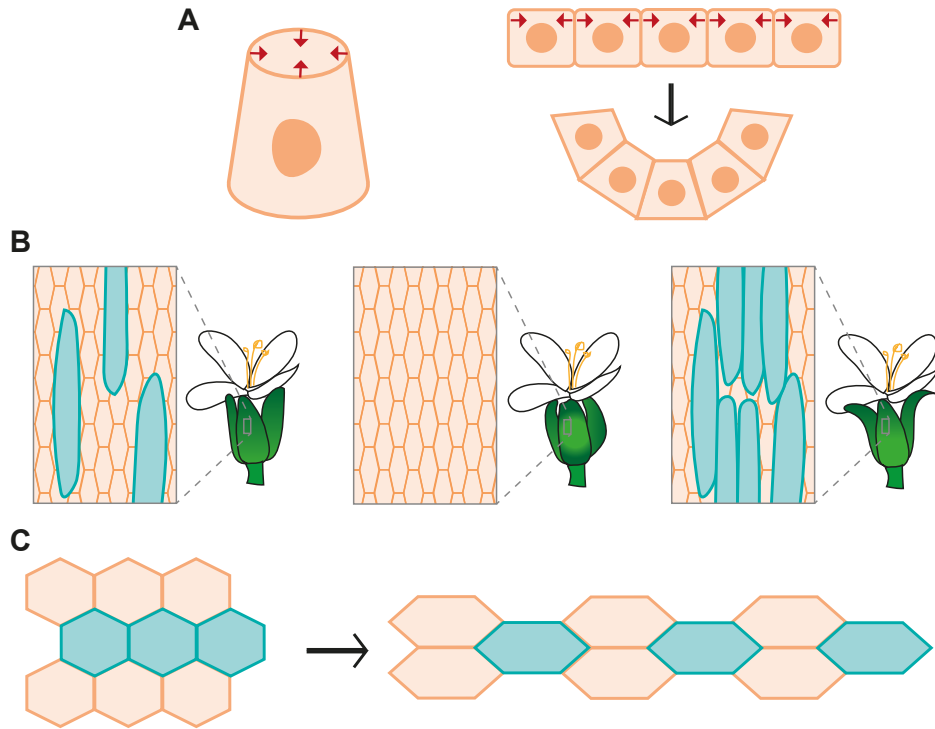


Figure 1.7 *Cell geometry dynamics driving tissue morphogenesis. (A) Apical constriction in a single cell causes a reduction of the apical-to-basal surface ratio (left). Apical constriction of a group of cells drives inward tissue bending (right; lateral view). (B) Cell size distribution in the sepal of *Arabidopsis thaliana* regulates tissue curvature (left: normal sepal, middle: inward-bent sepal, right: outward-rolling sepal). (C) Tissue convergence-extension driven by the coordination of cell rearrangements and cell elongation, akin to the initial extension of *Drosophila* anterior germ-band. Apical view.*

tributes to morphogenesis. In a planar epithelium, cells must divide within the plane of the tissue for their offspring to be fully integrated to the cell sheet and to have proper apical and basal domains. Then, within the plane, the 2D orientation of the division axis is also crucial. As observed more than a century ago, the division axis tends to align with the longest axis of the cell, an observation which became known as Hertwig's rule (named after the German biologist Oscar Hertwig). Cells in a variety of tissues appear to follow Hertwig's rule and to have their anisotropy predict the axis of their division. However, exceptions to this rule have been reported as well, such as some cells in the midline of the developing *Drosophila* notum (Lam et al. 2020).

A study in the *Drosophila* notal epithelium uncovered a mechanism by which cell shape regulates the positioning of the mitotic spindle (Bosveld, Markova, et

al. 2016). This study found that the protein Mud, which recruits the microtubule-associated molecular motor Dynein, is localised at tricellular junctions (TCJs, whose positions are tightly related to both cell shape and cell topology). Mud and Dynein activities control the pulling forces exerted at the tricellular junctions on astral microtubules and by which the mitotic spindle is correctly centered. Because the distribution of TCJs generally aligns well with the cell long axis, TCJs polarity could explain Hertwig's rule in the fly epithelium. Strikingly, in cases where the TCJs distribution and the cell anisotropy predict different division axes, the orientation of TCJs works as a better predictor than the long axis (Bosveld, Markova, et al. 2016). Interestingly, Mud is the *Drosophila* homologue of NuMa which has been linked to the cortical control of spindle positioning in a variety of organisms (reviewed in Morin and Bellaïche 2011).

Later work in the *Xenopus* found a similar role for TCJs in providing geometric cues that orient divisions (Nestor-Bergmann et al. 2019). In this study, the authors dissected and applied a 20%-uniaxial stretch on *Xenopus* cap tissue using PDMS membranes. In cells that elongate, both the TCJs distribution and the axis of division tend to align on the principal axis of stress. But in cells that do not elongate along the direction of stretch, the distribution of TCJs is a better predictor of division orientation than the tissue stress. Cadherin and LGN are enriched at the TCJs and are necessary for spindle orientation in the *Xenopus* cap.

In cells that do not have mature tricellular junctions where Dynein regulators localise, or in cells that fail to orient the spindle along their long axis, tissue tension pattern can provide orientational cues. During segmentation of the *Drosophila* embryo, actomyosin is enriched along supracellular cables at the compartment boundaries which locally generate a tension orthogonal to their axes. The division axis of cells adjacent to the cables aligns with their long axis in very elongated cells; however, in mildly elongated cells, division orientation is set by the local tissue tension which overrides the information of cell shape (Scarpa et al. 2018). In the *Drosophila* notal midline, cells are under little tension and are less efficient at correcting deviations from Hertwig's rule. Increasing Myosin activity, and hence local tissue tension, improves their ability to rotate their spindle towards the long axis; conversely, decreasing Myosin activity or disturbing the mechanical environment of cells using laser ablations decreases further the efficiency of spindle rotation and alignment (Lam et al. 2020).

Overall, division in multicellular tissues is oriented within the tissue plane by ge-

ometric and mechanical cues related to the cell shape. But what about the upstream role of cell geometry in triggering division?

1.2.4.2 Cell size and the decision to divide

During development as well as adult tissue homeostasis, the coordination between cell proliferation and cell loss controls the number of cells and, in contexts of moderate growth, cell density. Dysregulation of this coupling can lead to hyperplasia which is associated with various diseases, including cancers. The specific existence of a coupling between cell cycle progression and cell growth rate to achieve size homeostasis is well established in yeast and bacteria, but remains a controversial, fast-changing field of study in multicellular animals (reviewed with great details in [Cadart 2017](#)). In the section below, we do not address this question; instead, we describe the mechanisms that link cell size or density with proliferation, and whose existence is hinted at by the control of cell number together with cell size in healthy organisms.

In 1978, [Folkman and Moscona](#) set out to test the effect of varying cell shape on DNA synthesis and proliferation. To do so, they seeded endothelial cells on substrates of different adhesiveness, which had the effect of varying cell height and projected area. This experimental set-up revealed the existence of a clear correlation between cell projected area and the tendency to enter into S phase ([Folkman and Moscona 1978](#)). However, it did not allow to distinguish between the effects of cell size and of the substrate composition. This distinction is made possible by the advance in micropatterning techniques, that [C. S. Chen et al.](#) took advantage of in order to vary the projected area of single endothelial cells without changing their cell-ECM contact area or the substrate composition. This work found that DNA synthesis scales with cell spreading independently of the cell-ECM contact surface, suggesting an autonomous control of proliferation via cell geometry ([C. S. Chen et al. 1997](#)). Later work confirmed the correlation between cell area and frequency of entry into S phase, irrespective of cell elongation ([Roca-Cusachs, Alcaraz, et al. 2008](#)).

Tissue culture cells have been known since the 1960s to reduce their growth and proliferation some time after reaching confluence ([Stoker and Rubin 1967](#)). This property is seen in most healthy epithelial cells and has been coined Contact Inhibition of Proliferation (CIP). As the name suggests, contact inhibition of proliferation is believed to be mainly driven by cell-cell contacts. However, an elegant study

established a role for cell density increase in driving CIP (Puliafito et al. 2012). In this study, MDCK cells were seeded in isolated colonies with room to expand. The authors noticed that proliferation was not reduced initially, when the cells formed confluent growing sheets with established cell-cell contacts. This first phase could last several days. Then, in a second phase, the cell density increased rapidly before slowing down; it was in this second phase that the cell proliferation rate would decrease and that CIP would be observed. This shows that cell-cell contacts are not sufficient to trigger CIP, which is rather associated with an increase of cell density. Conversely, reducing cell density promotes cell proliferation: a 1.4-fold stretch of MDCK monolayers on a PDMS membrane is quickly (within 1h) followed by a 5-fold increase in the number of cell divisions (Gudipaty et al. 2017). Altogether, these studies reveal that changes in cell density (and, through it, changes in cell size) modulate the proliferation rate of confluent epithelial tissues. Future work will be needed to characterise the role of static cell size in the control of division, as has been found in single micropatterned cells, and to assess the relevance of this mechanism in the context of *in vivo* morphogenesis.

Perhaps unsurprisingly, the known molecular regulators of proliferation inhibition in dense cell sheets are linked to mechanotransduction. Gudipaty et al. showed that Piezo1 mechanosensitive ion channels are necessary for stretch-induced increase of proliferation (Gudipaty et al. 2017). In mammalian cells, YAP activity is decreased upon reaching confluence, while over-expression of YAP overcomes CIP, indicating a regulation of CIP by the Hippo/YAP pathway (Zhao et al. 2007). Finally, E-cadherin, the core transmembrane protein of adherens junctions and as such a key component of cell-cell contacts, has been repeatedly shown to modulate CIP (see Mendonsa et al. 2018 for a review).

1.3 The mechanics of apoptosis

In the previous sub-chapter, we saw how cell geometry, which is tightly linked to cell and tissue mechanics, impacts epithelial architecture and morphogenesis. Tissue morphogenesis is a complex process that can be described in terms of the single-cell behaviours (rearrangements, proliferation, cell loss, geometry changes) whose spatio-temporal regulation control tissue deformations. We showed that cell geometry, and in particular by cell size, contributes to the regulation of division. The counterpart of division in the control of cell number is cell loss, via either cell death or live-cell

removal. Cell death exists in many forms depending on whether it is physiological or damage-induced, and on the mode of elimination of the cell (Yan et al. 2020). Apoptosis is a prominent type of programmed cell death which plays a key role in the morphogenesis of epithelial tissues. In this sub-chapter, we describe apoptosis, its role in epithelial morphogenesis and its regulation, from a biomechanical point of view.

1.3.1 A short history of apoptosis discovery

Apoptosis was first described in 1842 by the German scientist Karl Vogt, who did not coin the term at the time (Vogt 1842). In his work, Karl Vogt gave the first description of physiological cell death during vertebrate development when he reported the death of notochord cells during toad metamorphosis. Interestingly, this discovery came very early when we consider that only a few years before, Schleiden and Schwann postulated that the cell is the fundamental unit of all living tissues (Schleiden 1838; Schwann 1839).

In the following decades, the field of developmental biology was the first to appreciate the widespread occurrence of cell death in a variety of developmental systems, as described in (Glücksman 1951). Glücksman's seminal work noted that local cell loss can precede tissue shape changes in many organisms. He hypothesised that cell death was a normal part of planned vertebrate development and not simply a by-product of mitosis, as some scientists suggested. This original view later turned out to be a fruitful strand of research (partly detailed in Section 1.3.3).

Glücksman's work came back into light two decades later when the foundational paper of John Kerr, Andrew Wyllie and Alastair Currie described a form of controlled cell deletion that they named "apoptosis", from an Ancient Greek word describing the "falling off" of leaves from trees (Kerr et al. 1972). John Kerr had been studying the morphological cell changes induced by vein ligation in rat livers when he noticed and described "shrinkage necrosis" in both control and ligated tissues (Kerr 1965, Kerr 1971). With Andrew Wyllie and Alastair Currie, they then proposed the concept of apoptosis as an active and programmed form of cell death. They suggested that apoptosis was a general phenomenon likely to play a key role in adult cell turnover (in coordination with proliferation), in embryonic development, as well as in cancer progression.

(Kerr et al. 1972) also gave a description of the morphological changes seen in apoptotic cells: there is visible chromatin condensation and nuclear fragmentation

(which he had noted earlier in [Kerr 1971](#)), followed by the formation of apoptotic bodies later degraded by macrophages. In contrast to necrosis, apoptosis does not elicit a wide-spread inflammatory reaction. Furthermore, in the context of our study, it is interesting to note that apoptosis in epithelial tissues elicits apical or basal cell shrinkage followed by extrusion from the epithelial sheet.

The next breakthrough in the nascent field of apoptosis research was genetic. In 1986, the first genes involved in the control of apoptosis were found with the discovery in *Caenorhabditis elegans* of *ced-3* and *ced-4* ([Ellis and Horvitz 1986](#)). These two genes encode caspases, the effector proteins of apoptosis (the molecular regulation of apoptosis is described in Section 1.3.2). The identification of components of the cell death control machinery earned H. Robert Horvitz a Nobel Prize in Physiology or Medicine in 2002, alongside colleagues Sydney Brenner and John Sulston.

1.3.2 Apoptotic signalling pathways

Since the identification of *ced-3* and *ced-4* in *C. elegans* ([Ellis and Horvitz 1986](#)), the core signalling pathways of apoptosis have been described in great details in various organisms, including *Drosophila* (**Figure 1.8**).

Caspases are proteins whose activation is central in the execution of apoptosis. Upon activation, caspases cleave a number of cellular proteins via proteolytic cascades, ultimately leading to cell death ([Timmer and Salvesen 2007](#)). As such, the control of caspase activity is at the core of apoptotic regulation. There is increasing evidence that the role of caspases is not restricted to apoptosis regulation; non-apoptotic functions of caspases have been described in excellent reviews (see for example [Nakajima and Kuranaga 2017](#); [Colon-Plaza and Su 2022](#)) and are out of the scope of this introduction.

In *Drosophila*, ectopic expression of the DIAPs proteins (Drosophila Inhibitor of Apoptosis) DIAP1 and DIAP2 reduces apoptosis ([Hay et al. 1995](#)). While inhibition of DIAP2 does not amplify apoptosis, as was shown using *diap2* null mutants ([Huh et al. 2007](#)), cell death is strongly activated when DIAP1 is inhibited ([Hay et al. 1995](#), [S. L. Wang et al. 1999](#)). This shows that the DIAP1 protein is a crucial negative regulator of caspase activity in *Drosophila*. DIAP1 activity can be inhibited by the RHG proteins encoded by the genes *reaper*, *hid*, *grim* and *sickle*, resulting in increased apoptosis within hours of RHG expression ([Hay et al. 1995](#); [Lisi et al. 2000](#); [Goyal et al. 2000](#), [Yoo et al. 2002](#)).

Less is known about the regulation of the core apoptotic machinery acting upstream of RHG proteins. This regulation appears to be complex and highly dynamic in space and time, with many different pathways able to trigger developmental apoptosis. We will now present some of these pathways which are of particular interest to the rest of this thesis.

The Hippo pathway, a mechanotransducing pathway we mentioned earlier in Section 1.1.4.3, regulates apoptosis. Inactivation of the gene *hippo* leads to reduced apoptosis and increased levels of DIAP1 (Harvey et al. 2003; Udan et al. 2003; Pantalacci et al. 2003), while overexpression of *hippo* enhances apoptosis and is associated with reduced DIAP1 activity (Udan et al. 2003; Pantalacci et al. 2003). Furthermore, while overexpression of *hid* increases apoptosis, this phenotype is restored by mutation of *hippo* (Udan et al. 2003). The action of Hippo on cell death involves Yki, a downstream target of the Hippo pathway which promotes cell survival and upregulates DIAP1 (Huang et al. 2005).

Notch signalling also impacts cell death by biasing the choice between apoptosis and survival in a variety of contexts. In the developing thoracic central nervous system of the *Drosophila*, neural stem cells undergo asymmetric cell divisions, with one of the daughters sometimes entering apoptosis. Notch activity controls the daughters' "decision" to survive or die, but can act in one direction or the other with the dying cell sometimes being Notch^{ON}, sometimes Notch^{OFF} (Truman et al. 2010, reviewed in Arya and White 2015). Similar binary decisions occur in the *Drosophila* optic lobe neurons. Interestingly, they are modulated by different elements of the central apoptotic pathway: Notch^{ON}-apoptosis depends on *reaper* activity, while the death of Notch^{OFF} neurons is modulated by *hid* (Bertet et al. 2014). Thus, Notch controls cell death in a context-dependent manner via the regulation of RHG proteins.

Another pathway involved in the regulation of developmental cell death is the MAPK/ERK signalling pathway. In the developing fly eye, activation of this pathway promotes cell survival via the downregulation of *hid*, while conversely, downregulation of this pathway upregulates *hid* and increases cell death (Kurada and White 1998; Bergmann, Agapite, et al. 1998), thus indicating the crucial role played by MAPK/ERK in controlling cell death (Bergmann, Tugentman, et al. 2002). Moreover, recent works in cell cultures (Gagliardi et al. 2021) and *Drosophila* dorsal thorax (Valon et al. 2021) showed that epithelial apoptosis triggers the activation of ERK in surrounding cells and that this activation promotes their survival, thus

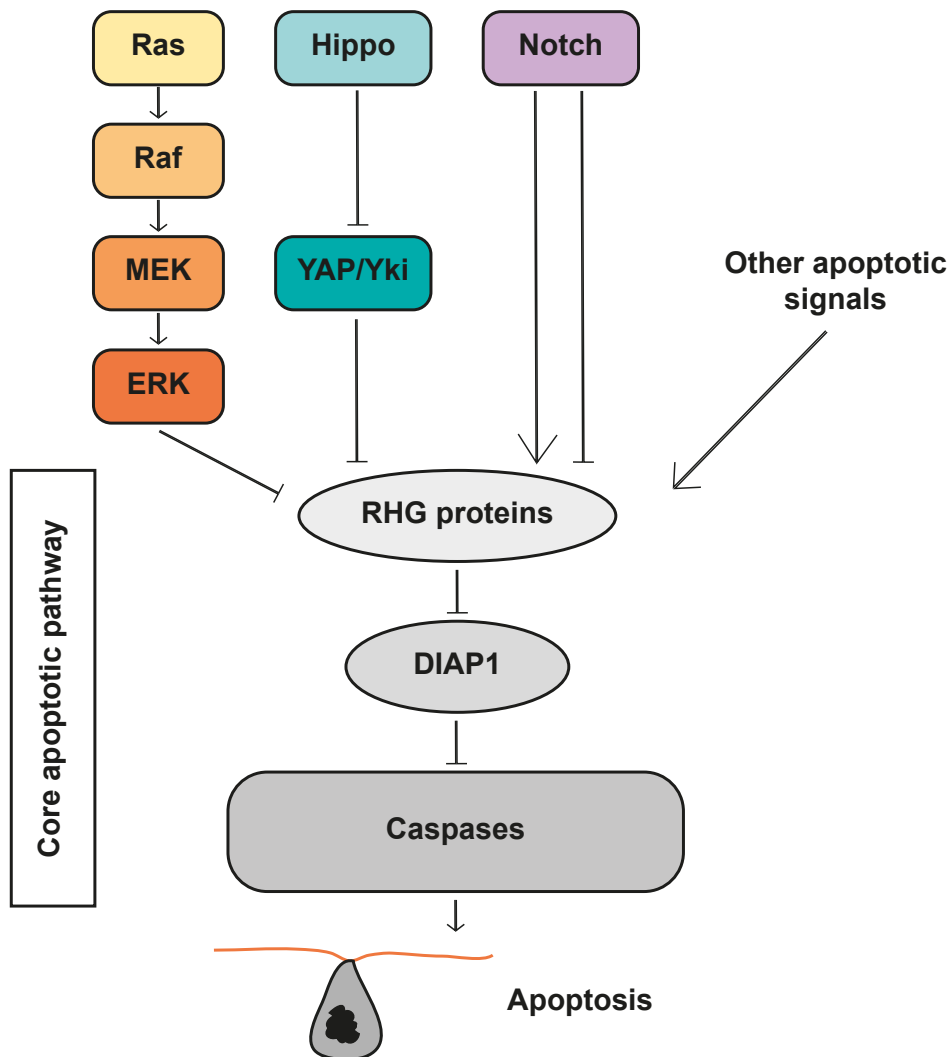


Figure 1.8 *Apoptotic signalling pathways in the Drosophila. See text for a full description.*

providing a mechanism to protect epithelial integrity during apoptosis.

The regulation of the core machinery of apoptosis is complex and of course not limited to these pathways; for example, the PI3-kinase pathway, the Wnt/Wingless pathway or BMP signalling all influence apoptosis in *Drosophila*, as reviewed in (Arya and White 2015).

1.3.3 Apoptosis in the mechanical regulation of morphogenesis

In addition to its coordinated action with proliferation in controlling cell number in adult organisms (Hall et al. 1994), apoptosis has proven instrumental in a variety of morphogenetic processes. Researchers in the late 19th and early 20th centuries found many examples of normal cell death occurring during embryonic development as described in (Glücksmann 1951), which led the author, German-British scientist Alfred Glücksmann, to conclude: "There can be no doubt that cell deaths occur regularly at certain developmental stages of all vertebrate embryos". An old example is the formation of digits in vertebrates (Hernández-Martínez and Covarrubias 2011). The developing limb has initially a more convex shape than the hand we are used to. In this system, developmental apoptosis occurs along a specific inter-digital pattern, thus freeing the digits by removing the tissues between them. This classical example may appear quite in line with a description of apoptosis as a cellular process that removes excess cells. In this section, we will describe other and more surprising morphogenetic roles of apoptosis which demonstrate its impact on the mechanics and dynamics of surrounding tissues.

1.3.3.1 Fusion of cell layers

By eliminating cells at the junction of two epithelial layers, apoptosis can mediate their fusion and remodel tissues. We present two examples: the mammalian palate fusion and the fly dorsal closure.

In mammals, the formation of the secondary palate requires two epithelial shelves to come into contact and fuse. This initial fusion of the shelves forms a transient epithelial seam which is later eliminated (**Figure 1.9A**). The presence of dead cells during palate fusion was described more than 50 years ago, before the term "apoptosis" was even coined (Farbman 1968), but it was not clear what the exact role of cell death was in this morphogenetic process. More recently, Cuervo, Valencia, et al. showed that apoptosis occurs along the entire epithelial seam upon shelves contact (Cuervo, Valencia, et al. 2002). Importantly, they also demonstrated that apoptosis of the seam cells plays a key role in the control of palate fusion, as inhibiting death results in poor fusion whereas amplifying death disturbs the relative timings of apoptosis and shelves contact and increases the risk of cleft palate. Shortly after, the same authors found that degradation of the basal ECM occurs as a consequence

of apoptosis. This process of matrix degradation in response to death, which they called "cataptosis", is especially interesting in that it indicates a role for apoptosis in impacting surrounding tissues (Cuervo and Covarrubias 2004).

Drosophila dorsal closure is another morphogenetic event during which two lateral cell layers migrate towards one another, this time to cover the dorsal side of the fly and the transient amnioserosa. In addition to eliminating the amnioserosa, apoptosis contributes to the good execution of dorsal closure by impacting its dynamics (Toyama et al. 2008): inhibiting apoptosis in the amnioserosa is associated with a reduction of the closure speed, while enhancing apoptosis accelerates dorsal closure. Interestingly, this role of apoptosis during dorsal closure is active and mediated by mechanical forces. Indeed, Toyama et al. showed with laser ablation experiments that apoptosis contributes to a third of the pulling force that the amnioserosa exerts on the migrating leading edge (Figure 1.9B).

1.3.3.2 Creation of folds and complex structures

As we saw from the example of *Drosophila* dorsal closure, apoptosis can lead to the generation of mechanical forces in developing tissues. These forces can control in-plane morphogenetic movements, such as the migration of the dorsal epithelium over the amnioserosa. Epithelial development is, however, not restricted to planar morphogenesis: the formation of complex shapes in the embryo stems from the emergence of robust 3D structures through processes such as folding or bending, implying the existence of out-of-plane forces.

It is only recently that apoptosis has been robustly linked to the induction of out-of-plane forces actively remodeling tissues. The study of the leg folding in *Drosophila* led to the elucidation of the cell mechanisms involved in the generation of an apoptotic folding force. The *Drosophila* leg epithelium is a cylindrical tissue around which folds develop and eventually form the leg joints that separate future leg segments. Joint morphogenesis in the distal leg crucially relies on Notch activity (reviewed in Córdoba and Estella 2020), as well as on the induction of apoptosis in the presumptive joints, an observation made by Manjón et al. who showed that inhibition of apoptosis impairs joint formation (Manjón et al. 2007). Interestingly, later works revealed that apoptosis causes the formation of an apico-basal actomyosin structure (Monier et al. 2015) connected to the nucleus (Ambrosini et al. 2019), akin to a cable inside the apoptotic cell which deforms the apical surface and pulls on neighbouring cells (Figure 1.9C). Cell-autonomous apical deformation is

repeated by frequent apoptoses. This repetition allows the tissue to fold on a large scale as force and cell shape changes (cell elongation and apical constriction) are transmitted via accumulation of cortical Myosin II in the neighbouring cells. Thus, the model of leg joint formation in *Drosophila* demonstrates that apoptotic cells can actively drive tissue remodelling by generating pulling forces.

Since this discovery, similar apico-basal acto-myosin cables were observed in other morphogenetic systems. The invagination of the mesoderm is a key out-of-plane process in *Drosophila* gastrulation. The use of laser ablations and numerical modelling revealed that impairing apico-basal forces prevents mesoderm invagination, highlighting their crucial role in driving mesoderm folding together with apical constriction (Gracia et al. 2019). Recently, it was shown that apoptotic cells similarly drive tissue bending via the formation of apico-basal cables in a vertebrate system: the neural tube closure of birds (chickens and quails) (Roellig et al. 2022). The neural tube is a precursor of the nervous systems in chordates. It starts as a flat neuroepithelium which then bends and closes on itself to form a tube. The observations of Roellig et al. in the bird neuroepithelium reveal that the capacity of apoptotic cells to exert pulling forces via acto-myosin structures is an evolutionary conserved mechanism. Interestingly, inhibiting apoptosis does not fully block avian neural tube morphogenesis, suggesting the existence of additional mechanisms in this system.

1.3.3.3 Regulation of tissue mechanical properties

By generating mechanical forces responsible for tissue deformation, apoptosis demonstrates an ability to alter the mechanical environment of the dying cell. Apoptosis can also affect the mechanical properties of a tissue, as is shown in the example of the fly genitalia rotation.

The *Drosophila* male genital plate, which later gives rise to genital and anal structures, rotates by 360° clockwise during metamorphosis. This dramatic rotation emerges from the added 180°-rotations of two concentric rings of cells (Suzanne et al. 2010) (Figure 1.9D). Interestingly, activation of the pro-apoptotic gene *hid* is required for the execution of genitalia rotation (Abbott and Lengyel 1991), an observation which motivated the investigation of the role of apoptosis during this morphogenetic process. It was found that apoptosis is triggered by the Jun kinase pathway at the boundaries of the motile rings, and that inhibiting apoptosis in any of the rings prevents its rotation (Suzanne et al. 2010). The authors of this

work proposed that local apoptosis could detach the rotating structures from one another, thus increasing the fluidity of their boundary domain and their overall degree of freedom. An alternative hypothesis is that apoptosis-driven forces may actively promote rotation, as we can see during *Drosophila* dorsal closure (Kuranaga et al. 2011). Indeed, changing the rate of apoptosis at the boundary between the concentric rings also impacts genitalia rotation, with an increase in apoptosis being associated to a faster rotation (Kuranaga et al. 2011). Nevertheless, the genitalia plate starts as a cohesive structure in which apoptosis is required for two sub-structures to appear and move relative to one another, indicating a coordinated change in the cohesiveness and local mechanical properties of the tissue.

Applying a hydrodynamic framework to the theoretical study of living tissues can inform us on the impact of apoptosis on tissue mechanical properties. In (Ranft et al. 2010), the authors modelled a tissue of adherent cells as an elastic solid in which cell proliferation and apoptosis actively change local stresses (in particular anisotropic stresses). In addition, divisions align on average with tissue anisotropy. Under these conditions, Ranft et al. show that the anisotropic stress obeys the following equation:

$$\left(1 + \tau \frac{D}{Dt}\right) \tilde{\sigma}_{\alpha\beta} = 2\eta \tilde{\nu}_{\alpha\beta} \quad (1.8)$$

where τ has the dimension of a time, $\frac{D}{Dt}$ is the convected corotational time derivative, $\tilde{\sigma}$ is the anisotropic part of stress, η is the shear viscosity which is proportional to τ , and $\tilde{\nu}$ is the traceless part of the strain rate tensor. Equation 1.8 corresponds to the constitutive equation of a Maxwell model of viscoelasticity, indicating that on large time scales, the tissue behaves as a viscoelastic fluid in which stress decays exponentially. Importantly, the relaxation time τ of the tissue is set by the rate of division k_d and by the rate of apoptosis k_a . Thus, on time scales long compared to cell division and loss, apoptosis can drive the fluidisation of a elastic tissue together with proliferation. It is important to note that highly apoptotic tissues can also display solid-like behaviours, such as the *Drosophila* leg fold in which apoptosis-driven apical stabilisation of Myosin II and F-actin induces an increase in tissue tension and a three-dimensional shape modification (Monier et al. 2015).

1.3.4 Biophysical modulation of apoptosis

Throughout the previous section, we saw that apoptotic cells contribute to the mechanical regulation of epithelial morphogenesis, by generating forces, by impacting

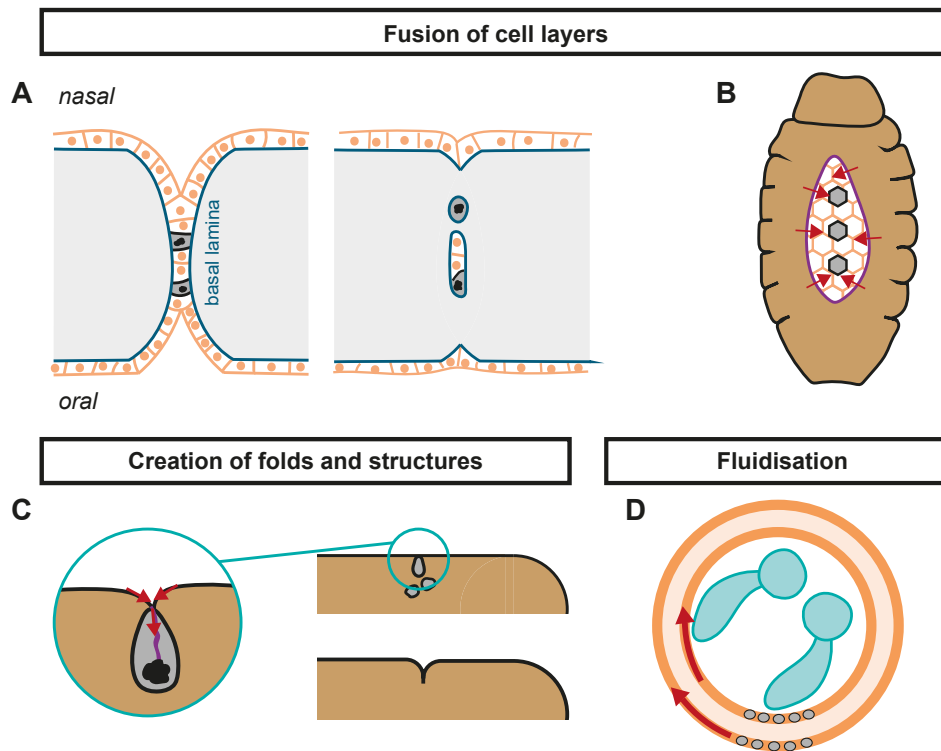


Figure 1.9 *Apoptosis in the mechanical regulation of morphogenesis.* (A) *Mammalian palate fusion.* Dark blue line: basal ECM. Inspired by (Cuervo and Covarrubias 2004). (B) *Drosophila dorsal closure.* Purple line: actomyosin cable. (C) *Drosophila leg folding.* (D) *Drosophila genitalia rotation.* Inspired by (Suzanne et al. 2010).

the extracellular environment such as the basal matrix, and by changing the fluidity and mechanical properties of epithelia. In a symmetrical manner, mechanical factors (and in particular tissue compaction) impact apoptosis.

1.3.4.1 Compaction-driven cell death

Recent works built on the use of perturbative approaches to explore the relationship between mechanical stresses and cell death in epithelial tissues. They revealed a role for tissue compaction in the control of apoptosis.

For instance, Eisenhoffer et al. showed that uniaxial strain reduction of epithelial cell cultures causes an increase in the cell extrusion rate (Eisenhoffer et al. 2012) (Figure 1.10A). In this work, MDCK cells were seeded on a pre-stretched PDMS membrane that was then released, causing a uniaxial compaction of the cell layer by 30%. Compaction caused a transient increase of cell density, from 110 to 150 cells per $(100 \mu\text{m})^2$; however, in approximately 6 hours, cell density was brought

back to pre-compaction levels by an increase in the rate of cell extrusion and subsequent death. This crowding-induced cell extrusion *in vitro* requires sphingosine-1-phosphate (S1P) signalling. The authors proposed that a similar mechanism of compaction-driven death is responsible for the extrusion of cells at zones of high density in the developing zebrafish epidermis, which relies on the stretch-activated channel protein Piezo1.

Local tissue compaction can also trigger *in vitro* epithelial apoptosis. Still in MDCK cell layers, spontaneous cell flows cause the emergence of $+\frac{1}{2}$ and $-\frac{1}{2}$ topological defects (Saw et al. 2017). The $+\frac{1}{2}$ comet-shaped topological defects are associated with local compressive stresses and activation of the mechanosensing Hippo pathway, as well as with a higher frequency of cell extrusion and death (**Figure 1.10B**). Moreover, using micropatterns to induce such comet-shaped topological defects in cell cultures, the authors observed an increase in the number of apoptoses.

These works connect apoptosis to global and local tissue dynamics driving tissue densification in *in vitro* systems. The role of ectopic compaction in inducing cell death was also studied *in vivo* during the morphogenesis of the *Drosophila* notum. The notum is a simple cuboidal epithelium formed by the fusion of two epithelial cell layers at the notum midline, a stripe of highly anisotropic cells which is subject to crowding induced by converging cell flows (Levayer et al. 2016). Around 30% of midline cells extrude during notum morphogenesis (Marinari et al. 2012; Levayer et al. 2016). Upregulating cell growth in the midline (by mutations in the PI3K and Hippo pathways which cause an increase in cell height) leads to a higher extrusion rate; conversely, inhibiting cell growth and causing midline cells to be shorter (via expression of *Tsc1* and *Tsc2*) decreases their extrusion rate (Marinari et al. 2012) (**Figure 1.10C**).

1.3.4.2 Mechanical cell competition

The ability for local increase of tissue crowding to trigger apoptosis is illustrated by the concept of mechanical cell competition. Competition is the context-dependent elimination of one cell population (loser cells) in favour of the expansion of another (winner cells) when the two populations are mixed. Mechanical competition is a form of cell competition driven by mechanical cues which was hypothesised a decade ago (Vincent et al. 2013) on the basis of influential theoretical works (Shraiman 2005; Basan et al. 2009) and of experimental observations of crowding-induced apoptosis

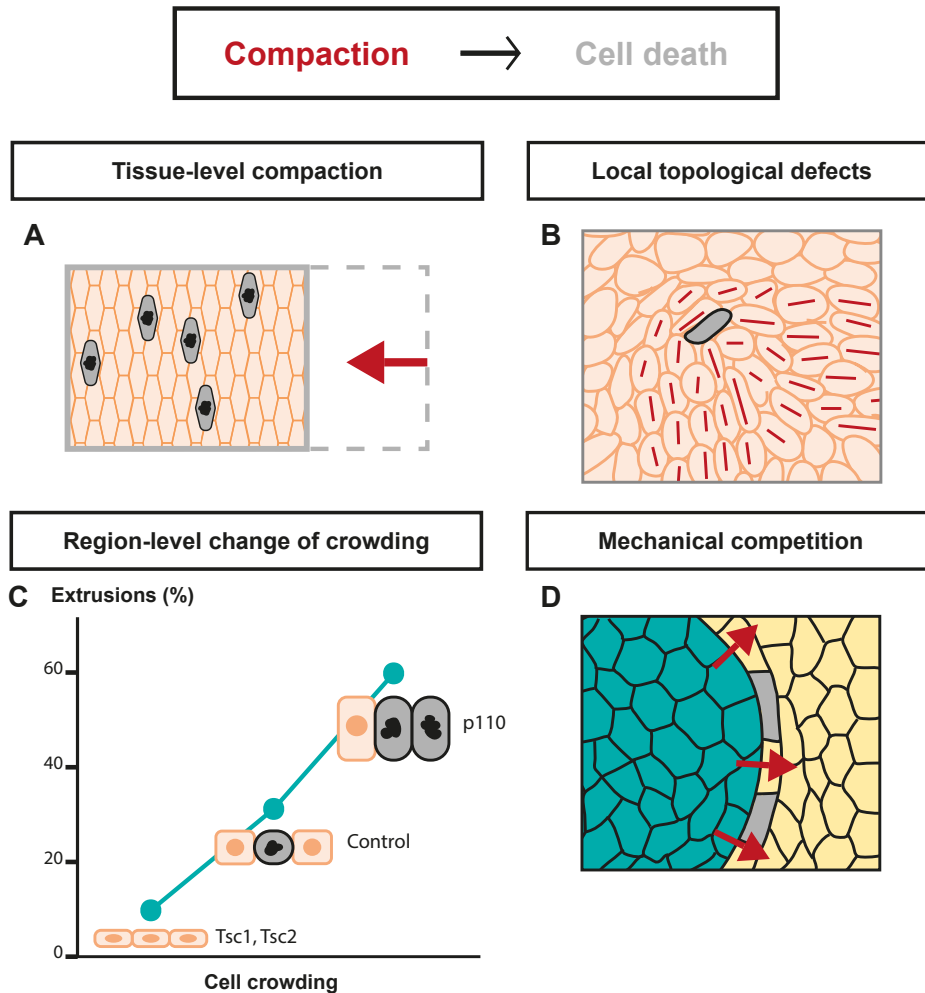


Figure 1.10 *Compaction-induced apoptosis*. (A) Global compaction of *in vitro* epithelial tissues increases the occurrence of apoptosis (Eisenhoffer et al. 2012). (B) Comet-shaped topological defects induce an increase of local tissue compaction that triggers apoptosis (Saw et al. 2017). Red lines: cell orientation. (C) Mutations that change cell growth in the *Drosophila* midline impact the rate of extrusion (Marinari et al. 2012; lateral view of cells). (D) Induction of winner clones in the *Drosophila notal* epithelium leads to the compaction and elimination of neighbouring cells (Levayer et al. 2016).

(Eisenhoffer et al. 2012; Marinari et al. 2012). It is the subject of several great reviews (Brás-Pereira and Moreno 2018; Matamoro-Vidal and Levayer 2019); here, we simply describe experimental evidences of apoptosis driven by mechanical compaction in the context of cell competition.

The phrase "mechanical cell competition" was first coined in an elegant study of *in vitro* cell competition. In MDCK cell cultures, clones of *scrb^{KD}* cells fully surrounded by wild-type cells are compacted, with their density increasing 4.5-fold up to 45 cells per $(100 \mu\text{m})^2$ compared to confluent pure *scrb^{KD}* cultures (Wagstaff et al. 2016). Using stretchable PDMS membranes, Wagstaff et al. found that crowding leads to the activation of the tumor suppressor *p53*. As a result, *scrb^{KD}* cells demonstrate high p53 activity which triggers their death. Interestingly, the authors showed that activating p53 into MDCK cells was sufficient to make them more sensitive to crowding and to induce their elimination when co-cultured with wild-type cells, thus demonstrating the key role of p53 activation in this process of mechanical competition. Later work verified that cell density upregulates apoptosis in *scrb^{KD}* cells (Bove et al. 2017); moreover, the authors found that wild-type cells in contact with *scrb^{KD}* neighbours are more proliferative, thus at this stage it is not known whether this increased proliferation is a cause or consequence of *scrb^{KD}* apoptosis.

A recent non-peer reviewed work also used *scrb^{KD}* MDCK cells co-cultured with wild-type cells to investigate the predictive morphological factors of loser fate in an analytical manner (Soelistyo et al. 2021). In this study, a minimally-supervised machine-learning convolution network was trained to predict cells' fate based on their behaviour over several hours. Strikingly, the model autonomously predicts cell density to be the strongest predictor of cell survival, in accordance with the rules of mechanical cell competition.

The concept of homeostatic pressure illustrates the different sensitivities to crowding between different cell types that could drive competition. The homeostatic pressure of a tissue is the equilibrium pressure at which cell division balances cell death within the tissue. If pressure is higher, apoptosis is triggered and pressure decreases, while if the tissue is under a lower mechanical stress than it can bear, it can continue to proliferate (Basan et al. 2009). If two cell types with different homeostatic pressures are in contact, the one with the lowest homeostatic pressure will recess and ultimately disappear under the pressure induced by the other, more proliferative one.

Mechanical cell competition was also observed *in vivo*. Clonal induction of the

oncogene Ras in the *Drosophila* midline leads to the compaction of the wild-type cells neighbouring the Ras clones, as shown by their reduced apical areas (Levayer et al. 2016) (Figure 1.10D). This compaction is associated with an increase in their apoptosis rate, suggesting a process of mechanical competition. Apoptosis of the compacted neighbour cells requires the local downregulation of the mechanosensitive MAPK/ERK pathway (Moreno et al. 2019) which acts upstream of the proapoptotic gene *hid* (Section 1.3.2).

1.4 Aims and outline of the thesis

Taken together, the works described in Section 1.3.4 highlighted the effect on apoptosis of impacting tissue compaction and changing cell sizes. They raise the following crucial questions: what is the physiological significance of biophysical regulators of apoptosis in developmental tissues? What is the role of cell geometry in triggering and controlling apoptosis? How are the well-characterised apoptotic pathways linked to the biophysical regulation of apoptosis?

In this thesis, I sought to answer these questions by identifying the biophysical determinants of epithelial apoptosis and their interplay with molecular mechanisms. To do so, I used the pupal *Drosophila* notum, a tissue which exhibits a reproducible spatiotemporal pattern of apoptosis. Apoptosis often occurs on short time spans (Glücksmann 1951), in scattered cells, making statistical analyses difficult (Kerr 1971), and can be hard to track over long periods in tissues undergoing complex 3D movements (Roellig et al. 2022). The notum is a relatively flat tissue which allows to track tens of thousands of cells in 2D over more than 20 hours, thus countering these difficulties and providing us with a wealth of data on the geometries, behaviours and fates of cells. I developed image and multi-scale data analysis solutions to characterise the pre-determining factors of apoptosis. We then further investigated the roles of these factors by combining our quantitative techniques with biological experiments. This work is interdisciplinary in essence and involved close collaboration with biologists in the team who performed the experiments: first and foremost Maria Balakireva, as well as Mélanie Gracia, Aude Maugarny-Calès and Floris Bosveld (exact contributions are detailed in each chapter). Our work provides important insights into how *in vivo* apoptosis is tuned in time and space.

The thesis is organised as follows. In Chapter 2, the results I obtained during my PhD are recapitulated in the form of a working paper. Chapter 3 presents a

preliminary study to extend this work in 3D. Finally, Chapter 4 discusses our results and suggests lines for possible future directions.

Chapter 2

Apical cell area controls apoptosis in developing epithelium

Contents

2.1 Contributions	49
2.2 Results	50

2.1 Contributions

Co-contributors:

Maria Balakireva*, Mélanie Gracia, Floris Bosveld, Aude Maugarny-Calès, Jesús López-Gay, Isabelle Gaugué, Lucas Sancéré, Cyril Kana-Tepakbong, Stéphane Rigaud, Boris Guirao[◊] & Yohanns Bellaïche[◊].

I developed methods and scripts for data analysis, designed the prediction model and analysed the data. Maria Balakireva* contributed equally to this work by performing experiments, correcting movie segmentations and generally participating in the design of the project. Mélanie Gracia set up and performed the compression experiments. Floris Bosveld and Aude Maugarny-Calès contributed several movies, in particular the *cycE^{OE}* and *trbl^{OE}* mutants. Floris Bosveld also quantified His2B:RFP movies. Jesús López-Gay contributed images of Ban-GFP and Diap1-GFP as well as *jub^{RNAi}* and *actn^{RNAi}* movies. Isabelle Gaugué made the ERK-KTR reporter. Lucas Sancéré, Cyril Kana-Tepakbong and Stéphane Rigaud developed and performed the denoising, enhancement, projection and segmentation of several movies. Stéphane

Rigaud and Boris Guirao developed the computational tools to track cells and locate extrusions and divisions. Boris Guirao[◇] & Yohanns Bellaïche[◇] contributed equally to this work by conceiving and supervising the project. Maria Balakireva, Boris Guirao, Yohanns Bellaïche and I wrote the manuscript. I made the figures, except for **Figure S5** which was made by Maria Balakireva.

2.2 Results

Results are described in the following manuscript.

Apical cell area controls apoptosis in developing epithelium

Victoire M. L. Cachoux*, Maria Balakireva*, Mélanie Gracia, Floris Bosveld, Aude Maugarny-Calès, Jesús M. López-Gay, Isabelle Gaugue, Lucas Sancéré, Cyril Kana-Tepakbong, Stéphane U. Rigaud, Boris Guirao[†] and Yohanns Bellaïche[†]

*[†] These authors contributed equally to this work.

ABSTRACT:

During development and homeostasis, cell apoptosis plays a crucial role in regulating cells number and tissue architecture. While the molecular pathways triggering apoptosis are well understood, how biophysical factors modulate apoptosis remains far less understood. Here, we used time-lapse microscopy of developing *Drosophila* epithelium and quantitative characterization of cell and tissue behaviors to study how apoptosis is controlled during epithelial tissue development. We find that early in their lives and well before their extrusion, future apoptotic cells are characterized by two distinct geometrical features: (i) a smaller absolute apical area; (ii) a smaller relative apical area with respect to their direct neighbors. By modulating the absolute apical area using genetics and mechanical approaches, we show that decreasing cell apical size leads to increased cell apoptosis. We found that the link between cell apical area and apoptosis is mediated by the Hippo pathway. Interestingly, we then found that the regulation by relative cell area is mediated by Notch whose inhibition is enough to reduce the preferential death of cells with smaller relative area and leads to clusters of apoptotic cells. Overall, by uncovering fundamental links between cell geometry and apoptosis, our work improves our understanding of the regulation of cell number and tissue architecture in a living tissue and introduces the concept of geometric cell competition.

INTRODUCTION

In living organisms, the number of cells is regulated by the balance between cell proliferation and cell loss. The acquisition of shape and size of developing organisms, as well as adult tissue homeostasis, rely on this crucial regulation (Ansari & Hall, 1992). In epithelial tissues, aberrant cell proliferation can drive tumor growth (Foster, 2000) while excessive cell death can jeopardize the barrier integrity (Valon et al., 2021).

Programmed cell death, or apoptosis, is a physiological and orderly process driving cell loss. In addition to regulating cell number, apoptosis plays a variety of morphogenetic roles during development. Indeed, apoptotic extrusion in epithelia is a phenomenon that actively engages both the apoptotic cell and its direct surroundings (Rosenblatt et al., 2001; Kuipers et al., 2014); as such, this cellular event can generate forces, cell rearrangements or deformations that remodel the apoptotic cell's environment. By doing so,

apoptosis can contribute to fusing cell layers (e.g., fly dorsal closure (Toyama et al., 2008) or the mouse palate (Cuervo et al., 2002)), creating folds and structures in developing tissues (e.g., *Drosophila* leg folding (Monier et al., 2015) or mammalian interdigit space, reviewed in (Hernández-Martínez & Covarrubias, 2011)), driving dynamic processes such as fly genitalia rotation (Suzanne et al., 2010), or fluidifying tissues (Ranft et al., 2010). The signaling pathways that regulate developmental apoptosis have been extensively characterized (Arya & White, 2015). Moreover, recent works suggested that epithelial apoptosis could arise from biophysical regulations linked to tissue crowding and resulting stresses, such as topological defects (Saw et al., 2017), cell density (Eisenhoffer et al., 2012), or tissue compaction (Marinari et al., 2012; Levayer et al., 2016; Moreno et al., 2019). However, these regulations have not explained the spatiotemporal patterning of *in vivo* apoptosis during development. More generally, how biophysical factors control apoptosis to regulate the growth, morphogenesis and homeostasis of tissues remains largely unknown.

To identify the biophysical factors controlling epithelial apoptosis *in vivo*, we studied the *Drosophila* pupal dorsal thorax, or notum, from 15 hours After Pupa Formation (hAPF) to approximately 35 hAPF. This time window covers a substantial part of the notum morphogenesis (Bosveld et al., 2012; Guirao et al., 2015), which is formed around 6 hAPF by the fusion of the two wing discs during thorax closure (Martín-Blanco et al., 2000). The two monolayered epithelial discs fuse at the dorsal notum midline, a highly-apoptotic stripe of cells along the antero-posterior axis of the notum. The study of the notum midline has provided a valuable model to explore the link between compression and apoptosis (Marinari et al., 2012; Levayer et al., 2016; Moreno et al., 2019). However, the midline is a restricted region of the notum whose cells express apoptotic factors at 15 hAPF (Fujisawa et al., 2019) prior to any morphogenetic movements or tissue deformations. Therefore, midline cells stand out among the other notum cells, which do not exhibit such a systematic apoptotic activity (Bosveld et al., 2012; Guirao et al., 2015). This calls for the study in a more general context, at the scale of the whole tissue, of the biophysical factors controlling life and death decisions.

Here, by combining time-lapse imaging of the developing notum with cell tracking, we characterized the spatiotemporal pattern of apoptosis in this tissue. By quantitatively analyzing the life-long behavior of future apoptotic cells, we found that long before their extrusion, these cells are characterized by two key geometric features related to cell apical area: a small apical area, and a small relative area compared to their neighbors. These distinct features are sufficient to globally predict the tissue-scale apoptotic pattern. We then studied each of these size features and identified molecular pathways involved in their respective regulations of apoptosis; in doing so, we also uncovered a novel interplay between proliferation and apoptosis.

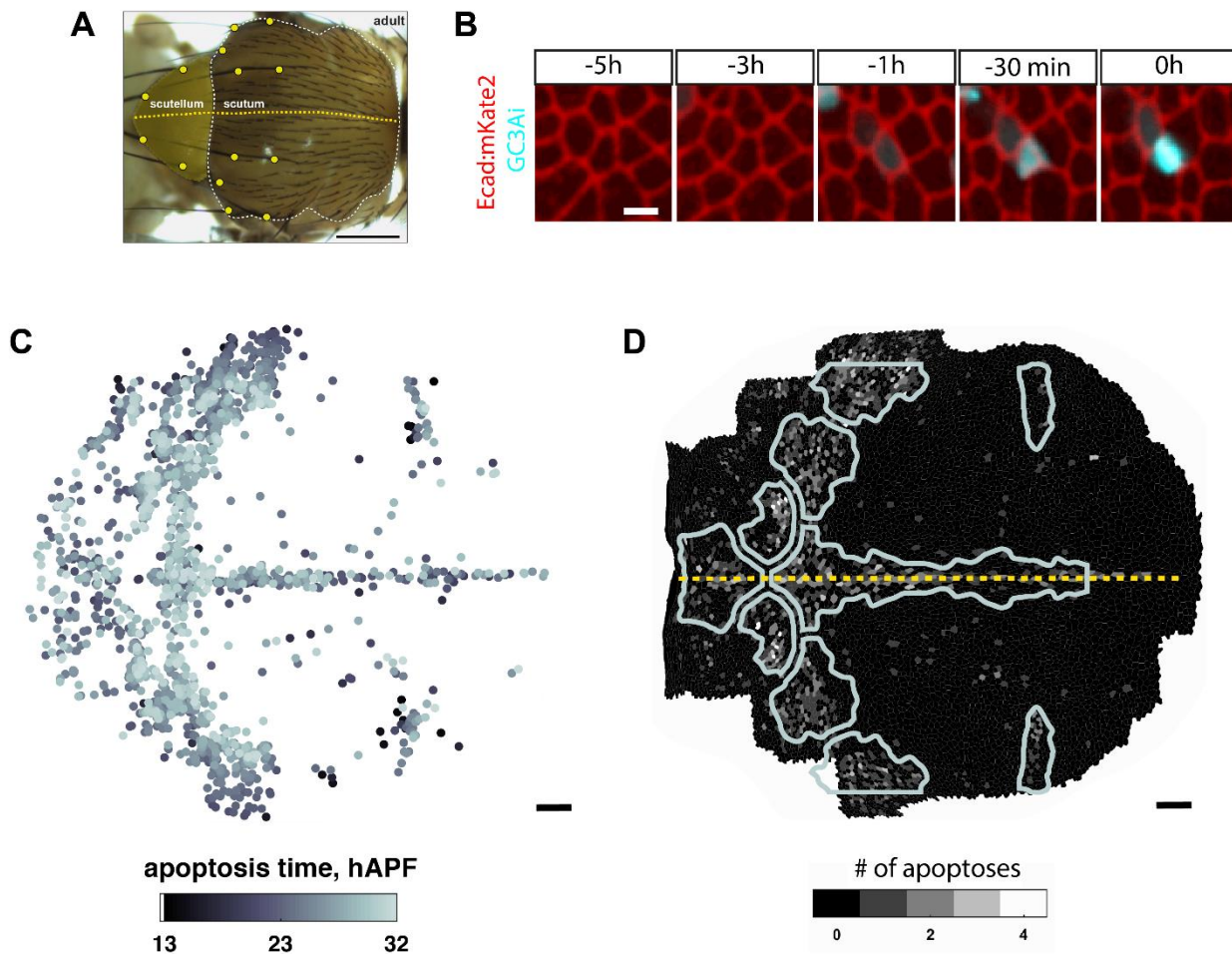


Figure 1. Spatiotemporal patterns of apoptosis in the *Drosophila* notum.

(A) *Drosophila* adult notum. Yellow dotted line: midline, yellow dots: macrochaetes. (B) Tracking of a representative apoptotic cell in a notum expressing Ecad:mKate2 and the GC3Ai caspase fluorescence reporter. Scale bar: 5 μ m. (C) Spatiotemporal distribution of apoptoses in a representative notum (see **Figure S1**). Dots indicate the last cell position for apoptoses occurring between 13h and 32 hAPF, color-coded according to their time of extrusion. Scale bar: 50 μ m. (D) Notum shown in (C), segmented, at 15 hAPF. Cells are color-coded according to the number of apoptoses in their progeny (black: no apoptosis, white: 4 and more apoptoses). Thick grey lines indicate the apoptosis pattern, which are regions with a higher apoptotic density. Yellow dotted line: midline. Scale bar: 50 μ m.

RESULTS

Characterization of the spatiotemporal pattern of apoptosis in the *Drosophila* notum

Past studies of apoptosis in the mono-layered *Drosophila* notum often analyzed a specific and highly apoptotic region of the tissue, the midline (**Figure 1A**). We have previously developed befitting tools that allow us to explore cell extrusion at the scale of a full epithelial tissue: we first labelled E-Cadherin with a fluorescent marker, then segmented the cells using deep neural networks and validation by manual corrections (Schmidt et al., 2018; di Pietro et al., 2021), in order to track them through time (Guirao et al.,

2015). This ultimately gave us access to large datasets of several tens of thousands of cells' positions and behaviors which we can relate to their contribution to morphogenesis. In particular, we can quantify the cell processes happening during morphogenesis, including cell extrusions (Guirao et al., 2015).

Extruding cells could be either alive, which would not rule out their later death, or apoptotic (Marinari et al., 2012). To characterize the nature of extruding cells in the entire notum, we performed time-lapse imaging with the E-Cadherin:mKate marker of adherens junctions and GC3Ai, a live caspase-activated fluorescent reporter (Schott et al., 2017). Caspases are proteases whose activation prompts the apoptotic cell to break into fragments later eliminated from the organism (Li & Yuan, 2008). Across the entire notum, we found that a sudden burst of caspase activity precedes cell extrusions (n=96 out of 100 cells in N=3 nota) (Figure 1B). In addition, we verified that extruded cells show chromatin condensation, indicative of late apoptosis (n=65 out of 65 cells, measured using His2B:RFP; data not shown). These data argue that most (at least 96%) of the extrusions in the *Drosophila* notum between 15 and 35 hAPF are apoptotic events.

To characterize the spatiotemporal pattern of apoptosis, we mapped apoptoses in the whole pupal notum between 15 and 32 hAPF. We found that apoptoses occur following a heterogeneous spatial pattern, with some regions being highly-apoptotic while others display nearly no cell death during this time window (Figure 1C). Using spatial landmarks on the notum (several macrochaetes and the midline), we verified that the spatial distribution of apoptoses is highly reproducible between animals (Figure S1). It is also strikingly symmetric with respect to the midline, even in a single animal (Figure 1C). These observations strongly suggest a spatial regulation, thereby ruling out the hypothesis of apoptoses randomly occurring in the tissue. Thus, we created an archetypal mask of apoptotic regions using the data from 5 half-nota (Figure 1D), that we later refer to as the “apoptotic pattern” versus “non-apoptotic regions” of the notum. This apoptotic pattern contains $77\% \pm 8.8\%$ (N=5 half-nota) of all apoptoses occurring between 15h and 30 hAPF, as well as non-apoptotic cells. Moreover, the temporal distribution of apoptosis is also reproducible (data from individual animals not shown; see Figure 6C for an average). Overall, these observations raise the question of how apoptosis is spatiotemporally regulated.

To identify the mechanisms driving this spatiotemporal regulation, we would like to determine whether the life-long behaviors of apoptotic cells display stereotypical features that could control the genesis of the apoptotic pattern. The last hour of life of apoptotic cells is characterized by major morphological changes, including the shrinkage of the cell apex, and by a burst of GC3Ai signal (Figure 1B). Therefore, to identify possible pre-determining factors of apoptosis, we studied future apoptotic cells prior to this last hour, during what we will refer to as the “pre-extrusion” phase of their lives. Our image analysis tools allow us to track future apoptotic cells throughout their lives and consequently to provide a description of their very early behavior, before they exhibit any known biological sign of apoptosis.

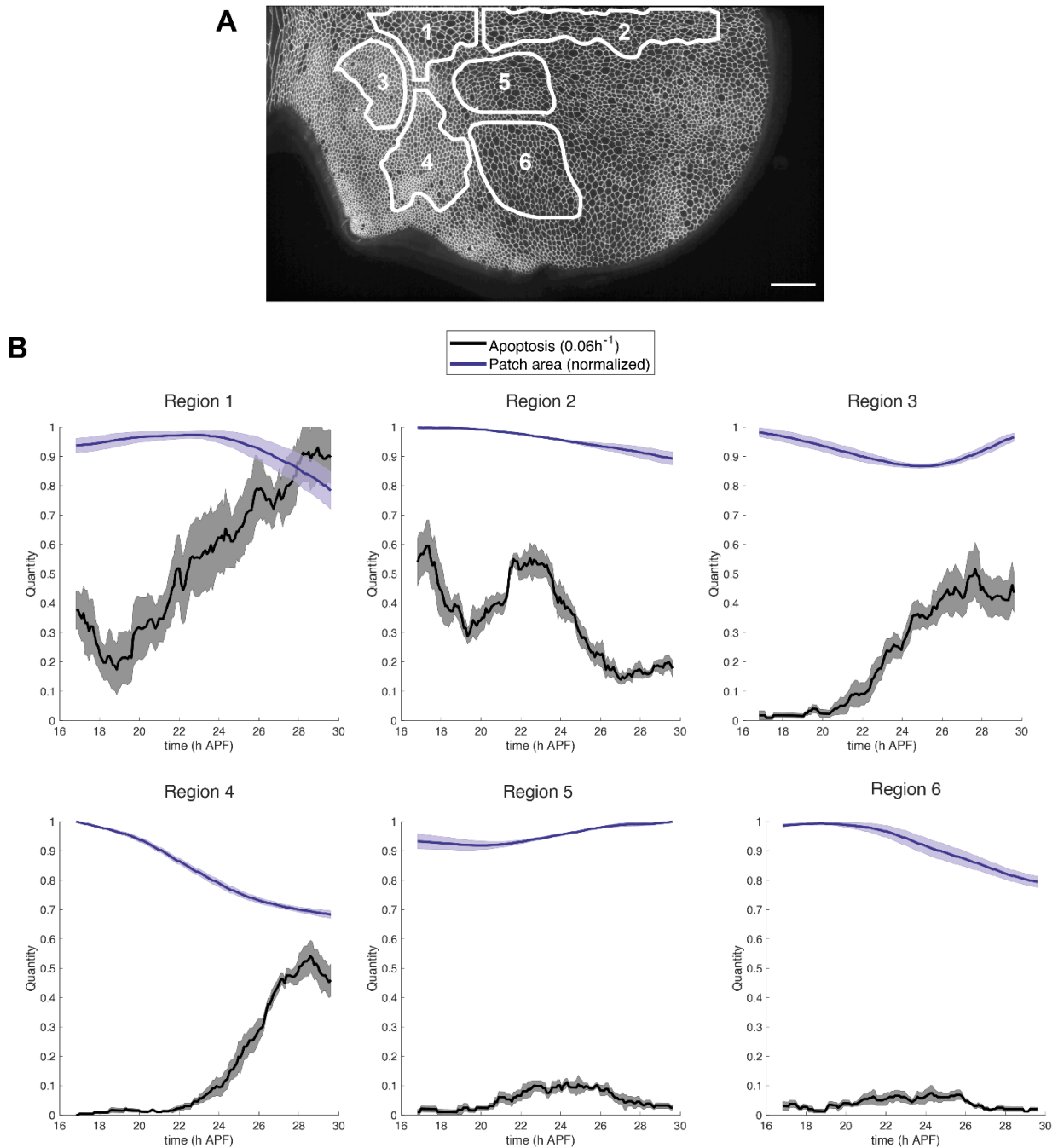


Figure 2. Relative timings of tissue compaction and apoptosis.

(A) Notum expressing Ecad:GFP at 17h30 APF. Thick white lines indicate the six regions in the tissue which are tracked over time. Scale bar: 50 μm . (B) Time evolution of the rate of apoptosis (black, mean \pm SEM) and the region surface area, normalized to its maximum value (blue, mean \pm SEM), in each of the six regions indicated in (A). A decrease in the region area (ex: region 2) indicates compaction, while an increase (ex: region 5) indicates extension. N=4 half-nota.

Early cell geometric features are predictive of apoptosis

During the fly metamorphosis, the notum undergoes tissue deformations, that can be characterized as a combination of isotropic contraction-expansion and anisotropic convergence-extension, and that can substantially vary over space and time (Guirao et al., 2015). Recent works linked tissue compression to cell

extrusion in a variety of systems, such as cell cultures, developing zebrafish epidermis and the surroundings of tumor cells (Eisenhoffer et al., 2012; Marinari et al., 2012; Levayer et al., 2016; Saw et al., 2017; Moreno et al., 2019). In order to explore whether the apoptotic pattern in the notum could stem from isotropic contraction, we studied the relative timings of mesoscopic tissue contraction and apoptosis in various regions of the notum. To study tissue deformation and its possible link with apoptosis, we tracked patches of cells corresponding to regions of interest over time and quantified their respective area variation (Figure 2A). A cell patch with decreasing area indicates patch contraction, whereas a patch with an increasing area indicates expansion. We found a wide variety of behaviors in the notum: while posterior lateral regions exhibit tissue contraction followed by cell apoptosis (regions 3-4, Figure 2B), other regions such as the central lateral zone exhibit contractions of similar magnitude without subsequent cell death (region 6, Figure 2B). Moreover, apoptosis sometimes precedes tissue contraction, as seen in the midline (regions 1-2, Figure 2B). Overall, tissue contraction does not always precede apoptosis, suggesting that tissue physiological contraction by itself cannot explain the apoptosis pattern observed in the developing notum.

Cell apical area is directly impacted by mechanical tissue deformations. It is also a read-out for some of their mechanical properties, such as cell stiffness in confluent cultures (Nehls et al., 2019). We hypothesized that the apical size of cells could play a role in the control of physiological apoptosis in the developing notum. To explore this role, we focused on cell apical size during the pre-extrusion phase.

First, we studied the autonomous role of individual cell apical area (Figure 3A). To do so, we quantified the apical area of apoptotic and non-apoptotic cells throughout their lives on segmented movies. We found that the apical areas of apoptotic cells, averaged over the pre-extrusion phase, is significantly smaller than the average notum cell area taken at the same time points (0.62-fold change, $p < 5 \times 10^{-4}$, Student's t-test, Figure 3B). Moreover, the distribution of their areas is more skewed towards small sizes. This suggests that smaller cells could be more likely to undergo apoptosis. We therefore quantified the probability of a cell to die as a function of its apical area and accordingly, we found that the probability of becoming apoptotic sharply increases with decreasing apical area (Figure 3C). Moreover, when we followed cells from their division to their death, we found that on average, apoptotic cells steadily shrink throughout their pre-extrusion phase, in sharp contrast with non-apoptotic cells whose apical area rather increases or remains constant after their birth (Figure 3D). Among future apoptotic cells, smaller cells have shorter lives (Figure 3D). These distinct behaviors, characterized by different size dynamics, can be observed as early as 1h after cell birth. Overall, during their pre-extrusion phase, future apoptotic cells are characterized by a smaller apical area that keeps decreasing.

To check whether a smaller cell area would be a consequence of apoptotic signaling, we then performed the simultaneous and local inhibition of the *rpr*, *hid* and *grim* genes (RHG) which promote apoptosis in *Drosophila* by clonally expressing *miRHG* (Figure S2A). To compare cell size in *miRHG* and wild-type (*wt*) cells despite the substantial cell size heterogeneity in the notum, we measured the apical area

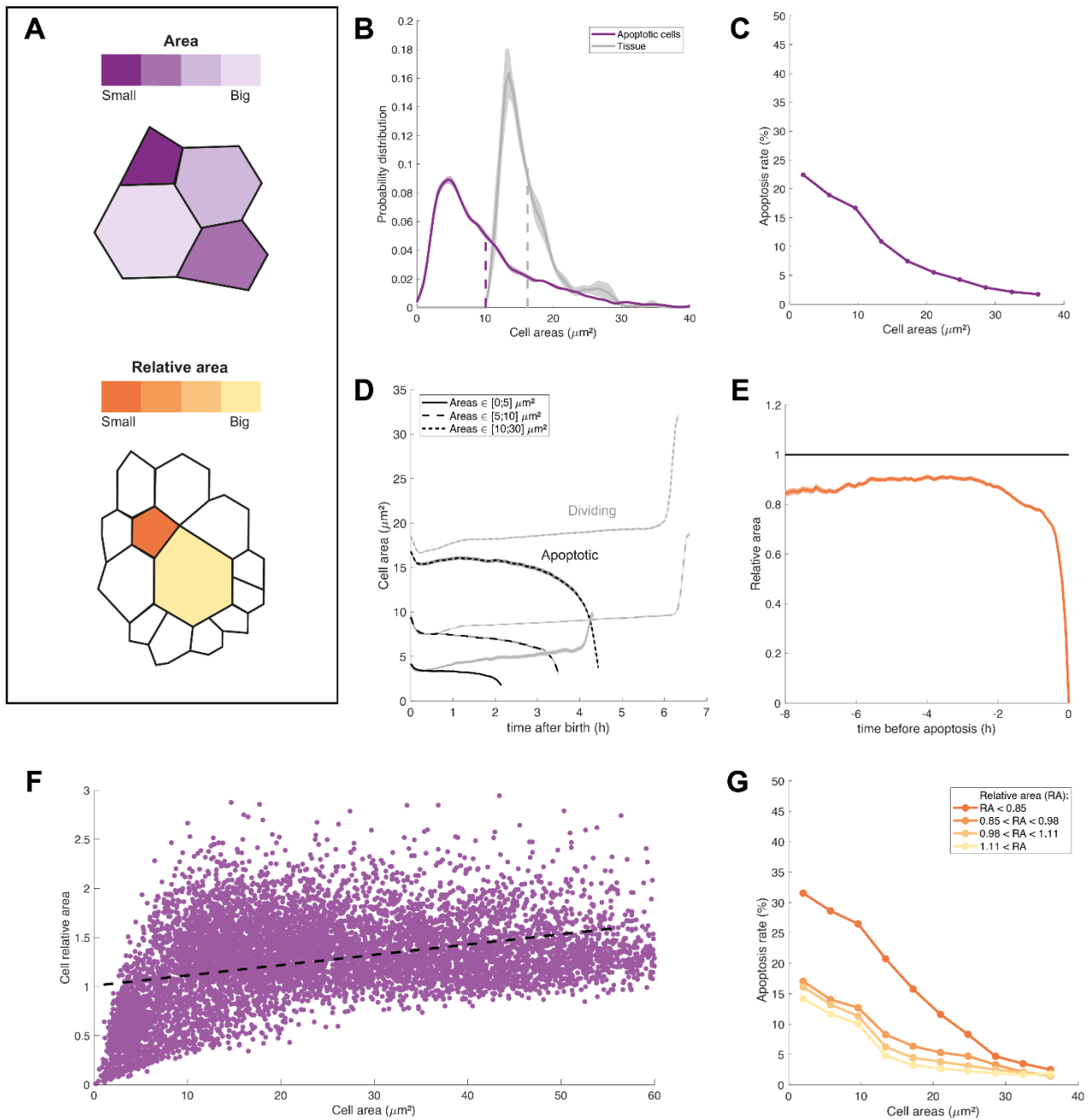


Figure 3. Apoptotic cells display early specific geometric features.

(A) Sketch of two geometric characteristics of cells: their absolute apical area (top) and their relative apical area (bottom). (B) Distribution of the mean apical areas of future apoptotic cells, averaged over their pre-extrusion phase (purple, mean \pm SEM), and average apical size of all cells of the tissue (grey, mean \pm SEM). For each time point where an apoptotic cell was detected, the region average is calculated by averaging the apical sizes of all the cells present in the tissue at the same time point. $n=4244$ cells from $N=4$ half-nota. Curves are smoothed over 3 data points. The area below each curve is one. (C) Probability to undergo apoptosis versus cell apical area. Cells whose fate is known are binned depending on their apical area (averaged over their lives minus the last hour), and the fraction of apoptotic cells is computed for each bin. The curve is then smoothed over 3 points. $n=32638$ cells from $N=4$ half-nota. (D) Average time-evolution of cell apical area after their birth, for cells of different fate (black: future apoptosis, grey: future division, mean \pm SEM). Cells are binned depending on their average apical area in the first hour after their birth (solid line: $0-5 \mu\text{m}^2$, $n = 1326$ apoptoses and 513 divisions; dashed line: $5-10 \mu\text{m}^2$, $n = 1308$ apoptoses and 2798 divisions; dotted line: $10-30 \mu\text{m}^2$, $n = 1201$ apoptoses and 7648 divisions). Then, cells are aligned on both their time of birth (left) and time of disappearance (right). The end of the resulting average curve is aligned to the average life duration of cells in the bin. $N=4$ half-nota. (\rightarrow)

(Figure 3 continued) (E) Relative apical area of apoptotic cells versus time before their death (mean \pm SEM). A relative area below 1 indicates a cell that is smaller than its direct neighbors. Cells are aligned to their time of apoptosis (right side of the graph). $n=4465$ cells from $N=4$ half-nota. (F) Relative apical area versus absolute apical area, both quantities averaged over their lives minus the last hour. Each dot represents a cell. Dashed black line: linear fitting, $y = 1.01 + 0.011x$, $R^2 = 0.15$. $n=8460$ cells from $N=4$ half-nota. (G) Probability to undergo apoptosis versus cell apical area (x-axis), depending on the relative apical area of cells (color-code). Notum cells whose fate is known between 15 and 29 hAPF are binned depending on their size and relative size (averaged over their lives prior to the last hour), and the rate of apoptotic cells is computed for each bin. Each curve is then smoothed over 3 points. $n=32638$ cells from $N=4$ half-nota.

of cells in *miRHG* clones and compared them to the corresponding wild-type (*wt*) cells located symmetrically with respect to the midline, in the same animal (Figure S2B). We found that inhibiting the RHG genes has only a very modest effect on cell apical area throughout tissue development (Figure S2C). This indicates that the small apical area of future apoptotic cells can be a predictive factor of cell apoptosis rather than a consequence of the expression of the RHG genes.

The notum displays several regions inside which cell area is locally quite homogeneous (Figure S3A-B). As a result, in the hypothesis of a regulation of cell death by apical area, entire regions of small cells could be primed to commit apoptosis, thereby potentially compromising epithelium integrity and its crucial role of barrier (Valon et al., 2021). Yet, apoptosis remains a relatively rare event that is not triggered in groups of multiple adjacent cells (Valon et al., 2021). We thus decided to investigate whether additional features could help distinguish a future apoptotic cell within its local environment. To do so, we investigated the role of the relative apical area (defined as $\mathcal{R}(A) = A_i / \langle A_j \rangle$, namely the apical area of a cell i divided by the average area of its direct neighbors j , a dimensionless metrics such that $\mathcal{R}(A) < 1$ if a cell apex is smaller than its neighbors) (Figure 3A). Strikingly, we found that future apoptotic cells are characterized by a small relative apical area (about 10-15% smaller than their neighbors) (Figure 3E). This observation holds true from their births; notably, on average, apoptotic cells are smaller than their immediate neighbors several hours before the extrusion phase.

As expected, given the ordered patterning of cell size in the tissue and the existence of large regions made up of cells with similar sizes, the absolute and relative apical areas are poorly correlated, suggesting that each quantity can carry different information (Figure 3F: linear regression, $R^2 = 0.15$). To evaluate the relative impacts of these two parameters on apoptosis, we used a multivariate logistic regression (Table 1) that models the probability to die as a function of these factors. Importantly, we found that both the absolute and relative areas significantly and independently correlate with the probability to undergo apoptosis ($p < 5 \times 10^{-4}$ in both cases), therefore arguing for distinct roles of these two parameters. This is confirmed when we plot the variation of the probability to undergo apoptosis as a function of both parameters: at areas below $30 \mu\text{m}^2$ (a threshold over which cells hardly enter apoptosis), we found that, for a given apical size, cells that are surrounded by neighbors that are substantially bigger have a higher probability to die than cells that

are surrounded by neighbors of similar size, or smaller (Figure 3G). Overall, we identified two distinct and early characteristics of future apoptotic cells.

	Estimate	Standard error	z	p-Value
Intercept	1.01	0.105	9.65	$< 5 \times 10^{-4}$ **
Absolute area	-0.104	0.003	-30.9	$< 5 \times 10^{-4}$ **
Relative area	-1.91	0.126	-15.1	$< 5 \times 10^{-4}$ **
R ²	0.172	No. obs	30 034	

Table 1. Multivariate logistic regression, Apoptosis ~ Absolute area + Relative area. ** p<0.01.

To evaluate to what extent cell apical size is sufficient to explain the spatial pattern of apoptosis, we developed a prediction model trained on experimental data. The training dataset consisted in the fate, absolute and relative apical areas (averaged over their lives minus the last hour) of cells from 7 half-nota; cells were then binned in clusters of 100 cells. The model then takes the absolute and relative areas of cells in the predicting dataset, assigns them to the nearest cluster and returns the apoptosis rate of the corresponding cluster. The model's F1-score is 0.56, versus 0.19 for a fully random model. Interestingly, we found that this model is successful in recapitulating and predicting most of the coarse-grained apoptosis pattern (Figure 4A-E). Notably, only few apoptoses are predicted in the highly-apoptotic anterior midline, indicating that midline cells are likely to follow a different apoptotic regulation compared to the rest of the tissue. This is consistent with their specific and systematic expression of apoptotic factors early in development (Fujisawa et al., 2019). Overall, we show that apical size characteristics alone can globally predict the distribution of apoptosis at the tissue scale.

Cell apical area modulates apoptosis

Our results indicate that future apoptotic cells are characterized by two distinct, predictive and early size features: a small apical area, and a small relative apical area. We next investigated the regulation of apoptosis by the first of these two parameters, the apical area.

To test the impact of apical area on apoptosis, we used stretchable PDMS membranes to exert uniaxial compaction by 20% along the medio-lateral axis on developing nota at ~15 hAPF. The uniaxial compaction was applied within 30 mins, then we studied tissue dynamics between 18 and 32 hAPF (Figure 5A). We focused on the posterior scutellum region of the notum, where a substantial part of apoptoses occur. In this region, cells after compaction are on average 21% apically smaller than in non-compressed tissues (Figure 5B). The uniaxial compaction resulted in a homogeneous cell size reduction over the region (data not shown). With our size-based prediction model, we predicted that this size change would be

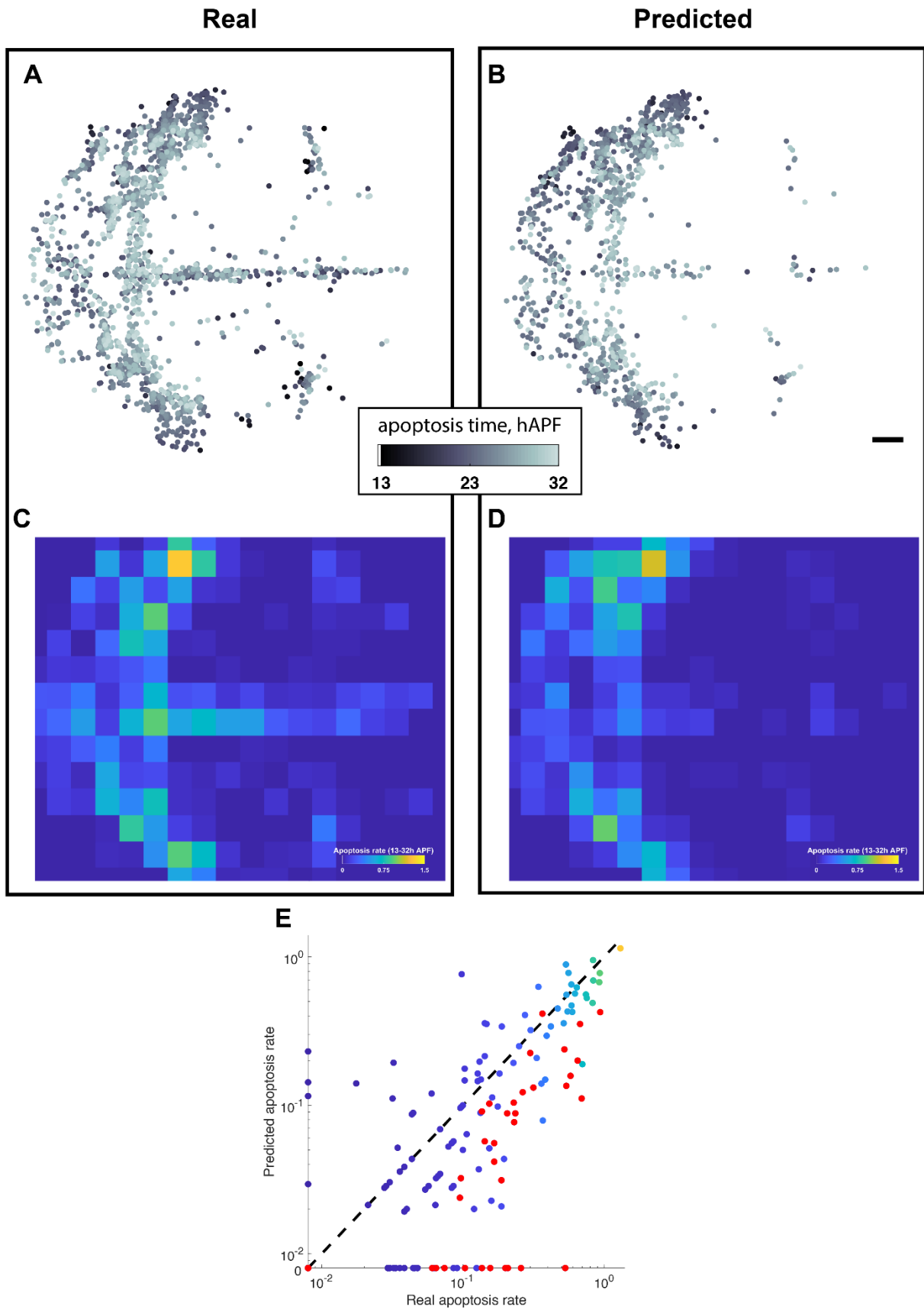


Figure 4. Prediction of the distribution of apoptoses using absolute and relative apical areas.

(A) Experimental spatiotemporal distribution of apoptoses in a representative notum (as in Figure 1C). (B) Predicted spatiotemporal distribution of apoptoses between 13 and 32 hAPF in the same notum. Dots indicate the positions of predicted apoptoses and are color-coded according to their time of apoptosis. Scale bar: 50 μm . (C) Map of the local rate of apoptosis in a notum, calculated in each box as the \rightarrow

(*Figure 4 continued*) number of apoptoses divided by the initial number of cells at 13 hAPF. Box size is $40 \times 40 \mu\text{m}^2$. Color-code: rate of apoptosis. **(D)** Map of the predicted local rate of apoptosis in a notum, calculated in each box as the number of predicted deaths divided by the initial number of cells at 13 hAPF. Same grid and color-code as (C). **(E)** Predicted apoptosis rate versus experimental apoptosis rate, for each box of the grid used in (C-D). Log-scales. Red dots: midline boxes. For the non-red dots, the color represents the real apoptosis rate. Dashed black line: $y = x$. $R^2 = 0.65$.

associated to an increase in the rate of apoptosis, measured as the number of apoptoses divided by the initial number of cells, by $23\% \pm 8.1\%$ ($N=3$). Importantly, we also predicted that this increase would not be spatially homogeneous, but instead that $86\% \pm 14\%$ of additional apoptoses would occur in the apoptotic pattern (*Figure 5C-D*). Experimentally, we observed that compressed pupae show a 25%-higher apoptosis rate than non-compressed ones, in accordance with the fold change we predict (*Figure 5D*). Moreover, the spatial distribution of apoptoses is not significantly changed by compression ($p = 0.14$, Student's t-test), with $81\% \pm 1.8\%$ of apoptoses occurring in the apoptotic pattern in compressed pupae versus $88\% \pm 4.6\%$ in control ones (*Figure 5E*). This conserved spatial distribution is in accordance with the predictions of the model. Moreover, it confirms that tissue compaction alone is not the main regulator of apoptosis, since a homogeneous reduction of cell sizes in the tissue drives a heterogeneous increase of apoptosis, biased towards regions of smaller cells.

Interplay between cell division and apoptosis

Cell division and growth are major regulators of cell size. In the pupal notum, apical growth is rather minor during the cell cycle: on average, cells grow by around 2% of their apical size per hour of life ($1.8 \pm 0.25\%$ per hour, $R^2 = 0.86$, $n = 400$ cells) (*Figure S4A*). Consequently, the average cell apical area decreases with each division wave (*Figure S4B*). Thus, we decided to study the interplay between division and apoptosis.

Before 12 hAPF, all cells are blocked in the G2 phase of the cell cycle and later divide in waves sweeping across the tissue, with a stronger division rate at the posterior side of the tissue as we described in (Guirao et al., 2015). First, comparing the spatial patterns of apoptosis and divisions reveals that apoptoses mostly occur in these regions of stronger division rate, and are uncommon in regions where cells divide only once; specifically, $\sim 75\%$ of regions of apoptoses overlap with regions where cells divide 2 times or more (*Figure 6A-B*). Second, we compared the global timings of both cell processes and found that apoptosis generally happens after the first wave of divisions is well advanced (*Figure 6C*). Third, after each division wave between 15-35 hAPF, we characterized the fate of the daughter cells (eliminating the cells whose fate was not known at 35 hAPF). We found that the more cells have divided, the higher their probability is to undergo apoptosis instead of entering another cycle of division (*Figure 6D*). These results suggest that cell division may influence apoptosis.

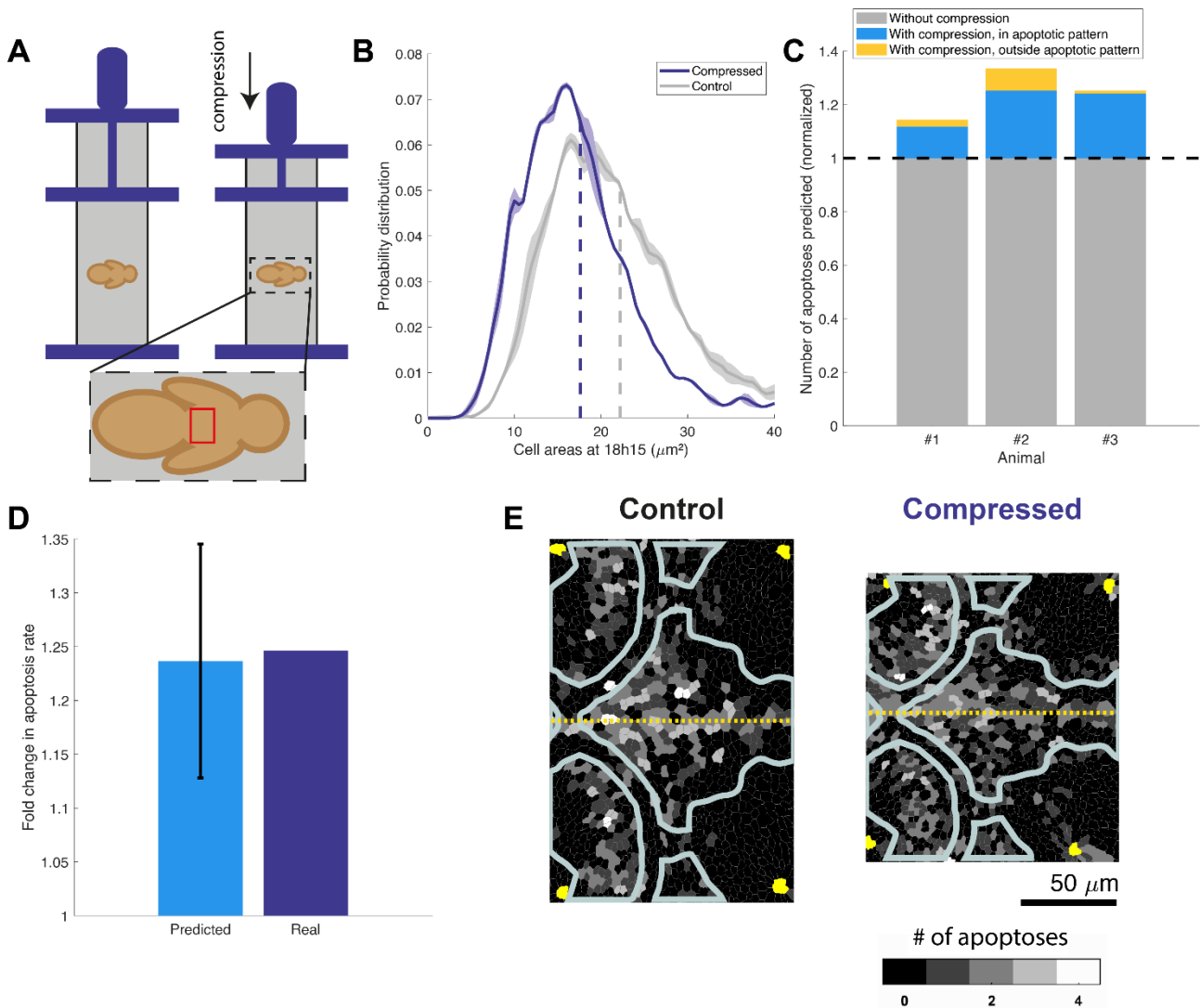


Figure 5. Uniaxial mechanical compression of developing pupae.

(A) Schematic representation of the experimental set-up. Compression is exerted between 15h and 15h30 APF. Experimental movies start at ~18h APF. Analyses are made in the scutellum region (red box, bottom sketch). (B) Distributions of the mean apical areas of cells at 18h15 APF in compressed (dark blue, $n=1910$ cells, $N=2$) versus non-compressed control (grey, mean \pm SEM, $n=2767$ cells, $N=3$) scutella. Curves are smoothed over 3 points. The area below each curve is one. Vertical dashed lines: average values. (C) Number of apoptoses predicted to occur following a 20%-tissue compaction in 3 control animals (x-axis). The prediction model is the same as in Figure 4. For each notum, three categories of apoptoses are shown: apoptoses predicted without compression (grey), compression-induced apoptoses predicted in the apoptosis pattern (blue), compression-induced apoptoses predicted outside the apoptosis pattern (yellow). The values are normalized by the number of apoptoses predicted without compression. (D) Fold change in the apoptosis rate induced by compression, predicted (blue) versus experimental (dark blue). Error bar: 95% confidence interval (CI). (E) Representative spatiotemporal distribution of apoptosis in a non-compressed scutellum (left) and a compressed scutellum (right), at 20 hAPF. Nota cells are color-coded according to the number of apoptoses in their progeny (black: no apoptoses, white: 4 and more apoptoses). Yellow cells: macrochaetae.

We then observed how caspase activity, estimated as the derivative of the GC3Ai signal (Valon et al., 2021), was modulated by divisions. Focusing on the cells located in the apoptotic pattern (Figure 1D), we found that in the first hours following a division, caspase activity generally peaks in daughter cells (Figure 6E-F). Importantly, this overall increase was both observed in future apoptotic and non-apoptotic cells ($p < 0.005$

in both cases, Student's t-test), with significantly stronger average activity in future apoptotic cells compared to non-apoptotic cells ($p < 0.005$ for both division waves, repeated-measures ANOVA). Moreover, and interestingly, this caspase burst of activity becomes stronger as cells undergo more divisions. Cell division is thus followed by a rapid peak of pro-apoptotic activity. Notably, this caspase activity is not linked to the occurrence of DNA segregation defects during mitosis that could trigger apoptosis: we used *His2B:RFP* to label chromatin in dividing cells that give at least one apoptotic offspring and saw that out of 32 cell divisions, only 1 displayed abnormal chromatin segregation (data not shown). Overall, our results indicate that cell division triggers an increase in caspase activity, that could be permissive for apoptosis.

To test the permissive role of division on apoptosis, we blocked epithelial divisions by overexpressing *tribbles* (*trbl^{OE}*), an inhibitor of the G2/M transition of the cell cycle (Figure 6G, 6K). Decreasing divisions number by *trbl^{OE}* led to the almost complete disappearance of apoptosis: the average apoptosis rate between 15-30 hAPF, measured as the number of apoptoses divided by the initial number of cells at 15 hAPF, falls to $1.5\% \pm 0.6\%$ (N=6 half-notums) versus $19\% \pm 2.7\%$ in *wt* (N=4) (Figure 6H, 6L). Alternatively, we also increased proliferation by overexpressing *cyclinE* (*cycE^{OE}*), a regulator of the G1/S transition (Figure 6I, 6K). *CycE* overexpression almost triples the occurrence of apoptosis, as the average number of apoptotic events per half-notum increases to $63\% \pm 15\%$ (N=4) (Figure 6L). Strikingly, this increase of programmed cell death is global and affects the entire notum, including the usually non-apoptotic regions of the tissue (Figure 6J). Altogether, we uncovered a central role of proliferation in the control of apoptosis.

Linking cell apical area, cell death, and Hippo pathway activity

In order to further understand how apical area regulates apoptosis, the pathways linking size inputs to programmed cell death need to be identified. We first hypothesized that the MAPK/ERK pathway could be involved. Indeed, divisions elicit ERK deactivation in the preimplantation mouse embryo (Pokrass et al., 2020) and human epithelium (Yang et al., 2017). In these latter cells, ERK has also been shown to control cell-cycle commitment (Yang et al., 2017). Moreover, ERK is a known regulator of apoptosis via the transcriptional regulation of the pro-apoptotic gene *hid* (Bergmann et al., 1998; Kurada & White, 1998; Moreno et al., 2019). We developed a ERK-KTR reporter based on the work described in (Regot et al., 2014) and validated the use of this reporter to quantify ERK activity, measured as the ratio between cytoplasmic and nuclear GFP fluorescence (Figure S5). Using this reporter, we found that ERK activity decreases immediately following division; however, this decrease is moderate (of ~14%, from 1.4 to 1.2) and ERK activity 30 min after division is already similar to its level 1h30 before division (Figure 7A) (n = 40). Besides, we found that ERK activity does not correlate with cell apical area in the notum (n = 60, $p = 0.80$, $R^2 = 1.2 \times 10^{-3}$) (Figure 7B). These results suggest that the MAPK/ERK pathway is unlikely to participate in the modulation of apoptosis by cell apical area.

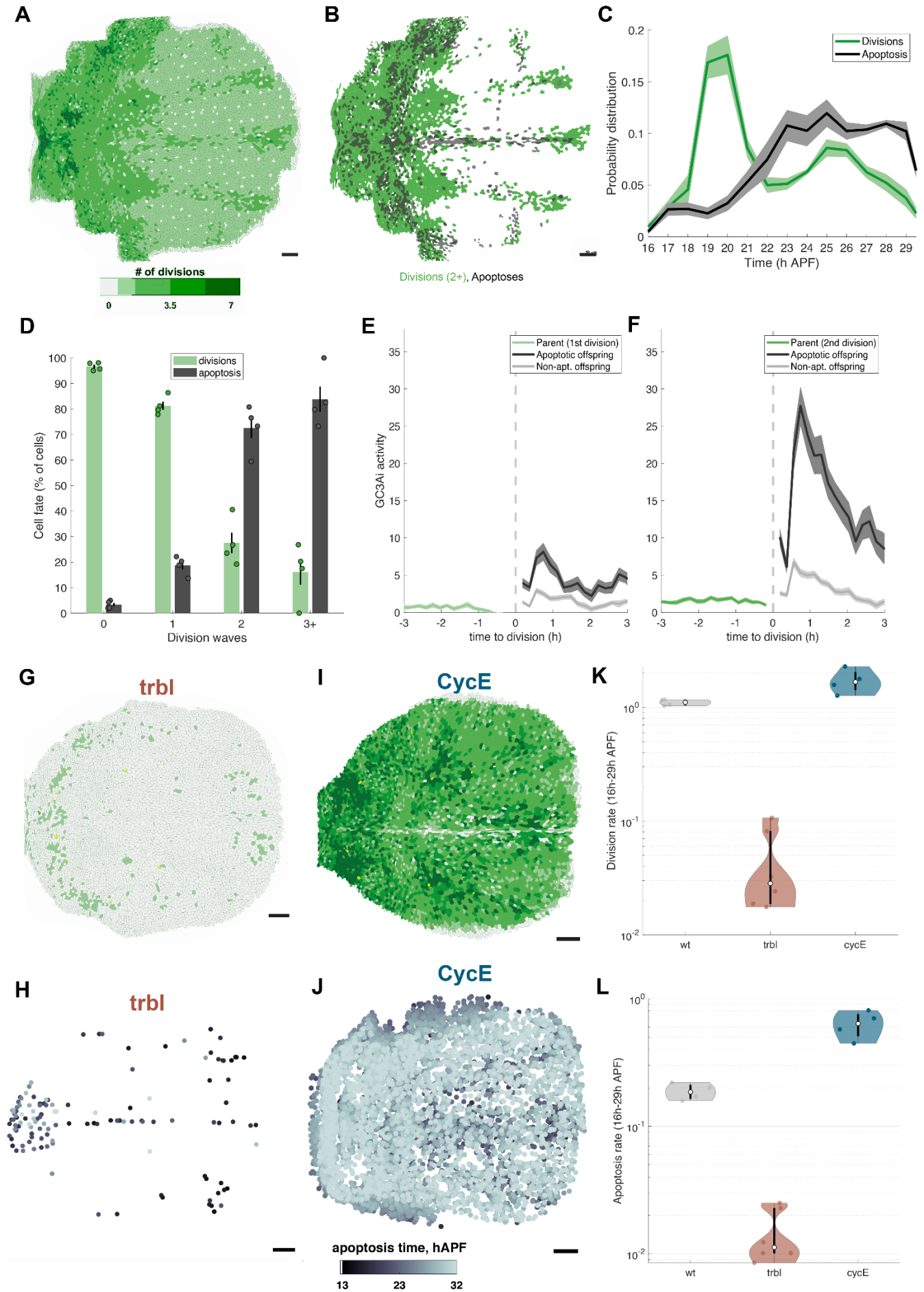


Figure 6. Coupling between proliferation and apoptosis in the developing notum. See legend next page.

Legend of Figure 6:

(A) Map of the total number of divisions in a segmented notum at 15 hAPF. Cells are color-coded depending on the number of divisions they and their progeny will do between 15 and 32 hAPF. Darker shades of green indicate more divisions. (B) Overlap of the apoptosis map (in dark grey, cells whose progeny or themselves will later apoptose) and the division map (in green, only 2+ divisions are shown, see (A)) in the same notum at 15 hAPF. (C) Distribution of divisions (green, mean \pm SEM) and apoptosis (black, mean \pm SEM) over developmental time. N=4. The area under each curve is 1. (D) Proportion of cells undergoing either division (green) or to apoptosis (dark grey), depending on the division wave the cells originate from. Error bars: SEM. Dots indicate individual data points (N=4 nota). (E-F) GC3Ai activity, measured as the time-derivative of the GC3Ai signal, in dividing cells and their offspring depending on whether the division belongs to the first wave (E) or the second one (F). Parent cells are shown in green while offspring are shown in dark grey (apoptotic offspring, mean \pm SEM) and light grey (non-apoptotic offspring, mean \pm SEM). First division wave: n=2879 parent cells giving birth to n=983 apoptotic and n=1896 non-apoptotic cells, second division wave: n=2325 parent cells giving birth to n=546 apoptotic and n=1779 non-apoptotic cells. N=3 nota. (G) Map of the waves of divisions in representative segmented *trbl^{OE}* notum at 15 hAPF. Cells are color-coded depending on the number of divisions they and their progeny will do. See (A) for more information. (H) Spatiotemporal distribution of apoptoses in the same representative *trbl^{OE}* notum. Dots indicate the death locus of apoptoses occurring between 13 and 32 hAPF, color-coded depending on their time of apoptosis. See Figure 1C for comparison. (I) Waves of divisions in a representative *cycE^{OE}* notum; see (G) for full description. (J) Spatiotemporal distribution of apoptoses in the same *cycE^{OE}* notum; see (H) for full description. (K) Division rate from 16h to 29 hAPF in wild-type (grey, N=4 half-nota), *trbl^{OE}* (brown, N=6) and *cycE^{OE}* (blue, N=4) flies. The division rate is computed as the number of divisions divided by the initial number of cells at 16 hAPF. White dot: average value, thick black line: first to third quartiles, thin black line: full range of values, dots: individual data points. Log-scale. (L) Apoptosis rate from 16h to 29 hAPF in wild-type (grey, N=4 half-nota), *trbl^{OE}* (brown, N=6) and *cycE^{OE}* (blue, N=4) flies. Apoptosis rate is computed as the number of apoptoses divided by the initial number of cells at 16 hAPF. See (K) for description. Scale bars: 50 μ m.

We then investigated the Hippo/YAP (Yorkie, Yki in *Drosophila*) pathway, which is involved in mechanosensing (Panciera et al., 2017), in cell proliferation (Tapon et al., 2002), and in the modulation of apoptosis via the control of the apoptosis inhibitor *diap1* (Tapon et al., 2002; Harvey et al., 2003; Udan et al., 2003; Huang et al., 2005) and of *bantam*, a transcriptional reporter of Yki (Brennecke et al., 2003). Unlike ERK, Hippo/YAP activity scales with apical size, a result which motivated our study of this pathway: indeed we recently showed that the intensity of *ban-nls:GFP* and of *diap1-nls:GFP* is proportional to cell apical area in the central posterior region of the notum, a region subjected to mechanical forces (López-Gay et al., 2020). Hence, we sought to verify that impacting Hippo activity could disturb the relationship between cell survival and apical size. Ajuba (Jub) is a regulator of Hippo signaling whose clustering with the Warts kinase upregulates Yki activity (Thakur et al., 2010; Reddy et al., 2013; Rauskolb et al., 2014; López-Gay et al., 2020). We locally inhibited Yki activity by clonal expression of *Jub^{RNAi}* in the posterior notum, and used the non-clonal regions symmetric relative to the midline as control. We found that, at a given apical area, inhibiting Jub enhances apoptosis (Figure 7C). Importantly, this effect is not homogeneous but instead increases with cell apical area (Figure 7D). This is consistent with a model in which the higher Yki activity in large cells would block their apoptosis. Since the scaling between Hippo activity and apical cell size is mediated by apical stress fibers (López-Gay et al., 2020) of which α -Actinin (*actn*) is a key component, we then disturbed this scaling by locally inhibiting α -Actinin in the posterior

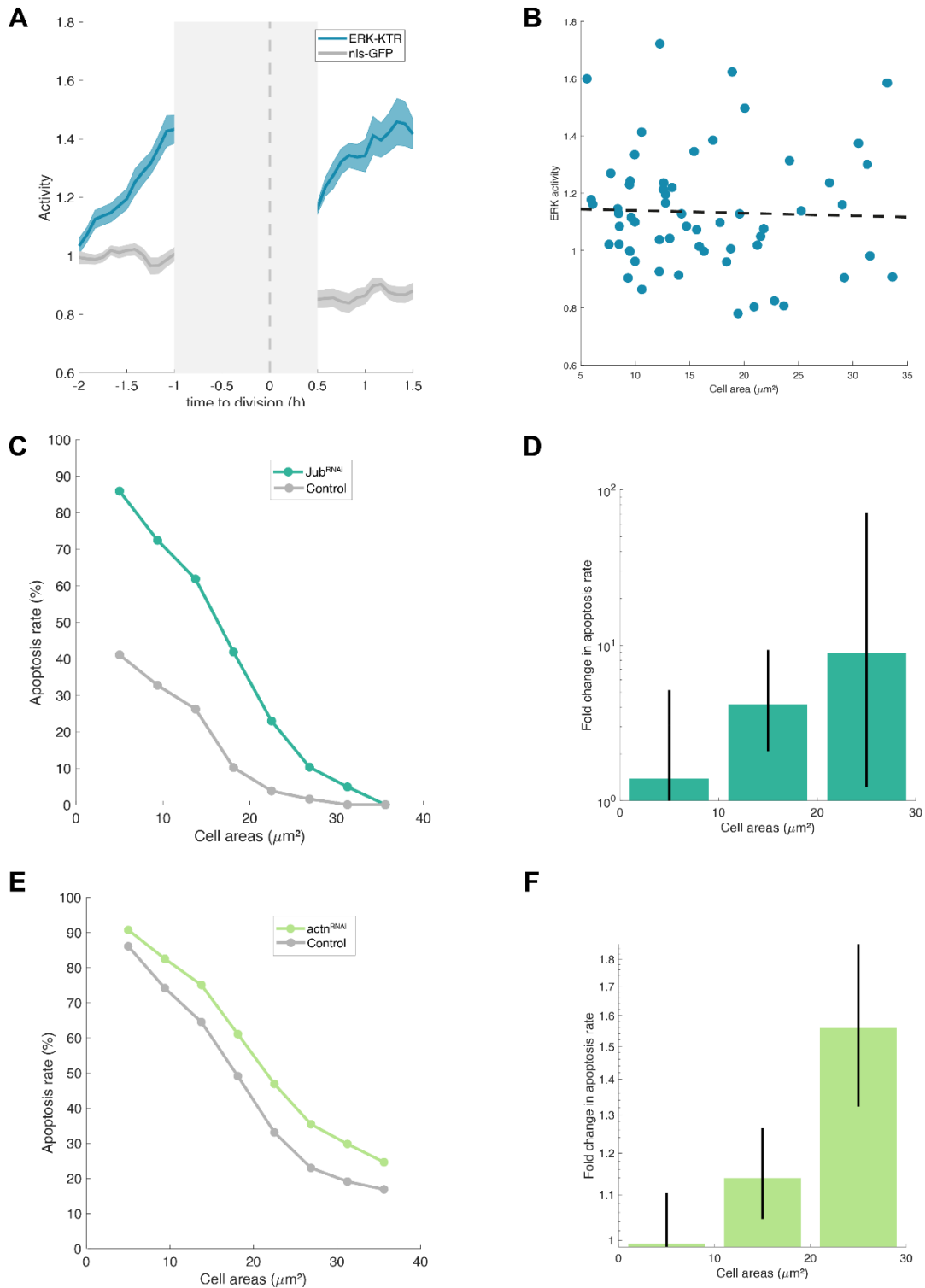


Figure 7. Cell area modulates apoptosis through Hippo/Yki activity.

(A) Time-evolution of ERK activity (blue, mean \pm SEM) measured as the cytoplasmic to nuclear intensity of the ERK-KTR sensor (see Figure S5 for description), in $n=40$ dividing cells and one of their offspring. Control: nls-GFP activity (grey, mean \pm SEM) in $n=37$ dividing cells and one of their offspring. Values around mitosis (1h before to 30 minutes after) are not included since the ERK-KTR sensor is also modulated by CDK activity in this time window (Ponsioen et al., 2021). (B) ERK activity versus cell apical area in $n = 60$ cells. ERK activity and cell apical area are averaged over 30 minutes. Measurements are made around 24 hAPF in the posterior half of the notum. Dashed line: linear fit ($p = 0.8$, $R^2 = 0.0012$). $N = 4$ nota. (\rightarrow)

(Figure 7 continued) (C) Apoptosis probability versus cell apical area, in *jub^{RNAi}* clone cells (green, n=193 cells) and control cells (grey, *wt* cells symmetric to *jub^{RNAi}* clones with respect to the notum midline, n=214 cells). Cells whose fate is known are binned depending on their apical area (averaged over their lives except the last hour), and the rate of apoptotic cells is computed for each bin. Each curve is then smoothed over 3 points. Clones were selected in the scutellum region. N=2 nota. (D) Fold change in apoptosis probability between *wt* and *jub^{RNAi}* clone cells, depending on cell apical area (averaged over their lives minus the last hour). Log-scale. Error bar: 95%-CI (Fisher test). n = 193 *jub^{RNAi}* and 214 *wt* cells from N = 2 nota. (E) Probability of apoptosis versus cell apical area, in *actn^{RNAi}* cells (green, n=1767 cells) and control cells (grey, *w^{RNAi}* cells, n=2729 cells). Scutellum cells whose fate is known are binned depending on their apical area (averaged over their lives minus the last hour), and the rate of apoptotic cells is computed for each bin. Each curve is then smoothed over 3 points. N=5 *pnr-G4>actn^{dsRNA}* nota, N=2 clonal *actn^{RNAi}* nota; control, N=5 *pnr-G4>w^{dsRNA}* nota, N=2 clonal *w^{RNAi}* nota. (F) Fold change in apoptosis probability between *w^{RNAi}* and *actn^{RNAi}* cells, depending on cell apical area (averaged over their lives minus the last hour). Log scale. Error bar: 95%-CI (Fisher test). n = 1767 cells from N=5 *pnr-G4>actn^{dsRNA}* nota, N=2 clonal *actn^{RNAi}* nota; n = 2729 control cells from N=5 *pnr-G4>w^{dsRNA}* nota, N=2 clonal *w^{RNAi}* nota.

notum. We found that in *actn^{RNAi}* regions, apoptosis is enhanced at a given apical area, and the fold change in apoptosis rate again increases with cell size (Figure 7E-F). Overall, our results indicate that a low YAP (Yki) activity as found in small *wt* cells is associated with an increased apoptosis probability. Preventing the scaling between Hippo/YAP activity and apical size by inhibiting *actn* (López-Gay et al., 2020) impacts the modulation of cell survival by cell apical area. Interestingly, reducing Hippo/Yki activity did not fully suppress the correlation between cell survival and apical area, suggesting the existence of additional mechanism that would contribute to the regulation of this scaling.

Notch signaling is required for the regulation of apoptosis by the cell relative apical area

Next, we studied the role of cell relative apical area, which is the second size feature of apoptotic cells that is predictive of epithelial apoptosis.

To test whether modulating relative cell size would change the apoptosis rate, we first sought to induce size heterogeneity in otherwise identical cells. To do so, we generated clonal populations of *Tor^{RNAi}* cells, which have reduced apical area (Figure 8A-C) although being as proliferative as *wt* cells (in N=2 pupae, the fold change in division rate between *Tor^{RNAi}* and *wt* cells is equal to 0.97 and 0.96). We turned our attention to the first (R1) and second (R2) rows of *wt* cells around *Tor^{RNAi}* clones (Figure 8D). These two different rows of *wt* cells have very slightly different apical areas (fold change of 1.08 ± 0.04 , R2/R1, n = 19 clones) (Figure 8E). More importantly, R1 cells are in direct contact with small *Tor^{RNAi}* cells; as a result, their relative areas are typically bigger than the ones of R2 cells, with a fold change of 1.17 ± 0.03 (Figure 8E). If a bigger relative area impedes cell death, we would expect apoptosis to be decreased in these cells that are otherwise wild-type. On the other hand, if R1 and R2 cells have similar apoptosis rate, it would suggest that the increased relative area of R1 cells does not impact apoptosis. We found that R1 *wt* cells have a 22%-lower probability to enter apoptosis, as compared to R2 *wt* cells which are not in contact with *Tor^{RNAi}* cells (p = 0.0047, Fisher test) (Figure 8F). Conversely, *Tor^{RNAi}* cells on the clone border, in contact with *wt* cells, are characterized by smaller relative areas than *Tor^{RNAi}* cells in the clone bulk (fold change of 0.85 ± 0.02 , Border/Bulk, n = 15 clones) (Figure 8G). We verified that these border clone cells die

significantly (170%) more than the bulk clone cells ($p = 2.8 \times 10^{-7}$, Fisher test) (Figure 8H). Accordingly, in *Tor^{RNAi}* clones, the vast majority of apoptoses (88% of $n = 222$ apoptoses) occur on the clone border, where size heterogeneities are the highest (Figure 8I). Overall, our data suggest that changing cell relative apical areas impacts apoptosis.

We then sought to identify the molecular pathways involved in the control of epithelial apoptosis by relative areas. The preferential death of cells smaller than their neighbors is a context-dependent form of cell elimination which involves comparison with adjacent cells. As such, it shares characteristics with cell competition mechanisms. The gene *azot* encodes a calcium-dependent protein whose role in cell competition has been shown in the *Drosophila* wing imaginal disc and pupal retina, as well as the adult fly brain and gut (Merino et al., 2015). We inhibited *azot* function during the notum development (*azot^{KO}*) and studied the impact on apoptosis in the posterior region of the notum (Figure S6B). In this region of *azot^{KO}* tissues, we found that apoptotic cells are still 10-15% smaller than their neighbors (Figure S6A) and that $79\% \pm 5.8\%$ of the apoptosis observed in *azot^{KO}* tissue overlapped with the wild-type apoptosis mask in the posterior notum (Figure S6B). Consequently, the elimination of cells smaller than their neighbors is not modulated by *azot*. This observation therefore prompted us to explore other pathways by which the relative apical areas of cells could impact their survival.

Apoptosis has been linked to cell-cell communication by the discovery of a local and transient inhibition of death in the neighbors of an apoptotic cell (Bilak et al., 2014; Gagliardi et al., 2021; Valon et al., 2021), which is regulated in the notum via the activation of ERK in the neighbors from 30 min to 1h30 after apoptosis (Valon et al., 2021). This spatiotemporal coordination of apoptosis prevents apoptosis clusters in which adjacent cells would die simultaneously and that would therefore jeopardize the integrity of the tissue. We decided to investigate if this process could be modulated by relative apical area. To do so, we measured ERK activity in cells of various sizes and found no scaling between ERK activity and the relative apical area of cells (Figure S7A). As a result, the regulation of apoptosis by relative size is unlikely to be ERK-dependent. Besides, it was proposed that the MAPK/ERK activation that blocks apoptosis clusters could be driven by the transient stretching of neighbor cells during apoptosis (Valon et al., 2021) (Figure S7B), as the MAPK/ERK pathway reacts to tissue deformations (Moreno et al., 2019). However, when studying this stretching proposed to counteract apoptotic cell loss, we found that neighbor apical expansion during apoptosis is not uniformly distributed among the dying cell neighbors, but is instead highly skewed towards one to three main neighbors (Figure S7C). Yet, ERK is activated in all neighbor cells during apoptosis (Valon et al., 2021). Moreover, neighbor cell stretching does not correlate with their probability to die in the few hours following extrusion of the apoptotic cell (Figure S7D). Overall, the local

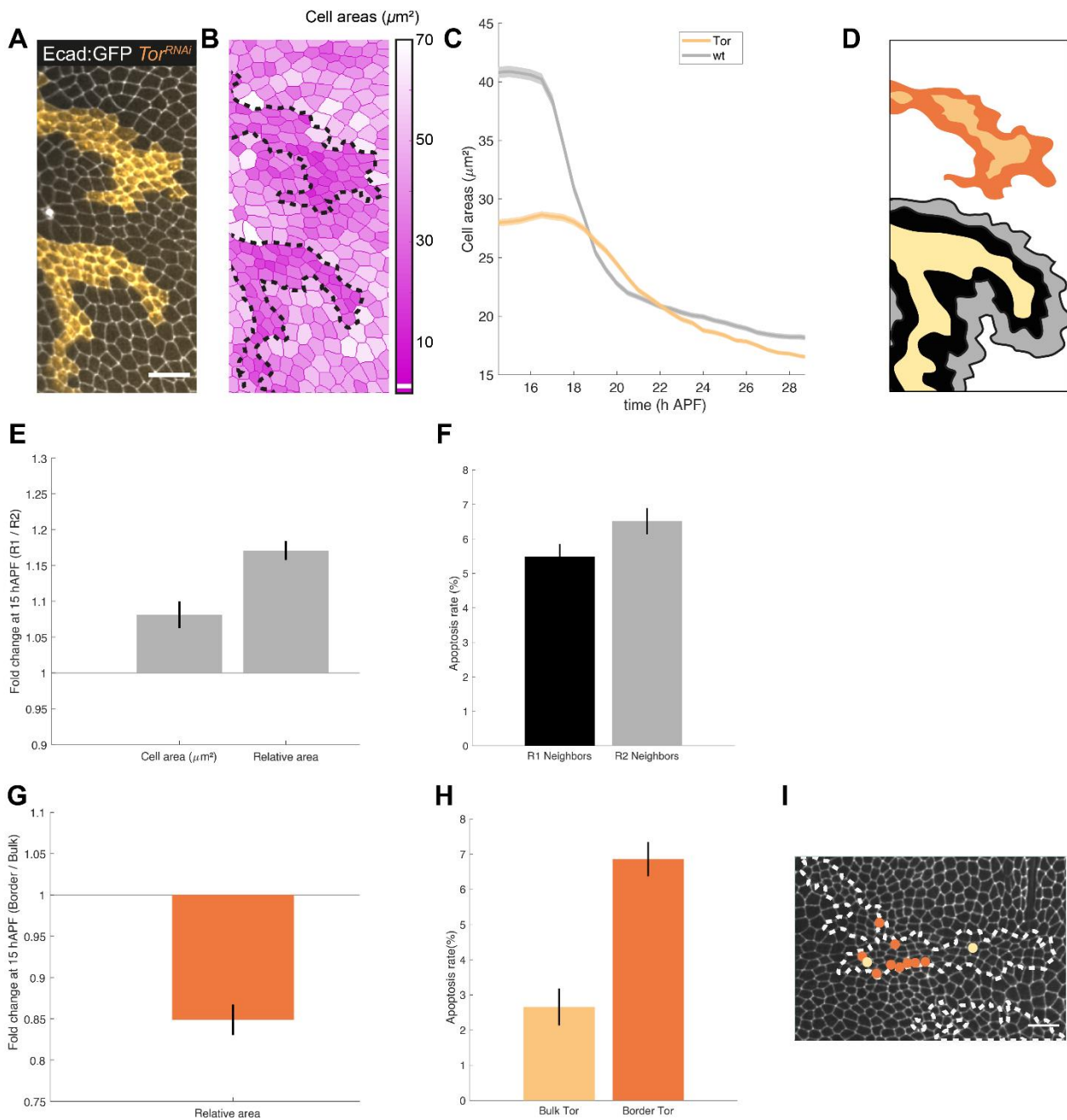


Figure 8. Loss of Tor function modulates cell size heterogeneity and apoptosis of surrounding wt cells.

(A) Close-up of a notum expressing Ecad:GFP with clonal expression of Tor^{RNAi} (orange) at 15 hAPF. Scale bar: 20 μ m. (B) Same tissue as (A), segmented. Cells are color-coded depending on their apical area. Black dotted lines: outlines of Tor^{RNAi} clones. (C) Time evolution of cell apical areas in Tor^{RNAi} clone cells ($n = 3326$ cells from $N = 2$ nota, orange) versus control ($n = 3073$ cells from same $N = 2$ nota, grey). Control cells are wt cells symmetric to Tor^{RNAi} clones with respect to the notum midline. Mean \pm SEM. (D) Schematic representation of Tor^{RNAi} clone cells (yellow: bulk, orange: border) and their wt neighbors (black: 1st row R1, grey: 2nd row R2). (E) Fold change in the apical areas and relative apical areas of wt neighbor cells, calculated for each clone as the ratio of the average quantity in R1 cells by the same quantity in R2 cells at 15 hAPF. Error bars: SEM. $n=19$ clones from $N=2$ nota. (F) Apoptosis probability of R1 neighbor cells (black, $n=3633$) and R2 neighbor cells (grey, $n=3844$) between 15 and 30 hAPF. Error bars: SEM. $N=2$ nota. (G) Fold change in relative apical area at 15 hAPF between border and bulk Tor^{RNAi} clone cells, calculated as the average relative area of border cells divided by the average relative area of bulk cells, for each clone. Error bar: SEM. $n=15$ clones from $N=2$ nota. (H) Apoptosis probability of bulk Tor^{RNAi} cells (yellow, $n=2700$) and border Tor^{RNAi} cells (orange, $n=940$) between 15 and 30 hAPF. Error bars: SEM. $N=2$ nota. (I) Close-up of a notum expressing Ecad:GFP with clonal expression of Tor^{RNAi} (dashed white lines) at 15h30 APF. Dots indicate future apoptosis; orange dots are border apoptotic cells, yellow dots are bulk apoptotic cells. Scale bar: 20 μ m.

coordination of apoptosis is not modulated by the stretching of apoptotic cell's neighbors during extrusion and by the activation of ERK in these neighbors.

We then investigated the possible involvement of the Notch (*N*) pathway: *N* regulates lateral inhibition, a process driving differential fate decisions between neighboring cells in a large variety of living systems (Lai, 2004; Artavanis-Tsakonas & Muskavitch, 2010; Sjöqvist & Andersson, 2019). Sensory organ precursor (SOP) patterning is an example of Notch-driven lateral inhibition in the notum (Simpson et al., 1999; Furman & Bukharina, 2008; Hunter et al., 2016). *N* also mediates asymmetric divisions resulting in binary cell fate decisions in the daughters, and sometimes leading to the apoptosis of one daughter cell, as seen again during the development of *Drosophila* bristles (Schweisguth, 2015) or of sea urchins' neural progenitors (Mellott et al., 2017). Besides, *N* signal has been shown to correlate with cell-cell contact area in *in vitro* contact assays of pairs of epithelial cells as well as in the developing chick inner ear, indicating its ability to sense geometric differences between adjacent cells and its possible relevance in our study (Shaya et al., 2017).

To investigate the role of this pathway, we used temperature-sensitive Notch allele (N^{ts}). We found that inhibiting Notch around 13 hAPF does not significantly change the rate of apoptosis (N^{ts} : $8.7 \pm 2.1 \times 10^{-2}$ apoptoses per initial cell at 16 hAPF, versus $9.5 \pm 1.8 \times 10^{-2}$ in control), nor the qualitative relationship between cell apical area and the apoptosis probability (Figure 9A). In sharp contrast, this inhibition is enough to significantly reduce the preferential death of cells smaller than their neighbors: the relative apical area of apoptotic cells is higher in N^{ts} condition compared to control, and this is seen throughout their lives, as early as 8h before apoptosis ($p = 2.33 \times 10^{-8}$, Student's t-test) (Figure 9B). Using a logistic regression, we found that a decrease of a N^{ts} cell relative area by 0.1 corresponds to a 4.2% increase in its probability to die, as compared to an 8.2% increase in control cells. This means that the coefficient of correlation between relative apical area and apoptosis, which measures the strength of the relationship between these two factors, is decreased twofold when Notch is inhibited. To verify that cell extrusion in N^{ts} tissue is still apoptotic, we used the GC3Ai caspase reporter and found that out of 110 extruding N^{ts} cells, all exhibited a burst of caspase activity before their extrusion (N = 4 pupae; Figure 9C). Moreover, in N^{ts} condition, we noticed the presence of apoptosis clusters usually not seen in epithelial tissues (Figure 9D). To quantify the occurrence of these clusters, for every apoptosis, we measured subsequent apoptoses occurring in a 5 μ m-radius (corresponding approximately to direct neighbors) and 3 h-time window around the position of the initial apoptotic cell. We found that inhibiting Notch leads to a significant increase in the probability of observing a nearby apoptosis in the 0h30-1h30 window after an apoptosis ($p = 0.002$, Fisher test, odds ratio = 1.32 ± 0.22) (Figure 9E).

Together, these results strongly suggest that Notch is important for the regulation of apoptosis by cell relative apical area. Notch activity contributes to the local coordination of apoptosis between

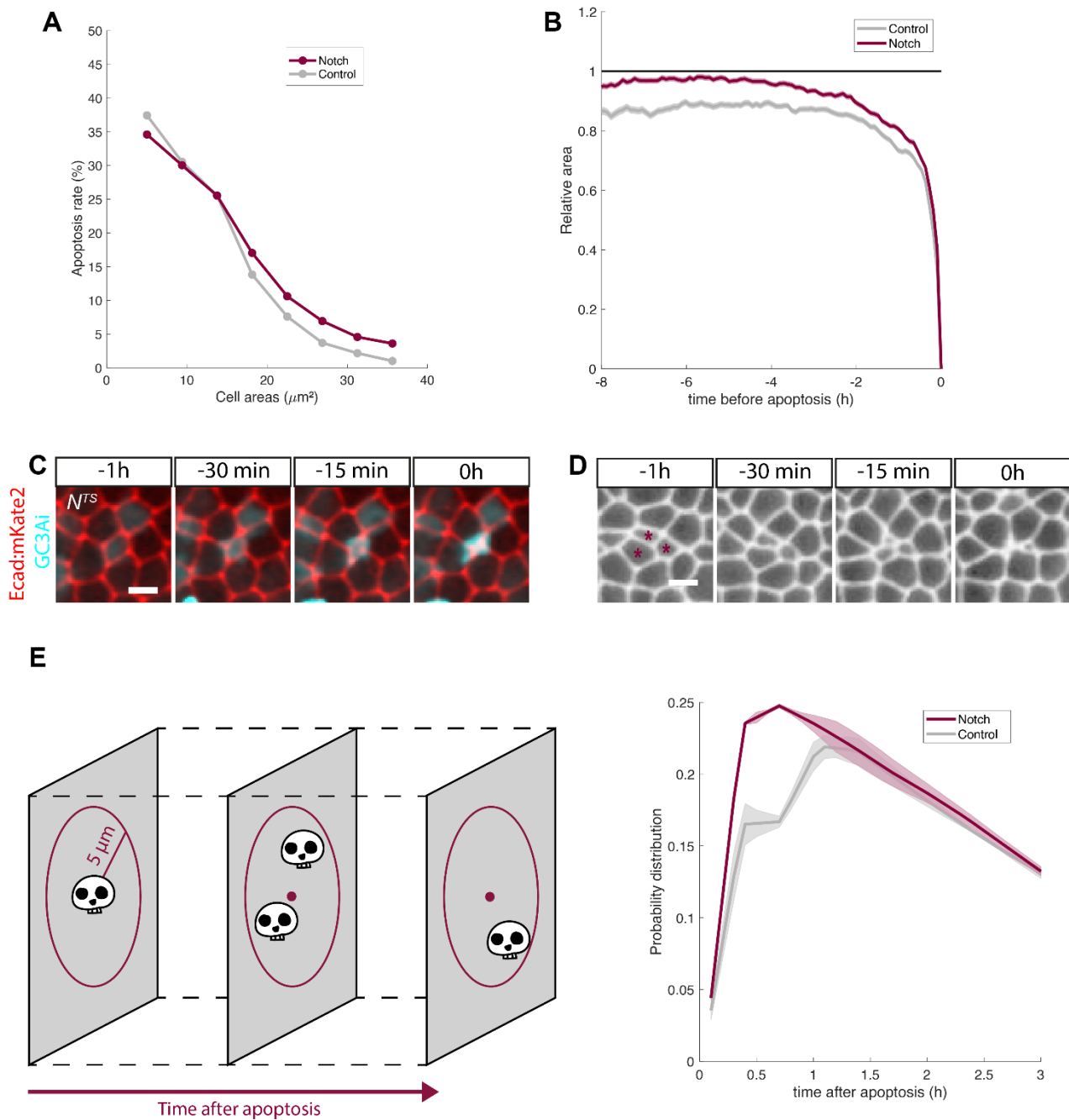


Figure 9. Cell relative apical area regulates apoptosis through Notch activity.

(A) Apoptosis rate versus cell apical area, in N^{ts} cells (dark red, $n=13217$ cells from $N=3$ nota) and control cells (grey, $n=9150$ cells from $N=2$ nota). Cells whose fate is known are binned depending on their apical area (averaged over their lives minus the last hour), and the fraction of apoptotic cells is computed for each bin. Each curve is then smoothed over 3 points. (B) Relative apical area of apoptotic cells versus time before their death, in N^{ts} (dark red, $n=2630$ cells from $N=3$ nota, mean \pm SEM) versus control (grey, $n=1600$ cells from $N=2$ nota, mean \pm SEM). Cells are aligned with respect to their time of apoptosis (right side of the graph). (C) Time-evolution of a representative apoptotic cell in a N^{ts} notum expressing Ecad:mKate2 and the GC3Ai caspase fluorescence reporter. Scale bar: 5 μm . (D) Cluster of apoptotic cells in a N^{ts} notum expressing Ecad:GFP: the 3 cells marked with asterisks die closely together, both in space and in time. Scale bar: 5 μm . (E) Schematic representation of the quantification of apoptosis clusters (left) and results (right) in N^{ts} (dark red, $n=2469$ cells, $N=3$ nota, mean \pm SEM) and control (grey, $n=1328$ cells, $N=2$ nota, mean \pm SEM). The graph shows the distribution of neighboring ($< 5 \mu\text{m}$) apoptoses after an initial death has occurred at $t=0$. The area under each curve is 1.

neighboring cells and prevent the occurrence of apoptotic cell clusters that would compromise tissue integrity.

DISCUSSION

The role of biophysical factors in the control of *in vivo* apoptosis, a process whose genetic regulation has been well characterized, remained mostly unknown. Here, we uncovered two distinct mechanisms of geometric control of cell death, both involving cell apical area but acting at two different scales and involving two different pathways: (i) globally, at the tissue level, regions displaying cells with smaller absolute area determines putative apoptotic zones; (ii) locally, at the cell level, cells with smaller relative area have a higher tendency to die, thereby determining putative apoptotic cells. To our knowledge, this constitutes one of the first characterizations of *in vivo* apoptotic cells that identified such early features.

We found that on the one hand, the global, cell-autonomous control of apoptosis by apical cell area involves the Hippo pathway. In addition, inhibition of Jub activity changes, but does not fully suppress, the correlation between apical area and apoptosis probability. This suggests the existence of additional mechanisms that regulate apoptosis depending on apical size, and whose elucidation should be the subject of future work. On the other hand, the local, non cell-autonomous modulation of apoptosis by relative apical area requires Notch. We showed that Notch activity prevents the occurrence of clusters of apoptotic cells dying together, by reducing the probability to die in the neighbors of an apoptotic cell between 0h30 and 1h30 after apoptosis. Interestingly, this timing is consistent with the time window recently found to correspond to the local and transient restriction of apoptosis in the neighbors of an apoptotic cell by ERK activation (Valon et al., 2021). Thus, the two mechanisms could cooperate to locally fine-tune apoptosis. Furthermore, recent reports highlighted the various and context-dependent modes of interplay between Notch and Hippo in the control of cell fate decisions (Totaro et al., 2018; Engel- Pizcueta & Pujades, 2021). Therefore, it will be interesting to explore the existence of crosstalk between these two pathways in the control of apoptosis in response to geometrical features.

In addition, our results uncovered and unexpected link between cell division and apoptosis. While it is known that stress-induced apoptosis can trigger compensatory proliferation (Fan & Bergmann, 2008), the impact of normal cell division on apoptosis remained unclear. We showed that cell division plays a key role in the control of apoptosis for which it is permissive. In particular, division triggers a peak of caspase activity which increases with the number of division waves, and which is visible (although a lot weaker) in non-apoptotic offspring as well. This peak of caspase activity can precede by several hours the final burst of caspase activation that is associated with apoptosis. Therefore, cell division might not only halve cell apical size but also promote a peak of caspase activity at cell birth that contributes to the future apoptotic fate of the cells. To better understand the link between cell division and apoptosis, it will be therefore

relevant to analyze the magnitude of caspase activity on the life duration of these cells, to explore whether this caspase activity peak depends on the Hippo pathway activity and to specifically modulate the level of caspase activity upon mitosis.

Our results also clarify and deepen our understanding of the link between of tissue contraction and apoptosis. Tissue contraction, which is linked to dynamic changes of cell size, was suggested to drive apoptosis in biological tissue (Eisenhoffer et al., 2012; Marinari et al., 2012; Levayer et al., 2016; Moreno et al., 2019). We found that the physiological contractions of the tissue cannot explain the tissue apoptosis pattern. In accordance with this finding, exerting a homogeneous compression on developing pupae resulted in a non-homogeneous increase of apoptosis. Instead, the important factor is cell apical size, whose dynamics and relative value compared to the cell's neighbors are distinct in future apoptotic and non-apoptotic cells early in their lives, sometimes hours before apoptosis. Previous studies on the biophysical regulation of apoptosis *in vivo* often analyzed the notum midline, a highly apoptotic stripe of cells (Marinari et al., 2012; Levayer et al., 2016; Moreno et al., 2019). Our prediction model, which recapitulates the global pattern of apoptosis in the notum, performed less well in the midline and predicted only few apoptoses. This indicates that the biophysical regulation of apoptosis in the notum midline might involve different mechanisms than the rest of the tissue. This, along with the fact that these cells globally express caspase 3 throughout the early notum development (Fujisawa et al., 2019), indicate that midline cells may be programmed to die during larval to pupal development regardless of any other specific single-cell characteristics such as cell geometry and that tissue contraction may rather be a facilitating than an instructive factor

We would like to conclude on the regulation of apoptosis by cell relative area. The regulation of apoptosis by cell relative apical area indicates that the context-dependent comparison between adjacent cells drives cell elimination in the notum. While this regulation is independent of *azot* activity, this is phenomenologically reminiscent of cell competition, which promotes the elimination of less-fit cells in mixed populations; in our case, cell fitness would correlate with cell apical area. Thus, we would like to propose that apoptosis can be akin to a process of physiological geometric competition.

REFERENCES

- Ansari, B., & Hall, P. A. (1992). The kinetic organisation of tissues. In *Assessment of Cell Proliferation in Clinical Practice* (pp. 45-62). Springer, Tokyo.
- Artavanis-Tsakonas, S., & Muskavitch, M. A. (2010). Notch: the past, the present, and the future. *Current Topics in Developmental Biology*, *92*, 1-29.
- Arya, R., & White, K. (2015). Cell death in development: signaling pathways and core mechanisms. In *Seminars in Cell & Developmental Biology* (Vol. 39, pp. 12-19). Academic Press.
- Bergmann, A., Agapite, J., McCall, K., & Steller, H. (1998). The *Drosophila* gene *hid* is a direct molecular target of Ras-dependent survival signaling. *Cell*, *95*(3), 331-341.
- Bilak, A., Uyetake, L., & Su, T. T. (2014). Dying cells protect survivors from radiation-induced cell death in *Drosophila*. *PLoS Genetics*, *10*(3), e1004220.
- Bosveld, F., Bonnet, I., Guirao, B., Tlili, S., Wang, Z., Petitalot, A., ... & Bellaïche, Y. (2012). Mechanical control of morphogenesis by Fat/Dachsous/Four-jointed planar cell polarity pathway. *Science*, *336*(6082), 724-727.
- Brennecke, J., Hipfner, D. R., Stark, A., Russell, R. B., & Cohen, S. M. (2003). *bantam* encodes a developmentally regulated microRNA that controls cell proliferation and regulates the proapoptotic gene *hid* in *Drosophila*. *Cell*, *113*(1), 25-36.
- Cuervo, R., Valencia, C., Chandraratna, R. A., & Covarrubias, L. (2002). Programmed cell death is required for palate shelf fusion and is regulated by retinoic acid. *Developmental Biology*, *245*(1), 145-156.
- de la Cova, C., Townley, R., Regot, S., & Greenwald, I. (2017). A real-time biosensor for ERK activity reveals signaling dynamics during *C. elegans* cell fate specification. *Developmental Cell*, *42*(5), 542-553.
- di Pietro, F., Herszterg, S., Huang, A., Bosveld, F., Alexandre, C., Sancéré, L., ... & Bellaïche, Y. (2021). Rapid and robust optogenetic control of gene expression in *Drosophila*. *Developmental Cell*, *56*(24), 3393-3404.
- Eisenhoffer, G. T., Loftus, P. D., Yoshigi, M., Otsuna, H., Chien, C. B., Morcos, P. A., & Rosenblatt, J. (2012). Crowding induces live cell extrusion to maintain homeostatic cell numbers in epithelia. *Nature*, *484*(7395), 546-549.
- Engel-Pizcueta, C., & Pujades, C. (2021). Interplay Between Notch and YAP/TAZ Pathways in the Regulation of Cell Fate during Embryo Development. *Frontiers in Cell and Developmental Biology*, *9*, 2314.
- Fan, Y., & Bergmann, A. (2008). Apoptosis-induced compensatory proliferation. The Cell is dead. Long live the Cell!. *Trends in Cell Biology*, *18*(10), 467-473.
- Foster, J. R. (2000). Cell death and cell proliferation in the control of normal and neoplastic tissue growth. *Toxicologic Pathology*, *28*(3), 441-446.
- Fujisawa, Y., Kosakamoto, H., Chihara, T., & Miura, M. (2019). Non-apoptotic function of *Drosophila* caspase activation in epithelial thorax closure and wound healing. *Development*, *146*(4), dev169037.
- Furman, D. P., & Bukharina, T. A. (2008). How *Drosophila melanogaster* forms its mechanoreceptors. *Current Genomics*, *9*(5), 312-323.
- Gagliardi, P. A., Dobrzyński, M., Jacques, M. A., Dessauges, C., Ender, P., Blum, Y., ... & Pertz, O. (2021). Collective ERK/Akt activity waves orchestrate epithelial homeostasis by driving apoptosis-induced survival. *Developmental Cell*, *56*(12), 1712-1726.
- Guirao, B., Rigaud, S. U., Bosveld, F., Bailles, A., López-Gay, J., Ishihara, S., ... & Bellaïche, Y. (2015). Unified quantitative characterization of epithelial tissue development. *eLife*, *4*, e08519.
- Harvey, K. F., Pflieger, C. M., & Hariharan, I. K. (2003). The *Drosophila* Mst ortholog, *hippo*, restricts growth and cell proliferation and promotes apoptosis. *Cell*, *114*(4), 457-467.

- Hernández-Martínez, R., & Covarrubias, L. (2011). Interdigital cell death function and regulation: new insights on an old programmed cell death model. *Development, Growth & Differentiation*, *53*(2), 245-258.
- Huang, J., Wu, S., Barrera, J., Matthews, K., & Pan, D. (2005). The Hippo signaling pathway coordinately regulates cell proliferation and apoptosis by inactivating Yorkie, the Drosophila Homolog of YAP. *Cell*, *122*(3), 421-434.
- Hunter, G. L., Hadjivasiliou, Z., Bonin, H., He, L., Perrimon, N., Charras, G., & Baum, B. (2016). Coordinated control of Notch/Delta signalling and cell cycle progression drives lateral inhibition-mediated tissue patterning. *Development*, *143*(13), 2305-2310.
- Kuipers, D., Mehonic, A., Kajita, M., Peter, L., Fujita, Y., Duke, T., ... & Gale, J. E. (2014). Epithelial repair is a two-stage process driven first by dying cells and then by their neighbours. *Journal of Cell Science*, *127*(6), 1229-1241.
- Kurada, P., & White, K. (1998). Ras promotes cell survival in Drosophila by downregulating hid expression. *Cell*, *95*(3), 319-329.
- Lai, E. C. (2004). Notch signaling: control of cell communication and cell fate. *Development*, *131*(5), 965-973.
- Levayer, R., Dupont, C., & Moreno, E. (2016). Tissue crowding induces caspase-dependent competition for space. *Current Biology*, *26*(5), 670-677.
- Li, J., & Yuan, J. (2008). Caspases in apoptosis and beyond. *Oncogene*, *27*(48), 6194-6206.
- López-Gay, J. M., Nunley, H., Spencer, M., Di Pietro, F., Guirao, B., Bosveld, F., ... & Bellaïche, Y. (2020). Apical stress fibers enable a scaling between cell mechanical response and area in epithelial tissue. *Science*, *370*(6514), eabb2169.
- Marinari, E., Mehonic, A., Curran, S., Gale, J., Duke, T., & Baum, B. (2012). Live-cell delamination counterbalances epithelial growth to limit tissue overcrowding. *Nature*, *484*(7395), 542-545.
- Martín-Blanco, E., Pastor-Pareja, J. C., & García-Bellido, A. (2000). JNK and decapentaplegic signaling control adhesiveness and cytoskeleton dynamics during thorax closure in Drosophila. *Proceedings of the National Academy of Sciences*, *97*(14), 7888-7893.
- Mellott, D. O., Thisdelle, J., & Burke, R. D. (2017). Notch signaling patterns neurogenic ectoderm and regulates the asymmetric division of neural progenitors in sea urchin embryos. *Development*, *144*(19), 3602-3611.
- Merino, M. M., Rhiner, C., Lopez-Gay, J. M., Buechel, D., Hauert, B., & Moreno, E. (2015). Elimination of unfit cells maintains tissue health and prolongs lifespan. *Cell*, *160*(3), 461-476.
- Monier, B., Gettings, M., Gay, G., Mangeat, T., Schott, S., Guarner, A., & Suzanne, M. (2015). Apico-basal forces exerted by apoptotic cells drive epithelium folding. *Nature*, *518*(7538), 245-248.
- Moreno, E., Valon, L., Levillayer, F., & Levayer, R. (2019). Competition for space induces cell elimination through compaction-driven ERK downregulation. *Current Biology*, *29*(1), 23-34.
- Nehls, S., Nöding, H., Karsch, S., Ries, F., & Janshoff, A. (2019). Stiffness of MDCK II cells depends on confluency and cell size. *Biophysical Journal*, *116*(11), 2204-2211.
- Panciera, T., Azzolin, L., Cordenonsi, M., & Piccolo, S. (2017). Mechanobiology of YAP and TAZ in physiology and disease. *Nature Reviews Molecular Cell Biology*, *18*(12), 758-770.
- Pokrass, M. J., Ryan, K. A., Xin, T., Pielstick, B., Timp, W., Greco, V., & Regot, S. (2020). Cell-cycle-dependent ERK signaling dynamics direct fate specification in the mammalian preimplantation embryo. *Developmental Cell*, *55*(3), 328-340.
- Ponsioen, B., Post, J. B., Buissant des Amorie, J. R., Laskaris, D., van Ineveld, R. L., Kersten, S., ... & Snippert, H. J. (2021). Quantifying single-cell ERK dynamics in colorectal cancer organoids reveals EGFR as an amplifier of oncogenic MAPK pathway signalling. *Nature Cell Biology*, *23*(4), 377-390.

- Ranft, J., Basan, M., Elgeti, J., Joanny, J. F., Prost, J., & Jülicher, F. (2010). Fluidization of tissues by cell division and apoptosis. *Proceedings of the National Academy of Sciences*, *107*(49), 20863-20868.
- Rauskolb, C., Sun, S., Sun, G., Pan, Y., & Irvine, K. D. (2014). Cytoskeletal tension inhibits Hippo signaling through an Ajuba-Warts complex. *Cell*, *158*(1), 143-156.
- Reddy, B. V. V. G., & Irvine, K. D. (2013). Regulation of Hippo signaling by EGFR-MAPK signaling through Ajuba family proteins. *Developmental Cell*, *24*(5), 459-471.
- Regot, S., Hughey, J. J., Bajar, B. T., Carrasco, S., & Covert, M. W. (2014). High-sensitivity measurements of multiple kinase activities in live single cells. *Cell*, *157*(7), 1724-1734.
- Rosenblatt, J., Raff, M. C., & Cramer, L. P. (2001). An epithelial cell destined for apoptosis signals its neighbors to extrude it by an actin-and myosin-dependent mechanism. *Current Biology*, *11*(23), 1847-1857.
- Saw, T. B., Doostmohammadi, A., Nier, V., Kocgozlu, L., Thampi, S., Toyama, Y., ... & Ladoux, B. (2017). Topological defects in epithelia govern cell death and extrusion. *Nature*, *544*(7649), 212-216.
- Schmidt, U., Weigert, M., Broaddus, C., & Myers, G. (2018). Cell detection with star-convex polygons. In *International Conference on Medical Image Computing and Computer-Assisted Intervention* (pp. 265-273). Springer, Cham.
- Schott, S., Ambrosini, A., Barbaste, A., Benassayag, C., Gracia, M., Proag, A., ... & Suzanne, M. (2017). A fluorescent toolkit for spatiotemporal tracking of apoptotic cells in living *Drosophila* tissues. *Development*, *144*(20), 3840-3846.
- Schweisguth, F. (2015). Asymmetric cell division in the *Drosophila* bristle lineage: from the polarization of sensory organ precursor cells to Notch-mediated binary fate decision. *Wiley Interdisciplinary Reviews: Developmental Biology*, *4*(3), 299-309.
- Shaya, O., Binshtok, U., Hersch, M., Rivkin, D., Weinreb, S., Amir-Zilberstein, L., ... & Sprinzak, D. (2017). Cell-cell contact area affects notch signaling and notch-dependent patterning. *Developmental Cell*, *40*(5), 505-511.
- Simpson, P., Woehl, R., & Usui, K. (1999). The development and evolution of bristle patterns in Diptera. *Development*, *126*(7), 1349-1364.
- Sjöqvist, M., & Andersson, E. R. (2019). Do as I say, Not (ch) as I do: Lateral control of cell fate. *Developmental Biology*, *447*(1), 58-70.
- Suzanne, M., Petzoldt, A. G., Spéder, P., Coutelis, J. B., Steller, H., & Noselli, S. (2010). Coupling of apoptosis and L/R patterning controls stepwise organ looping. *Current Biology*, *20*(19), 1773-1778.
- Tapon, N., Harvey, K. F., Bell, D. W., Wahrer, D. C., Schiripo, T. A., Haber, D. A., & Hariharan, I. K. (2002). salvador Promotes both cell cycle exit and apoptosis in *Drosophila* and is mutated in human cancer cell lines. *Cell*, *110*(4), 467-478.
- Thakur, M. D., Feng, Y., Jagannathan, R., Seppa, M. J., Skeath, J. B., & Longmore, G. D. (2010). Ajuba LIM proteins are negative regulators of the Hippo signaling pathway. *Current Biology*, *20*(7), 657-662.
- Totaro, A., Castellán, M., Di Biagio, D., & Piccolo, S. (2018). Crosstalk between YAP/TAZ and Notch signaling. *Trends in Cell Biology*, *28*(7), 560-573.
- Toyama, Y., Peralta, X. G., Wells, A. R., Kiehart, D. P., & Edwards, G. S. (2008). Apoptotic force and tissue dynamics during *Drosophila* embryogenesis. *Science*, *321*(5896), 1683-1686.
- Udan, R. S., Kango-Singh, M., Nolo, R., Tao, C., & Halder, G. (2003). Hippo promotes proliferation arrest and apoptosis in the Salvador/Warts pathway. *Nature Cell Biology*, *5*(10), 914-920.
- Valon, L., Davidović, A., Levillayer, F., Villars, A., Chouly, M., Cerqueira-Campos, F., & Levayer, R. (2021). Robustness of epithelial sealing is an emerging property of local ERK feedback driven by cell elimination. *Developmental Cell*, *56*(12), 1700-1711.
- Yang, H. W., Chung, M., Kudo, T., & Meyer, T. (2017). Competing memories of mitogen and p53 signalling control cell-cycle entry. *Nature*, *549*(7672), 404-408.

SUPPLEMENTARY INFORMATION

Material and Methods

Fly stocks and genetics

Supplementary Table 1 lists *Drosophila melanogaster* stocks used and associated references. Loss-of-function and gain-of-function experiments were carried out using the Gal4/UAS system utilizing the temperature sensitive Gal80^{ts} (1, 2). To tune the transcriptional activity of the *Act-GAL4* drivers, animals were raised at 18°C and incubated at 29°C before mounting for 4 h (UAS-*cycE*) or 24 h (UAS-*trbl*). For clonal loss-of-function analyses the FLP/FRT flip-out was employed using the Act>CD2>Gal4, UAS-Caax:tBFP line to express Gal4 and labelled the clones by membrane localized BFP (3, 4). Larvae were raised at 25°C, somatic clones were induced in the third instar larval stage by heat shock at 37°C for 10 min (UAS-*Ras*^{V12}, UAS-*Notch*^{dsRNA}, UAS-*Tor*^{dsRNA}, UAS-*diap1*, UAS-*trbl*, UAS-*miRHG*) or 20 min (UAS-*trbl*, UAS-*Jub*^{dsRNA}, UAS-*actn*^{dsRNA}) and then incubated at 29°C for 24 h (UAS-*Ras*^{V12}, UAS-*Notch*^{dsRNA}, UAS-*Tor*^{dsRNA}) or 48 h (UAS-*diap1*, UAS-*trbl*, UAS-*miRHG*) before mounting. To tune Notch activity male pupa *N^{ts}* were raised at 18°C, and then shifted to 29°C 3 hours prior to imaging. Analyses were then performed in pupa that exhibited a “bold” (absence of microchaetae) phenotype indicative of sensory organ cell fate mis-determination. Analysis of caspase activation in *Notch* context was done using ShineGal4 (ubi-Gal4^{MagHigh}) (9) of GC3Ai reporter of caspase activity with light exposure 1 day before mounting.

Supplementary Table 1. *Drosophila* alleles and transgenes.

<i>Drosophila</i> stock	Reference or Source
Ubi-Ecad::GFP	Ref (15); (5); gift of Yang Hong.
Ecad::3xGFP	Ref (6)
Ecad::3xmKate2	Ref (6)
Ecad::3xTagRfp	Ref (6)
Ubi-KTR::GFP	This study.
UAS- <i>trbl</i>	(7)
<i>azot</i> ^{KO}	(8) (Cell 160, 461); gift from Eduardo Moreno
<i>Ubi-2xpMagHigh1:AD</i>	(9)
<i>Ubi-Gal4DB:2xnMagHigh1</i>	(9)
UAS- <i>Diap1</i>	Bloomington Stock Center (#6657)
UAS- <i>w</i> ^{dsRNA}	Bloomington Stock Center (#33644)
UAS- <i>Tor</i> ^{dsRNA}	Bloomington Stock Center (#34639)
UAS- <i>miRHG</i>	Triple dsRNA against Hid, Rpr and Grim. Gift from Marco Milan.
UAS- <i>actn</i> ^{dsRNA}	Bloomington Stock Center (#34874)
UAS- <i>jub</i> ^{dsRNA}	Bloomington Stock Center (#41938)
<i>N^{ts}</i>	Gift from Michel Gho
Ban-GFP	(10)
UAS-GC3Ai	(14)
UAS- <i>CycE</i> ; UAS- <i>CycE</i>	(11); gift from Michel Gho.
<i>diap1</i> ^{3.5} -GFP	(12)
<i>w</i> ^{I118}	Bloomington Stock Center (#56326)
Ubi-His2B::RFP	(13)
hs-flp	Bloomington Stock Center (#8862)
Act>CD2>Gal4, UAS-Caax:tBFP	Ref (7)
Act-GAL4	Bloomington Stock Center (#3954)
Ubi-GAL80 ^{ts}	Bloomington Stock Center (#7017)
UAS- <i>Ras</i> ^{V12}	Karim & Rubin, 1998; Bloomington Stock Center (#64196)

Pupa and adult mounting and imaging

Time-lapse live imaging

Notum live imaging was performed as described previously (13, 6). Pupae were collected at the white stage (0 hour after pupal formation, hAPF) and mounted at head eversion (12 hAPF). Samples were imaged with an inverted confocal spinning disk microscope from Carl Zeiss using 40x/1.4 OIL DIC H/N2 PL FLUOR, 60x/1.4 OIL PL APO, 63x/1.4 OIL DICII PL APO VC objectives and a sCMOS camera (Orca Flash4, Hamamatsu). Unless otherwise stated, all movies were done at 29°C using tile imaging (6 to 10 tiled positions), z stacks (0.5 μm /slice), every 5 min using autofocus. The autofocus was performed using Ecad fluorescent signal as a reference.

Pupal tissue fixation, staining and imaging

Pupal nota were dissected, fixed and stained into MatTek glass bottom dish. Briefly, the nota were dissected in PBS, fixed in 4% formaldehyde solution, permeabilised/washed in PBT 0.4% triton, stained with primary antibody solution washed and then stained with secondary antibody solution. Primary antibodies used: rabbit anti-dpERK (Cell signaling, #4370, 1/100), chicken anti-GFP (abCam, #13970, 1/500). Secondary antibodies used: donkey anti-rabbit Cy3 and donkey anti-chicken Alexa488 (Jackson Immunoresearch). Dissected nota were mounted in Vectashield with DAPI (Vectorlab).

They were imaged using an inverted confocal spinning disk microscope from Carl Zeiss using 40x/1.4 OIL DIC H/N2 PL FLUOR and sCMOS camera (Orca Flash4, Hamamatsu). Images shown are maximal (dpERK and DAPI) or average (KTR-ERK) z-projections.

*Compression of *Drosophila notum* and imaging*

White pupae (0hAPF) were collected with a wet paintbrush and placed on double-side tape with a coverslip on top of the pupae to flatten the notum and ease the compression. In parallel, a 3,5 by 1 cm polydimethylsiloxane (PDMS – from Gel Pack: Gel Film PF_60_x4) stripe was attached to a custom-made compression device and stretched to 150%. After 15h of development at 25°C, the pupal case was fully removed and the flattened pupae were carefully grabbed by the head with a plastic tip to be glued, with heptane glue, on the pre-stretched PDMS. Using the micrometric screw of the compression device, the pre-stretched PDMS was progressively release over 30 minutes to allow a 15% compression of the area of interest. At each step, a confocal image was taken to follow the course of compression. For live-imaging, the compression device was fixed to the stage of an inverted confocal spinning disk from Nikon and pupae were imaged at 25°C with an 40x NA 0.95 Air dry PL APO objective from 17h30APF to 30hAPF.

Image processing for display

Unless otherwise stated, all images and movies for display represent maximal z-projections. Movies were restored and projected using the CARE deep neural network (19). In the few cases where focus was lost at a given time point, these time-point images were replaced by a previous time-point acquisition to allow for segmentation and tracking.

Generation of Ubi-KTR:GFP reporter

The Ubi-KRT:GFP reporter was generated by cloning the KTR:GFP sequence (16) in a modified pUbi vector (17). Cloning was performed using SLIC (18). All embryo transgenesis injections were performed by Bestgene and transgenes were confirmed by sequencing. Detailed plasmid maps and their DNA sequences are available upon request.

Quantification of KTR:GFP reporter and GC3Ai sensor activities

All images and movies for KTR:GFP reporter and GC3Ai sensor represent average z-projections of 20x0.5 μ m slices containing (centered on) nucleus plane.

Quantifications of tissue dynamics

Spatial and temporal registration of time-lapse movies

Between 14-17 hAPF the presumptive neck-thorax boundary, the most medial and posterior pair of head macrochaetes, the anterior macrochaetes of the scutum and the midline provide reproducible spatial landmarks easily identifiable using cortical markers such as *Ecad::3xGFP*. We used their positions before 18 hAPF to register all time-lapse movies in space.

To register time-lapse movies in time, the maximum of the tissue rotation rate in a reference window was used, as described in details in (13; 20). To correct for the difference in developmental time between 25°C and 29°C, a correction factor of 1.11 was applied to data acquired at 29°C to match the 25°C timing. Note that each experimental condition was compared to a control condition acquired at the same temperature, so this correction factor does not impact any of our conclusions.

Segmentation and Tracking

Cell outlines labelled with fluorescent markers for E-cadherin were segmented using a homemade segmentation software based on watershed and on the StarDist deep neural network (21). Cell tracking was performed using MATLAB and C++ codes as previously described in details (13; 20).

To quantify the absolute and relative apical areas of cells expressing the ERK-KTR reporter, manual segmentation was performed using Fiji. Cells were segmented in their apical plane over several time points corresponding to half an hour, then these values were averaged.

For clonal analysis, tissue counterparts which are symmetric to clones with respect to the midline were sometimes used as control (specified in text and figure legends). These counterparts were rigorously defined based on the positions of the macrochaetae and midline. The symmetric regions were identified at the first frame of the movies, then the corresponding cells were tracked through time.

Cell apoptosis and division quantification

Apoptoses and divisions were tracked in the tissue on the basis of the cell tracking and using MATLAB and C++ codes as previously published (13; 20).

To create a mask of apoptosis at the notum scale, we used the grey level maps of the offspring apoptotic rates (as shown in Figure 1D) for 5 half-nota, taken at the same time points. 3 masks were created, at 15 hAPF, 17h30 APF and 20 hAPF, to adapt for movies with different beginning times. The grey level maps were binarized and a Gaussian blur was performed. They were then rescaled so that the origin and spatial landmarks of all animals would match (the full description of the rescaling process has previously been described (20)). The 5 rescaled maps were added together and the resulting map was slightly blurred so that coarse-grained regions of apoptosis would emerge. The boundaries between close regions were drawn by hand.

Tissue compaction measurements

Tissue regions where compaction was measured were tracked over time, and their total area quantified using cell segmentation. The region areas were then averaged over 2h-wide sliding time windows, with a 96%-overlap, so that each time frame would be the center of an averaged time window. The resulting smoothed region area was normalized so that its maximum value over time would equal 1.

Statistics

Sample sizes vary in each experiment and animal samples were randomly selected within a given genotype for subsequent analyses. Experiments were repeated at least twice. Only animals correctly mounted for microscopy and without developmental delay were included in the analyses. The numbers of analyzed animals and analyzed cells are indicated in figures or figure legends. For all graphs, each error bar/error area represents the standard error to the

mean (sem), unless specified otherwise. Statistical analyses were performed using Matlab or Python. P-values are given with a 5%-level of significance.

Prediction model

To build a prediction model, segmented data from 7 half-nota were used. Cells whose future fate was known were selected, and their absolute and relative apical areas were averaged over their entire lives minus the last hour, to avoid the bias induced by this last hour of drastic cell shrinkage in the life of an apoptotic cell. Outliers were removed. Cells were then clustered in equal size-bins of 100 cells, and for each bin, the apoptosis rate was calculated. To create clusters, initial values were chosen using the k-means++ algorithm (REF) and the clusters were then optimized through an iterative process. The optimal size of clusters and prediction threshold were estimated via a k-fold cross validation with 5 subsets. The prediction dataset consisted in segmented data from 1 full notum. The data was pre-processed similarly to the training dataset. Then, each cell was assigned the apoptosis rate corresponding to the cluster it belonged to. Cells whose apoptosis rate was above the prediction threshold were predicted to die.

Data and Code availabilities

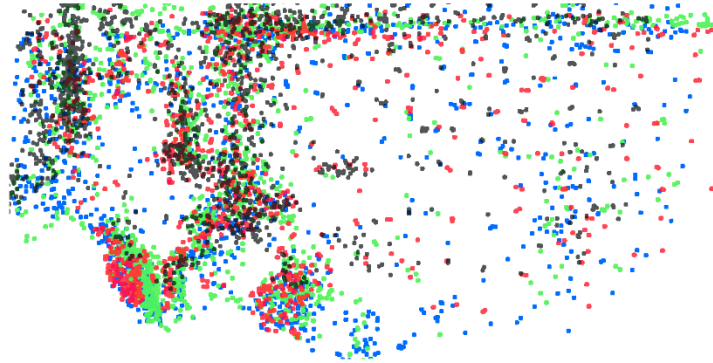
All data are available upon reasonable requests. All scripts and codes are accessible upon request.

Supplementary References

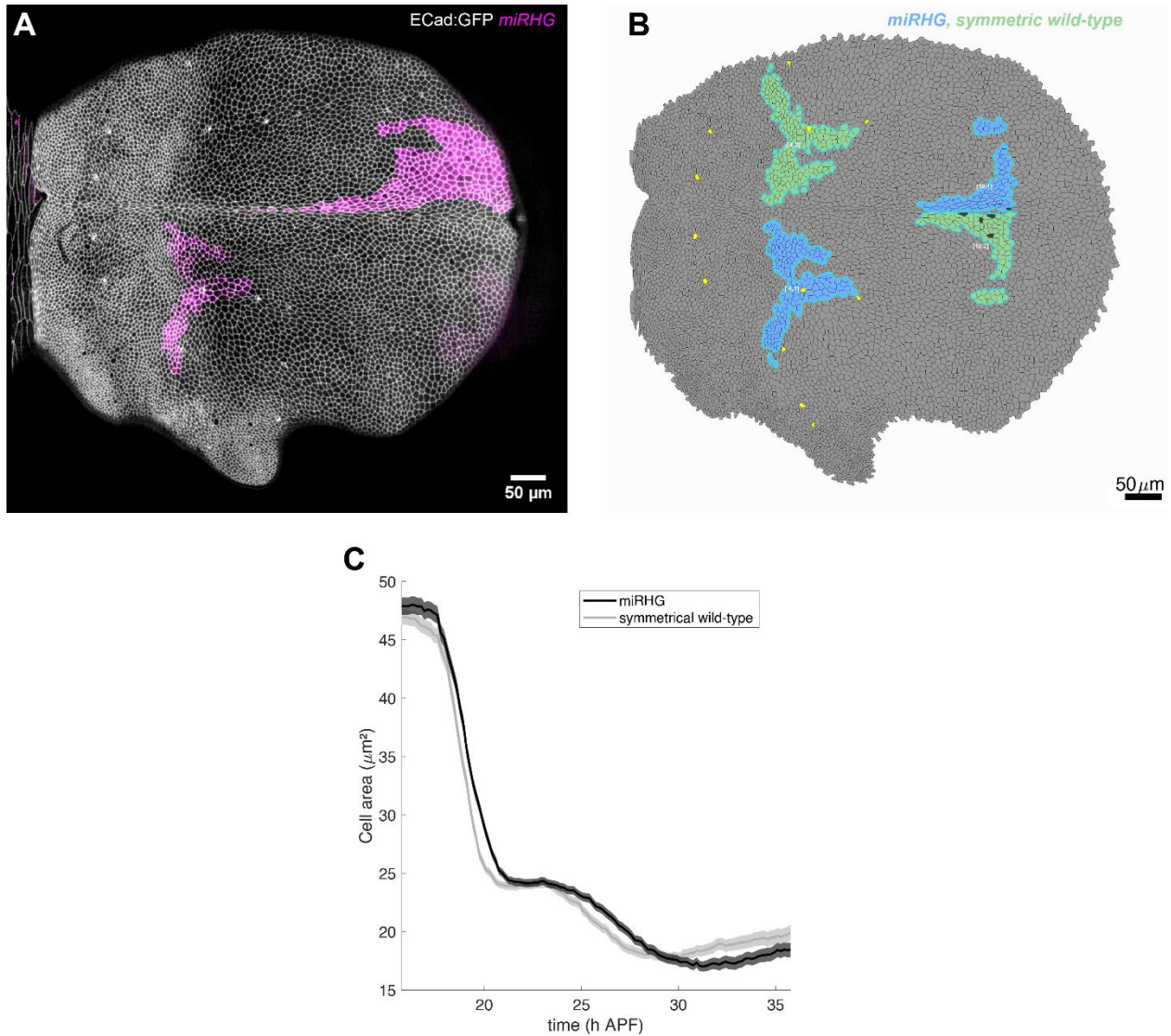
1. Brand, A. H., & Perrimon, N. (1993). Targeted gene expression as a means of altering cell fates and generating dominant phenotypes. *development*, *118*(2), 401-415.
2. McGuire, S. E., Le, P. T., Osborn, A. J., Matsumoto, K., & Davis, R. L. (2003). Spatiotemporal rescue of memory dysfunction in *Drosophila*. *Science*, *302*(5651), 1765-1768.
3. Xu, T., & Rubin, G. M. (1993). Analysis of genetic mosaics in developing and adult *Drosophila* tissues. *Development*, *117*(4), 1223-1237.
4. Golic, K. G., & Lindquist, S. (1989). The FLP recombinase of yeast catalyzes site-specific recombination in the *Drosophila* genome. *Cell*, *59*(3), 499-509.
5. Huang, J., Zhou, W., Dong, W., Watson, A. M., & Hong, Y. (2009). Directed, efficient, and versatile modifications of the *Drosophila* genome by genomic engineering. *Proceedings of the National Academy of Sciences*, *106*(20), 8284-8289.
6. Pinheiro, D., Hannezo, E., Herszterg, S., Bosveld, F., Gaugue, I., Balakireva, M., ... & Bellaïche, Y. (2017). Transmission of cytokinesis forces via E-cadherin dilution and actomyosin flows. *Nature*, *545*(7652), 103-107.
7. Großhans, J., & Wieschaus, E. (2000). A genetic link between morphogenesis and cell division during formation of the ventral furrow in *Drosophila*. *Cell*, *101*(5), 523-531.
8. Merino, M. M., Rhiner, C., Lopez-Gay, J. M., Buechel, D., Hauert, B., & Moreno, E. (2015). Elimination of unfit cells maintains tissue health and prolongs lifespan. *Cell*, *160*(3), 461-476.
9. Di Pietro, F., Herszterg, S., Huang, A., Bosveld, F., Alexandre, C., Sancéré, L., ... & Bellaïche, Y. (2021). Rapid and robust optogenetic control of gene expression in *Drosophila*. *Developmental Cell*, *56*(24), 3393-3404.
10. Matakatsu, H., & Blair, S. S. (2012). Separating planar cell polarity and Hippo pathway activities of the protocadherins Fat and Dachshous. *Development*, *139*(8), 1498-1508.
11. Simon, F., Fichelson, P., Gho, M., & Audibert, A. (2009). Notch and Prospero repress proliferation following cyclin E overexpression in the *Drosophila* bristle lineage. *PLoS Genetics*, *5*(8), e1000594.
12. Zhang, L., Ren, F., Zhang, Q., Chen, Y., Wang, B., & Jiang, J. (2008). The TEAD/TEF family of transcription factor Scalloped mediates Hippo signaling in organ size control. *Developmental Cell*, *14*(3), 377-387.
13. Bosveld, F., Bonnet, I., Guirao, B., Tlili, S., Wang, Z., Petitalot, A., ... & Bellaïche, Y. (2012). Mechanical control of morphogenesis by Fat/Dachshous/Four-jointed planar cell polarity pathway. *Science*, *336*(6082), 724-

727.

14. Schott, S., Ambrosini, A., Barbaste, A., Benassayag, C., Gracia, M., Proag, A., ... & Suzanne, M. (2017). A fluorescent toolkit for spatiotemporal tracking of apoptotic cells in living *Drosophila* tissues. *Development*, *144*(20), 3840-3846.
15. Rauzi, M., Lenne, P. F., & Lecuit, T. (2010). Planar polarized actomyosin contractile flows control epithelial junction remodelling. *Nature*, *468*(7327), 1110-1114.
16. Regot, S., Hughey, J. J., Bajar, B. T., Carrasco, S., & Covert, M. W. (2014). High-sensitivity measurements of multiple kinase activities in live single cells. *Cell*, *157*(7), 1724-1734.
17. Ségalen, M., Johnston, C. A., Martin, C. A., Dumortier, J. G., Prehoda, K. E., David, N. B., ... & Bellaïche, Y. (2010). The Fz-Dsh planar cell polarity pathway induces oriented cell division via Mud/NuMA in *Drosophila* and zebrafish. *Developmental Cell*, *19*(5), 740-752.
18. Li, M. Z., & Elledge, S. J. (2019). SLIC: A method for sequence- and ligation-independent cloning. *Methods in Molecular Biology*, **852**, 51–59.
19. Weigert, M., Schmidt, U., Boothe, T., Müller, A., Dibrov, A., Jain, A., ... & Myers, E. W. (2018). Content-aware image restoration: pushing the limits of fluorescence microscopy. *Nature Methods*, *15*(12), 1090-1097.
20. Guirao, B., Rigaud, S. U., Bosveld, F., Bailles, A., López-Gay, J., Ishihara, S., ... & Bellaïche, Y. (2015). Unified quantitative characterization of epithelial tissue development. *Elife*, *4*, e08519.
21. Schmidt, U., Weigert, M., Broaddus, C., & Myers, G. (2018, September). Cell detection with star-convex polygons. In *International Conference on Medical Image Computing and Computer-Assisted Intervention* (pp. 265-273). Springer, Cham.

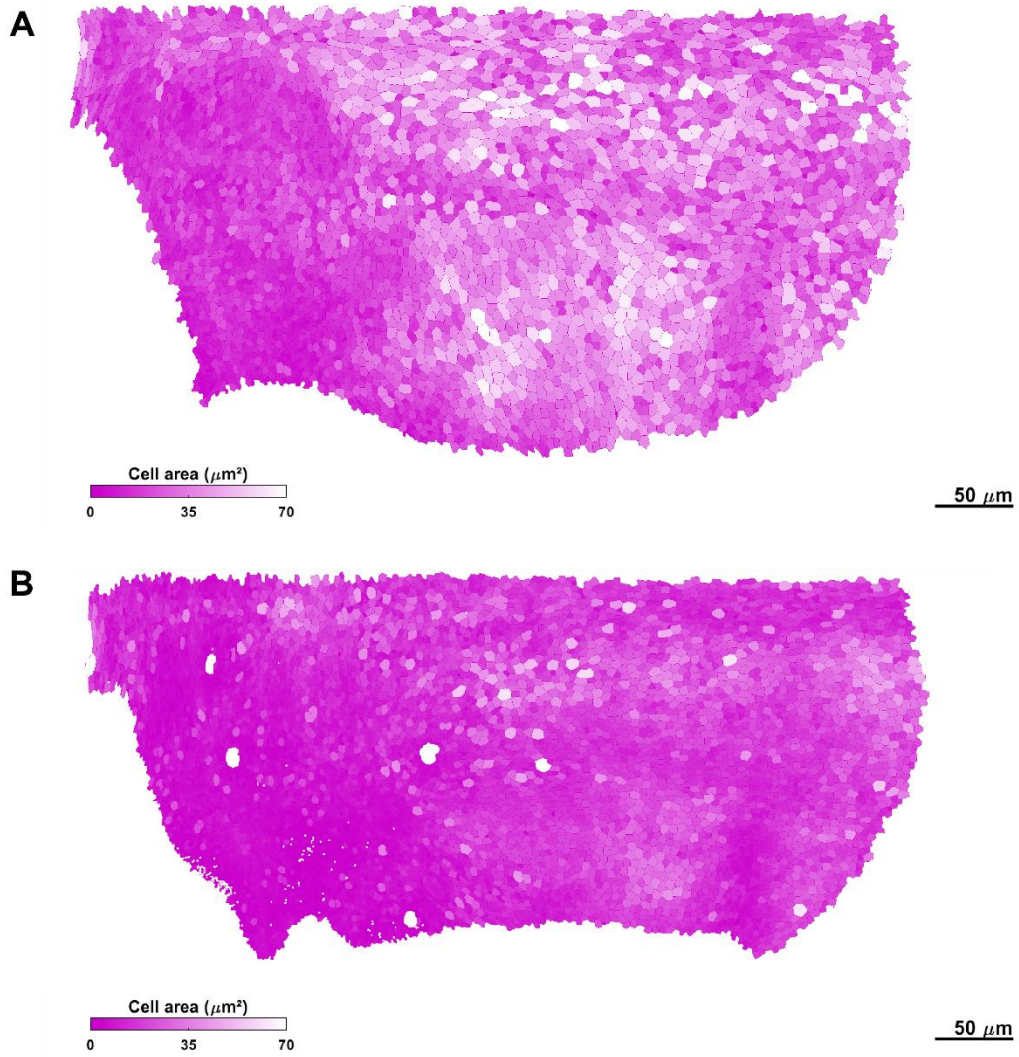
Supplementary Figures**Supplementary Figure 1. Spatial distribution of apoptosis in the notum.**

Spatial distributions of apoptoses in N=4 half-nota (shown in blue, red, green, and black). For each half-notum, the apoptosis distribution between 15 and 29 hAPF (see Figure 1C) was rescaled so that all animals are aligned to one another, using spatial landmarks (the midline and 4 macrochaetes).



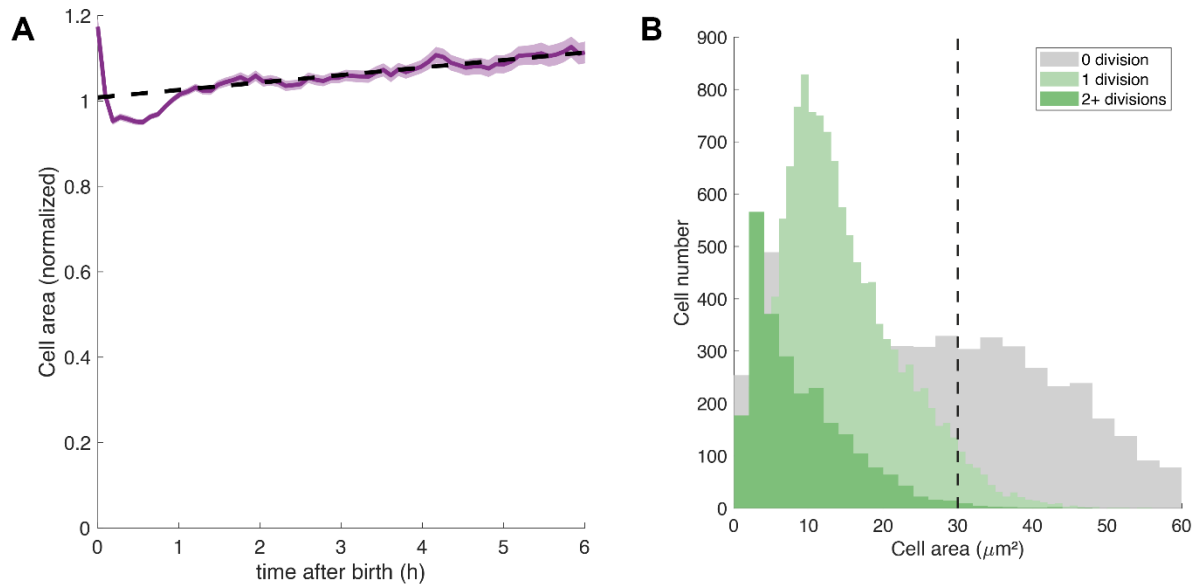
Supplementary Figure 2. Expression of *miRHG* only has a mild impact cell apical size.

(A) Notum expressing Ecad:GFP and clonal expression of *miRHG* (magenta), which inhibits the expression of the pro-apoptotic genes *hid*, *reaper* and *grim*. 16 hAPF. Scale bar: 50 μm . (B) Same notum, segmented, with the *miRHG* clones shown in blue and the *wt* cells symmetric to the clones with respect to the midline shown in green. Scale bar: 50 μm . Yellow dots: macrochaetae. (C) Time evolution of cell apical area in *miRHG* clones (black, $n = 1968$, $N = 1$, mean \pm SEM) and control (grey, $n = 2167$, $N = 1$, mean \pm SEM). Control cells are the *wt* symmetric cells.



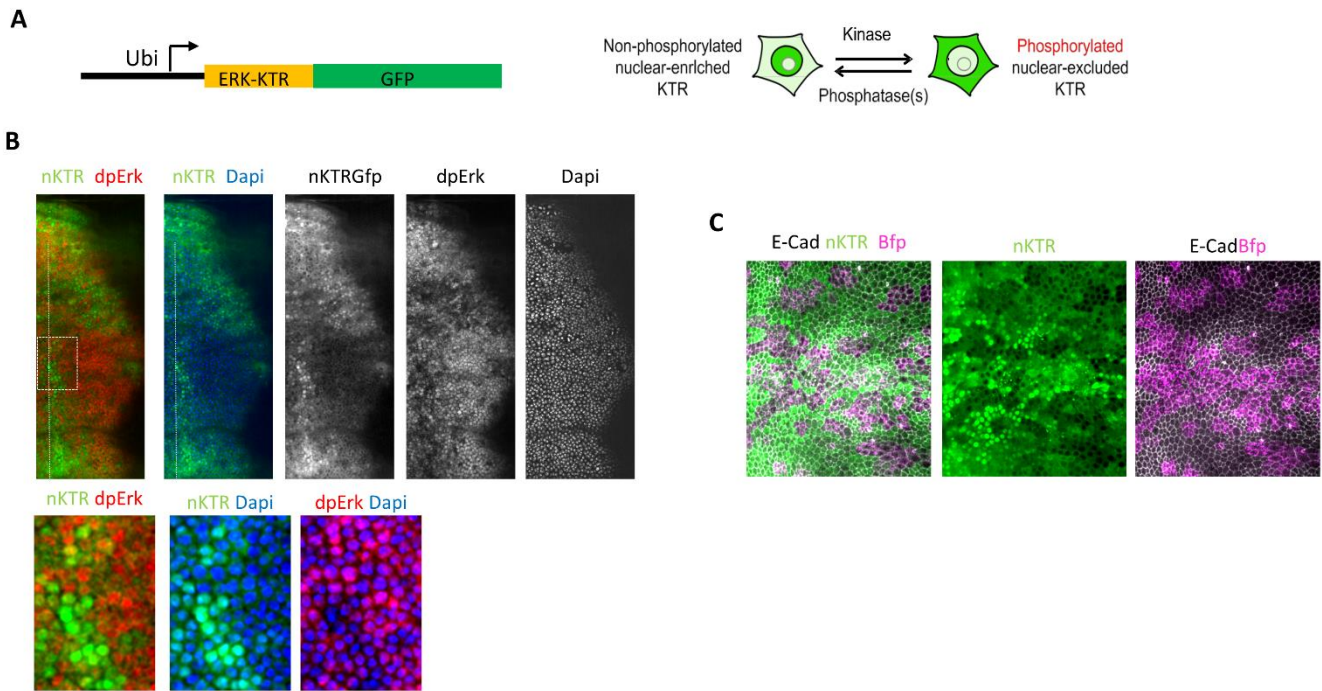
Supplementary Figure 3. Map of cell apical areas in the tissue.

(A) Segmented notum at 15 hAPF where cells are color-coded depending on their apical area. (B) Same as (A) at 25 hAPF. Scale bars: 50 μm .



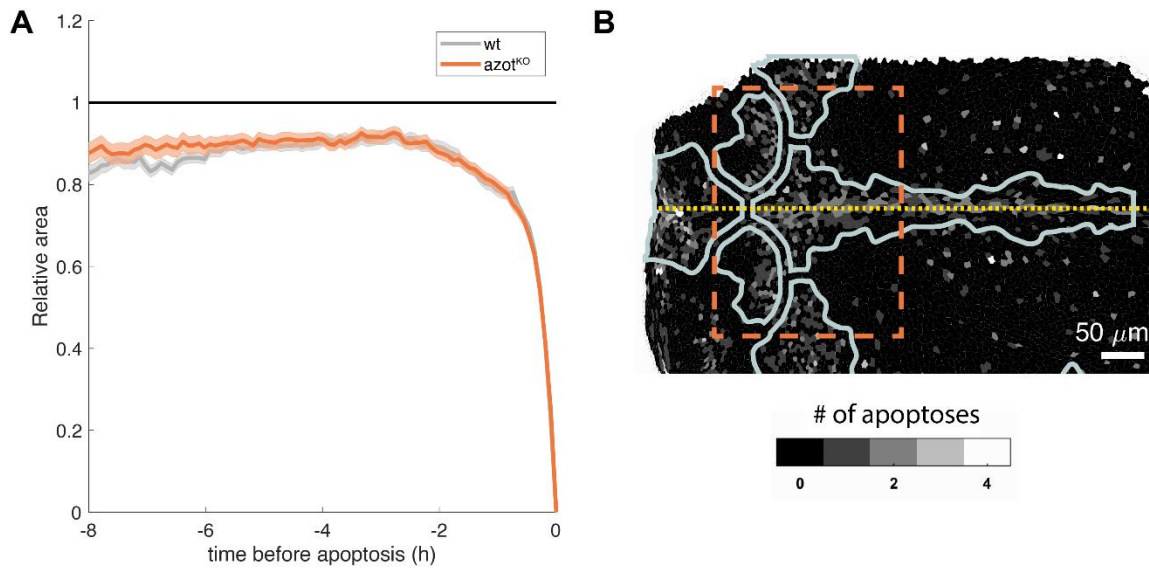
Supplementary Figure 4. Apical area of cells: impact of growth and proliferation.

(A) Apical area of $n = 400$ non-apoptotic cells versus the time after their birth. Areas are normalized. Dashed line: linear regression on values after 1h of life, $y = 1.01 + 0.02x$, $R^2 = 0.86$. Mean \pm SEM. $N = 4$ half-nota. (B) Histograms of the average apical area of cells depending on the division wave they are born from (grey: 0 division, light green: 1 division, dark green: more than 2 divisions). The apical areas are averaged over the lives of cells minus the last hour. Black dashed line: $30 \mu\text{m}^2$.



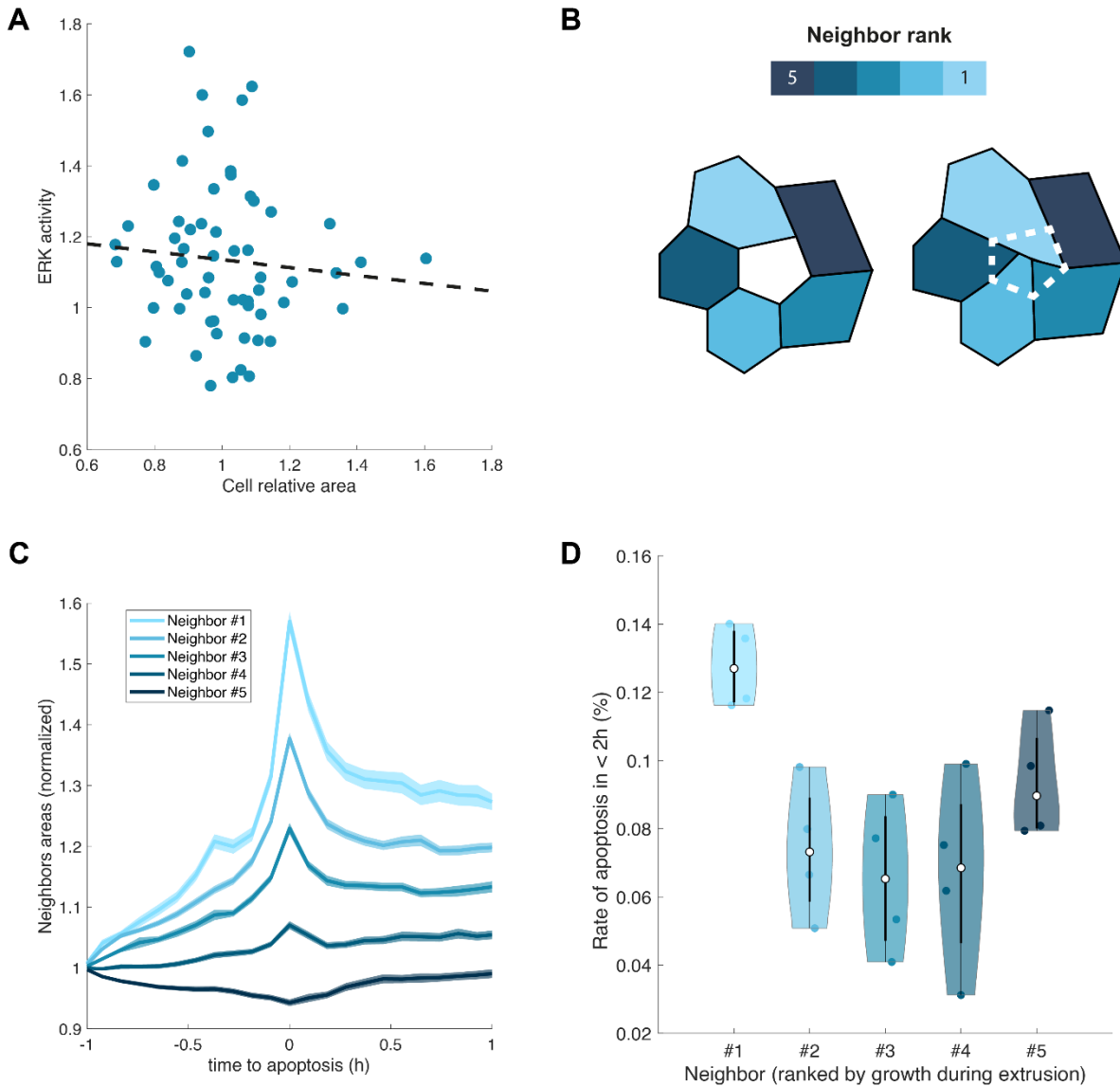
Supplementary Figure 5. Validation of a new live sensor for ERK.

(A) Schematic of the nKTR::GFP construct. Right cartoon: expected localisation of nKTR::GFP. The sensor accumulates in the nucleus when ERK is not activated, and in the cytoplasm otherwise. Taken from (de la Cova et al., 2017). (B) z-projection of immunostainings of a pupal notum (24 hAPF, top) and Close-up views (bottom) stained for nKTR::GFP (anti-GFP, green), dpERK (red), and DAPI (blue); a, anterior; p, posterior; dashed line, midline. (C) Live pupal notum (E-Cad::mKate,white) with clones overexpressing RasV12 (magenta). Activation of Erk (GFP, green) in clones is shown.



Supplementary Figure 6. Inhibition of *azot* and absence of impact on apoptosis.

(A) Relative apical area of apoptotic cells in the scutellum versus time before their death, in *azot* (orange, n=533 cells from N=2 nota, mean \pm SEM) versus wild-type (grey, n=1198 cells from N=4 nota, mean \pm SEM). Cells are aligned to their time of apoptosis (right side of the graph). (B) Segmented *azot* notum, where cells are color-coded depending on the number of apoptoses in their progeny (black: no apoptosis, white: 4 and more apoptoses). Thick grey lines: apoptosis pattern. Yellow dotted line: midline. See Figure 1D for comparison. Orange dashed rectangle: scutellum. Scale bar: 50 μ m.



Supplementary Figure 7. ERK activity and neighbor stretching during apoptosis.

(A) ERK activity versus cell relative apical area in $n = 60$ cells. ERK activity and cell relative area are averaged over 30 minutes of cells' lives. Measurements are made around 24 hAPF in the posterior half of the notum. Dashed line: linear fit ($p = 0.48$, $R^2 = 0.0085$). $N = 4$ nota. (B) Schematic representation of neighbors stretching during apical extrusion. (C) Apical areas of the neighbors of extruding apoptotic cells during apoptosis, normalized. For each apoptosis, the neighbors are sorted depending on their area increase during extrusion (in descending order, with #1 neighbors being the highest-growing neighbors). Neighbors of apoptotic cells are then binned depending on their rank. $n = 2678$ apoptotic cells, $N = 4$ half-nota. Mean \pm SEM. (D) Rate of apoptosis in the next 2 hours following an extrusion, for the neighbors of the initially extruding cells. Neighbor cells are sorted depending on their area increase during extrusion (see (C) for description and color code).

Chapter 3

Early 3D Geometry in the Posterior Notum

Contents

3.1	Introduction	89
3.2	Contributions	90
3.3	3D segmentation of the posterior notum	90
3.3.1	Segmentation method	90
3.3.2	Results	92
3.4	Study of 3D cell shapes	93
3.4.1	Geometric features of interest	93
3.4.2	Notum cells under the apical surface	96
3.5	Characteristics of cells with apoptosis-related geometries	98
3.5.1	Cells with small apical areas	98
3.5.2	Cells with small relative apical areas	99
3.6	Discussion	104

3.1 Introduction

In the previous chapter, we uncovered a key role for cell apical geometry in the control of epithelial apoptosis. Future apoptotic cells are both small in the tissue and smaller than their neighbours, and these 2D geometric characteristics impact

their survival via the activity of well-known signalling pathways. Although the study of the apical plane provides great insights to our understanding of the behaviour of simple planar epithelia, tissues have a certain thickness and extend below the apical surface. This motivated us to analyse the 3D shape of notum cells with the aim of complementing our results and answering this question: do the 2D characteristics of apoptotic cells reflect 3D geometric differences?

In this chapter, we describe our methodology and preliminary results. Unless specified otherwise, the term "depth" refers to the depth along the apico-basal axis, and "plane" to a two-dimensional plane orthogonal to the apico-basal axis (as is the apical plane for example).

3.2 Contributions

Co-contributors:

Floris Bosveld*, Chloé Roffay, Stéphane Rigaud, Boris Guirao[◊] and Yohanns Bellaïche[◊].

I defined the 3D geometric features of interest, developed tools to extract these features from the segmentation and performed analyses on the dataset. Floris Bosveld* contributed equally to this work by performing the 3D imaging of the developing notum and segmenting the cells in a large posterior region. Chloé Roffay and Boris Guirao developed the segmentation pipeline, as well as tools to display the segmentation output as seen in **Figure 3.2**. Stéphane Rigaud helped with the development of computational tools and of an alternative 4D segmentation pipeline. Boris Guirao[◊] & Yohanns Bellaïche[◊] contributed equally to this work by conceiving and supervising the project.

3.3 3D segmentation of the posterior notum

3.3.1 Segmentation method

In order to analyse the 3D shape of cells, we developed a semi-automated 3D segmentation pipeline whose principle is described in **Figure 3.1**.

First, the pipeline requires user input to acquire the cell contours at different depths along the apico-basal axis. On a 3D image of an epithelium where cells

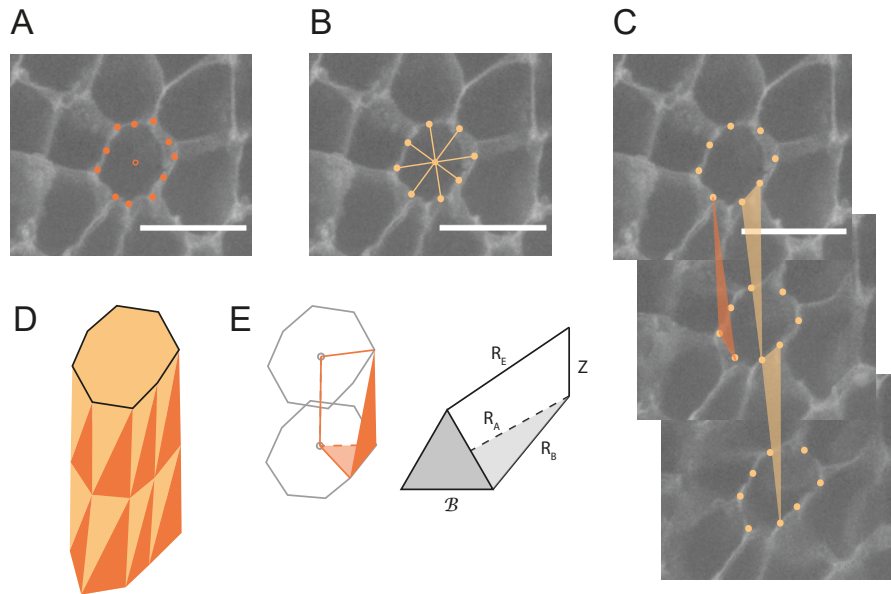


Figure 3.1 *3D segmentation method.* (A) 2D image of a notum cell whose membranes are labelled using *E-Cadherin:GFP* and are clicked in several points (orange dots). The point coordinates are used to calculate the position of the cell centroid (orange circle). (B) Same cell with 8 points computed at a constant angular distance from each other along the cell contour (yellow dots). (C) This operation is repeated at each plane where the cell is visible, and the points are connected to form triangular facets along the lateral membrane. (D) Schematic representation of the 3D reconstruction of a cell segmented along 3 different planes using 8 points per plane. (E) Schematic representation of the volume element associated with a triangular facet connecting segmentation points in a cell (left) and close-up (right). Scale bars: 25 μm .

membranes are labelled with a fluorescent marker, the pipeline user makes a series of clicks around the cell contour on each plane where the cell is visible, starting with the apical plane (**Figure 3.1A**). The cell centroid in the plane can then be calculated as the barycenter of these clicked points. Second, at each plane, the pipeline computes a fixed number of points (typically 50 to 100 points) along the cell perimeter defined by the clicked points. The computed points are chosen at constant angular distance from each other with respect to the cell centroid (**Figure 3.1B**). Third, the computed points are connected between consecutive planes as shown in **Figure 3.1C**, forming triangular facets which, together, define the lateral cell membrane (**Figure 3.1D**).

3.3.2 Results

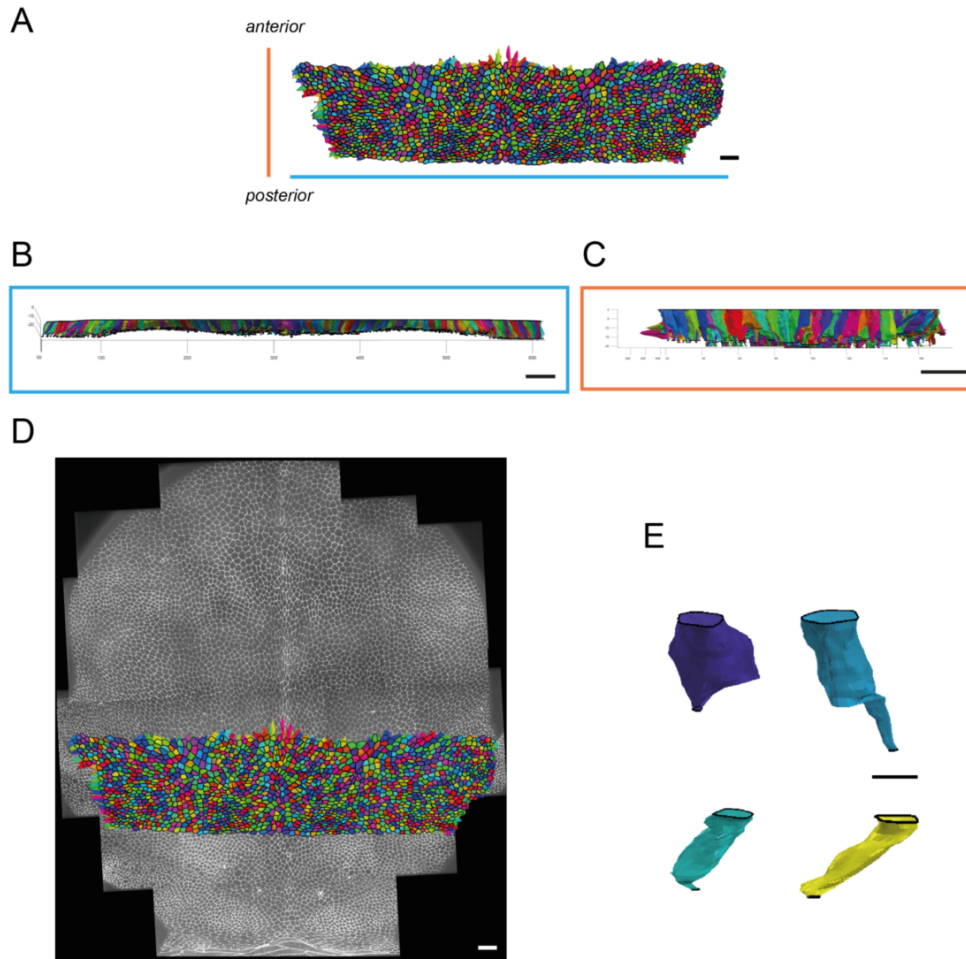


Figure 3.2 *Segmented posterior notum.* (A-C) 3D reconstructions of all the segmented cells, as seen (A) from the apical side, (B) along the left-right axis and (C) along the antero-posterior axis. The cell apices can be found at different depths in the tissue, but are brought back to the same plane for visualisation purposes. Scale bars: 25 μm . (D) Segmented region overlaid on the equivalent region of another notum at 13 hAPF where membranes are labelled using *E-Cadherin:GFP*. Scale bar: 25 μm . (E) 3D reconstruction of sample segmented cells. Scale bar: 10 μm .

The segmentation pipeline was used to segment a region of more than 1500 cells at a given time point, corresponding approximately to 13 hAPF. This region is located in the posterior notum, at the scutum-scutellum boundary (Figure 3.2A-D).

A quick evaluation of the 3D shape of cells in this region shows that the typical cell has a larger apical than basal surface. The cells can display various 3D morphologies but often end up stretched in a thin basal extension (**Figure 3.2E**).

These adjacent cells at 13 hAPF represent a large dataset of cell positions and 3D morphologies. In the following sections, we focus our attention on the analysis of this dataset. Our work illustrates how this novel approach can be used to characterise new features of cells and tissues.

3.4 Study of 3D cell shapes

3.4.1 Geometric features of interest

In order to analyse the 3D shape of cells, we first defined geometric features at the single-cell level which can be extracted from the segmentation. These features are the following ones (**Figure 3.3**):

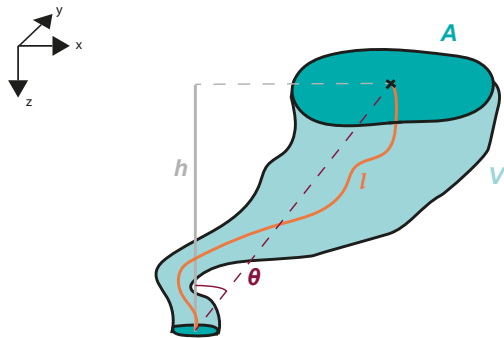
- The cell volume V , in μm^3 . The cell volume is calculated as the sum of the volume elements associated with each triangular facets of the segmentation (**Figure 3.1E**): $V = \sum_{k=1}^F V_k$, where F is the total number of facets. To calculate V_k , the volume element associated with facet k , we integrate its section area parallel to the triangular base (light grey in **Figure 3.1E right**) along the element's vertical axis. This vertical axis of length Z joins the centroids of the two consecutive planes which are linked by the facet. We use Heron's formula to calculate the areas of the triangular sections and, after integrating, we end up with the following formula:

$$V_k \simeq \frac{ZR_E\sqrt{\alpha}}{4} \left(1 + \frac{\beta}{3} + \frac{\gamma}{4}\right), \quad (3.1)$$

where $\alpha = (\mathcal{B} + R_B - R_A) \times (\mathcal{B} + R_A - R_B)$, $\beta = \left(\frac{R_A+R_B}{R_E} - 2\right)$ and $\gamma = \frac{(R_A+R_B-2R_E)^2 - \mathcal{B}^2}{4R_E^2}$ (see **Figure 3.1E** for the notations).

- The cell apical area A , in μm^2 . With $\mathbf{x}_0, \mathbf{x}_1, \dots, \mathbf{x}_n$ the positions of the contour points in the apical plane such that $\mathbf{x}_n = \mathbf{x}_0$, $A = \frac{1}{2} \sum_{k=0}^{n-1} \|\mathbf{x}_k \times \mathbf{x}_{k+1}\|$ (inspired by [Ishihara and Sugimura 2012](#)).
- The cell height h , in μm , defined as the depth the cell reaches in the tissue along the apico-basal axis.

- The cell length l , in μm . It is calculated as the sum of the distances between cell centroids in two consecutive planes.
- The cell in-plane extension, $\frac{l}{h}$, dimensionless. The cell length can differ from the cell height if the cell deviates from a simple cylinder-like shape oriented along the apico-basal axis. The ratio $\frac{l}{h}$ measures this deviation from an apico-basal cylindrical shape.
- The cell tubularity T , dimensionless. $T = \frac{l}{\sqrt{\mu(A_z)}}$, where $\mu(A_z)$ is the average cross-sectional area along the apico-basal axis. T is typically low for a squamous cell and high for a long, columnar cell.
- The cell z-Area Variation zAV , dimensionless. $zAV = \frac{\sigma(A_z)}{\mu(A_z)}$, where $\sigma(A_z)$ is the standard deviation of the cross-sectional areas along the apico-basal axis.
- Finally, the cell tilt angle θ , in radians. With \mathbf{v} the projection in the apical plane of the vector joining the apical and basal centroids, $\theta = \arctan \frac{\|\mathbf{v}\|}{h}$.



V	Volume (μm^3)	A	Apical area (μm^2)	h	Height (μm)	l	Length (μm)
T	Tubularity $= l / \sqrt{\mu(A_z)}$	zAV	z-Area Variation $= \sigma(A_z) / \mu(A_z)$	θ	Tilt angle (rad)		

Figure 3.3 *Some relevant cell geometric features in 3D. See text for a full description.*

For each segmented cell, we can calculate this set of quantities. We can then represent the relationships between any two quantities in the full dataset in the form of a matrix of pairwise scatter plots (**Figure 3.4**). This is useful to see how

geometrical features correlate with each other in the segmented region, which we will further interpret in the following sections.

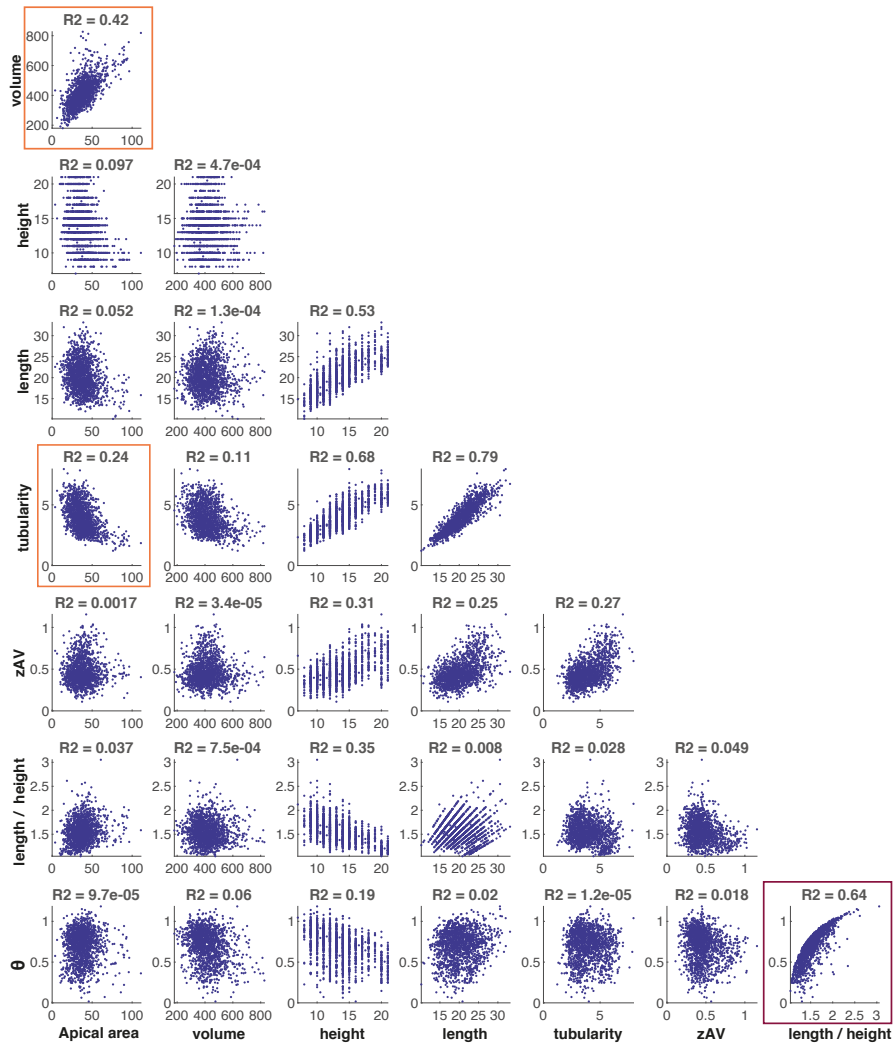


Figure 3.4 Pairwise scatter plots of cell geometric features. The y-axis variables are listed on the left of the first column of plots, while the x-axis variables are listed on the bottom of the last row of plots. For each pair of variables, the coefficient of determination R^2 of the linear regression between the two variables is indicated above the scatter plot. Plots which are in rectangular boxes (orange, dark red) are further discussed in the main text.

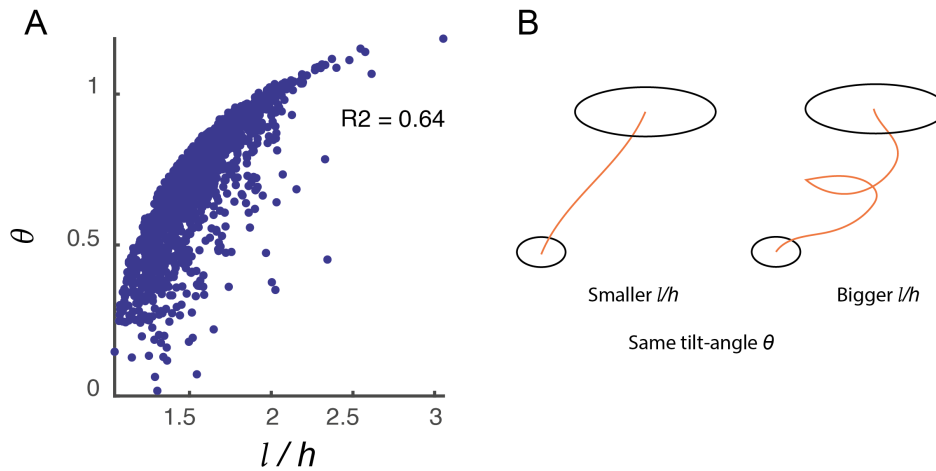


Figure 3.5 *Cell tilt angle versus in-plane extension.* (A) Scatter plot of θ versus l/h . (B) Simplified drawing of two cells with same apical and basal surfaces, same heights and same tilt angle θ , but different shapes corresponding to different in-plane extensions. Left: straight cell for which l/h correlates very well with θ ; right, twisted cell for which l/h does not correlate with θ .

3.4.2 Notum cells under the apical surface

What is the posterior epithelium like in 3D? Looking at **Figure 3.4**, a first observation we can make is that amongst the most correlated variables are the tilt angle θ and in-plane extension $\frac{l}{h}$. A magnified view of their scatter plot is given in **Figure 3.5A**. The correlation between these two variables indicates that notum cells are typically rather straight, as are the sample cells shown in **Figure 3.2E**, than twisted or spiralling (**Figure 3.5B**). Otherwise, an increased cell extension would not necessarily be associated with a higher tilt angle.

As a result, we can define an apico-basal orientation for each cell which, combined with the cell height h , gives a fairly accurate impression of the cell orientation in space. The cell orientation is the apical projection of the vector joining the apical and basal centroids. **Figure 3.6C** shows the vector field of cell orientations in the segmented region. We can see that cells are usually tilted: the magnitude of the orientation vectors are in the range of $10 \mu\text{m}$, indicating that the apical and basal surfaces of cells are not vertically aligned, or in other words, that cells are not perfectly orthogonal to their apical plane. This result can be seen as well from the distribution of tilt angles: their values are rarely close to 0, and in the vast majority of cells, $\theta > 0.25 \simeq \frac{1}{12}\pi$ radians. Moreover and interestingly, the orientation field is

quite smooth, as adjacent cells have similar directions and magnitudes of orientation.

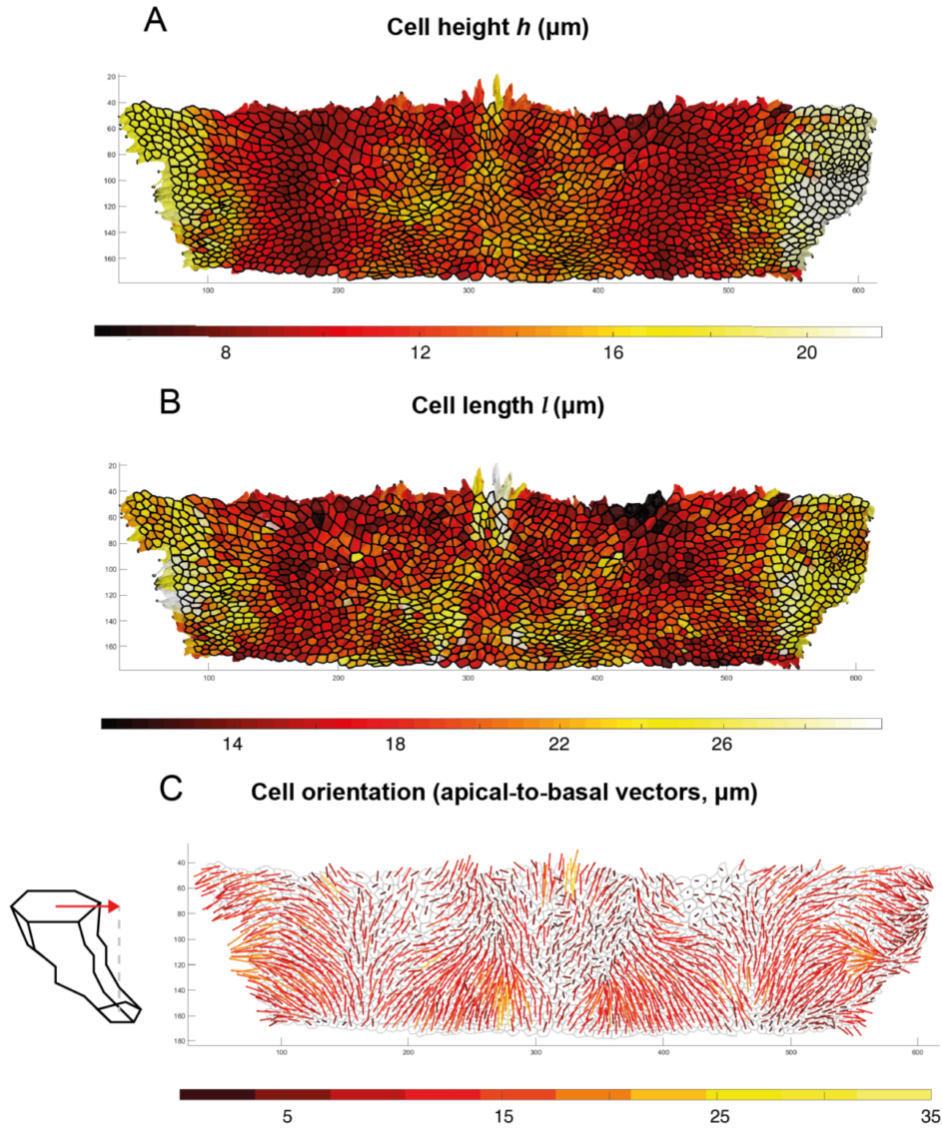


Figure 3.6 Maps of cell height, length and orientation. The midline would be a vertical line dividing the tissue in two equal parts. The x - and y -axes represent the tissue dimensions in the apical plane and are in μm . (A) Map of cell height, color-coded by intensity; (B) map of cell length, color-coded by intensity. (C) Vector field of cell orientations. A cell orientation is defined as the apical projection of the vector connecting its apical centroid with its basal centroid (see schematic representation on the left). The vectors are color-coded according to their magnitude, in microns.

We then focused on the cell height h and length l . To assess how the tissue depth changes in space, we mapped these quantities over the entire segmented region

(**Figure 3.6A-B**). We found that both quantities, and particularly h , are locally homogeneous, indicating that cells tend to have the same height as their neighbours. As a result, cells in a same sub-region align together, which would allow us to define a rather smooth basal surface.

Furthermore, the cell height, orientation, and to a lesser extent the cell length, display patterns which are symmetric with respect to the tissue midline, a clear indication that we are not measuring noise.

3.5 Characteristics of cells with apoptosis-related geometries

In the 2D apical plane, we found that apoptotic cells are characterised by specific geometric features, namely a small area and a small relative area. We also uncovered molecular mechanisms by which these 2D geometric features are connected with the cell's survival.

In order to identify possible features of apoptotic cells in 3D, which could ultimately deepen our understanding of the biophysical mechanisms regulating apoptosis, we analysed the relationships between cell area and other geometric features. The results are described in Section 3.5.1. We also compared cells with their neighbours, by calculating their relative geometric features, and linked these relative features with the relative apical area (Section 3.5.2).

3.5.1 Cells with small apical areas

Observation of the pairwise relationships between cells's geometric features in **Figure 3.4** shows that the two quantities which are the most correlated with the cell apical area are the cell volume V ($R^2 = 0.42$, positive correlation) and the cell tubularity T ($R^2 = 0.24$, negative correlation). All other geometric quantities have a coefficient of determination R^2 that is lower than 0.1. This suggests that there could be two ways for a posterior notum cell to have a small apical area: it could either have a small volume, or have a high tubularity (and a columnar shape).

Indeed, regions of small apical areas seem to correlate with regions of small volume, or large tubularity, or both (**Figure 3.7**). Conversely, regions where cells have large apical areas seem to correspond to regions where cells have a big volume and/or a small tubularity. Furthermore, these three quantities are patterned symmetrically

with respect to the midline, as are the cell height, length and orientation (**Figure 3.6**).

To estimate the strength of the relationship between cell area, volume, and tubularity, we fitted a linear regression model for A as a linear function of V and T (Table 3.1).

Table 3.1 *Linear regression model for cell area A*

	Estimate	Standard error	t-Stat	p-Value
Intercept	19.5	1.69	11.6	8.89e-30**
Volume	0.0785	2.77e-03	28.3	1.04e-141**
Tubularity	-3.59	0.225	-16.0	2.55e-53**
R^2	0.507	No. obs	1494	

* $p < 0.05$, ** $p < 0.01$.

We verified that both the volume and tubularity are indeed significantly ($p < 0.01$) correlated with the cell area, and that the coefficients are positive for V and negative for T . The coefficient of determination R^2 is equal to 0.507, indicating that 50% of the total variability of cell apical area is explained by a linear combination of the volume and tubularity.

Overall, our results indicate that cells with small apical areas (which we previously found are at a higher probability to die) typically tend to have small volumes, or to be more tubular, compared to the rest of the tissue.

3.5.2 Cells with small relative apical areas

We then studied the geometry of a cell relative to its neighbours. In 3D, establishing neighbour relationships is more challenging than in 2D. For a cell whose apical centroid is C and whose radius is $R = \sqrt{\frac{A}{\pi}}$, the neighbours were defined as the cells whose apical centroids were at a distance of less than $3R$ from C . For a cell i , for any given geometric quantity Q , we could then calculate its value relative to the cell neighbours:

$$\mathcal{R}(Q)_i = \frac{Q_i}{\mu(Q_j)} \quad (3.2)$$

where $\mu(Q_j)$ is the average value of quantity Q in the neighbours of cell i . In the same manner as with absolute geometric features, we can then represent the relationships between any two relative geometric quantities (**Figure 3.8**).

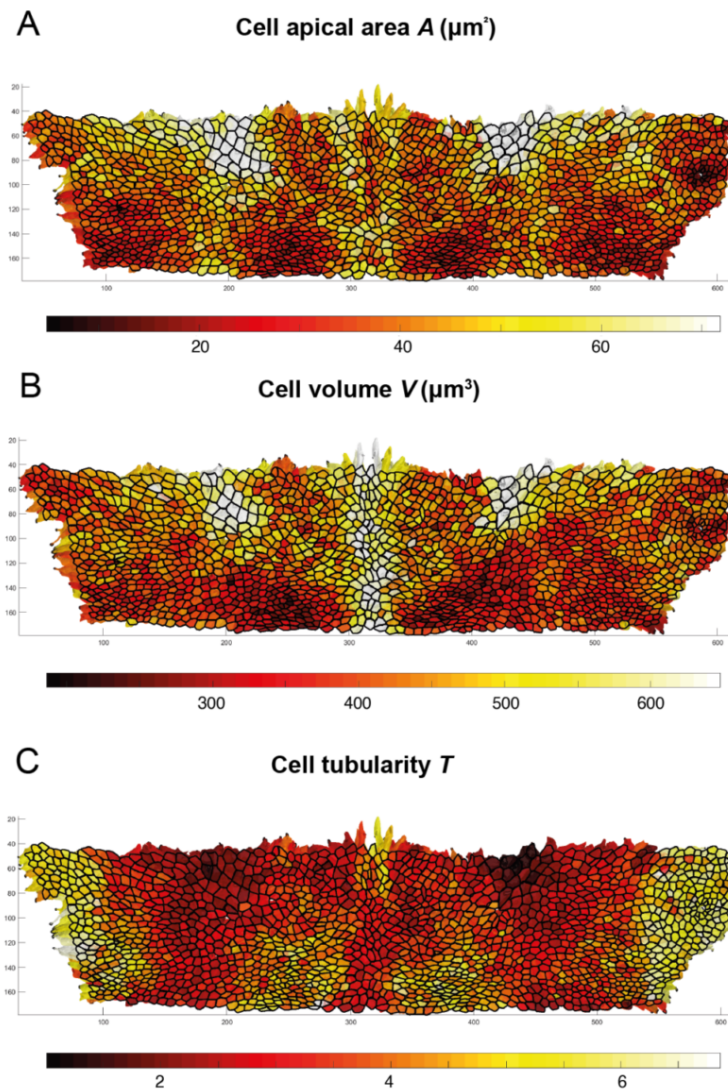


Figure 3.7 Maps of cell area (**A**), volume (**B**) and tubularity (**C**), color-coded by intensity. The midline would be a vertical line dividing the tissue in two equal parts. The x- and y-axes represent the tissue dimensions in the apical plane and are in μm .

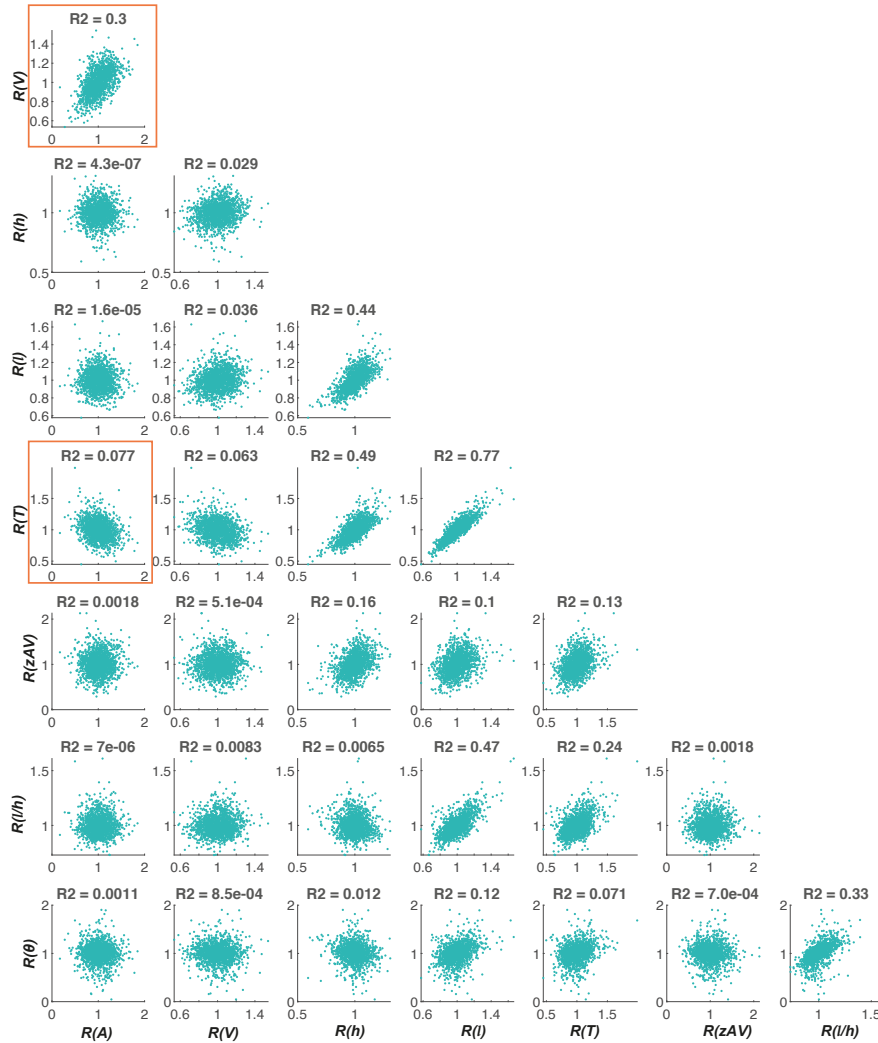


Figure 3.8 *Pairwise scatter plots of cell relative geometric features. $\mathcal{R}(Q)$ is the relative quantity Q compared to the neighbours. The y-axis variables are listed on the left of the first column, while the x-axis variables are listed on the bottom of the last row. For each pair of variables, the coefficient of determination R^2 of the linear regression is indicated above the scatter plot.*

On average, future apoptotic cells have a smaller apical area than their neighbours, and this is true early in their lives. Thus, we wondered which relative geometric quantities correlate the most with $\mathcal{R}(A)$. The best correlated feature is the relative cell volume $\mathcal{R}(V)$ ($R^2 = 0.3$). The next best correlated feature is the relative cell tubularity $\mathcal{R}(T)$, although the correlation is weak compared to the correlation between A and T ($R^2 = 0.077$). All other geometric quantities have a coefficient of determination R^2 that is less than 0.002. Overall, differences in apical areas between neighbour cells could partly reflect differences in volume or, to a lesser extent, differences in tubularity.

We performed a linear regression fitting $\mathcal{R}(A)$ as a linear function of $\mathcal{R}(V)$ and $\mathcal{R}(T)$ (Table 3.2). Both variables were found to significantly correlate with the cell relative area ($p < 0.01$). However, as expected from the smaller R^2 of the relationship between $\mathcal{R}(A)$ and $\mathcal{R}(T)$, the model explained less of the variability of $\mathcal{R}(A)$ ($R^2 = 0.324$) than the previous linear regression did for A .

Table 3.2 *Linear regression model for cell relative area $\mathcal{R}(A)$*

	Estimate	Standard error	t-Stat	p-Value
Intercept	0.388	0.0522	7.43	1.83e-13**
$\mathcal{R}(V)$	0.823	0.0352	23.4	2.11e-103**
$\mathcal{R}(T)$	-0.204	0.0305	-6.70	3.00e-11**
R^2	0.324	No. obs	1494	

* $p < 0.05$, ** $p < 0.01$.

Next, since apoptotic cells are characterised by smaller-than-average relative apical areas, we focused our attention on cells whose apical sizes greatly differ from the sizes of their neighbours. We defined cells with "extreme" relative areas as cells for which $\mathcal{R}(A)$ is either lower than 0.8, on the lower side, or greater than 1.2, on the greater side. Overall, the apical areas of these cells differ from their neighbours' ones by at least 20%.

We analysed the distributions of the relative geometric features $\mathcal{R}(Q)$, $Q \in V, T, \dots$, in these cells with extreme relative areas, and compared them with the general distributions of the same features in all cells. In accordance with our previous results, we found that cells which are substantially smaller (or bigger, respectively) in apical area than their neighbours tend to have a significantly smaller relative volume $\mathcal{R}(V)$, and bigger tubularity $\mathcal{R}(T)$, than normal (or a smaller $\mathcal{R}(T)$ and bigger $\mathcal{R}(V)$, respectively) (**Figure 3.9**; p-values for significance are shown in the legends).

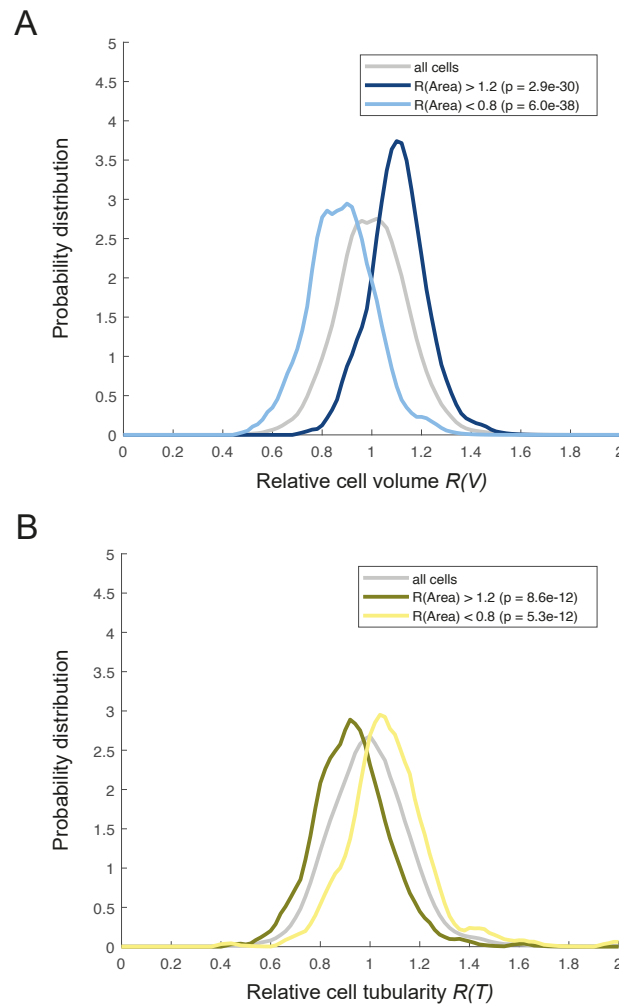


Figure 3.9 Probability distributions of (A) $\mathcal{R}(T)$ and (B) $\mathcal{R}(V)$ for cells with extreme relative areas. The grey curve indicates the probability distribution for all cells, independent of their relative areas. For cells apically smaller (light curve) or bigger (dark curve) than their neighbours, the legend indicates the p -value of a Student's t -test comparing the mean $\mathcal{R}(Q)$ in the cells in question with the mean $\mathcal{R}(Q)$ in all cells (grey curve).

In contrast, the distributions of the other relative quantities are not significantly different in cells with extreme relative areas (**Figure 3.10**).

Finally, we wondered how many of the cells with small relative areas, which would present a higher risk to die, fall either in the category of cells with small relative volumes or in the category of big relative tubularities. To answer this question, we focused on the cells at least 20%-smaller than their neighbours ($\mathcal{R}(A) < 0.8$). We found that 83% of these cells are smaller in volume than their neighbours ($\mathcal{R}(V) < 1$), while 71% of them are more tubular than their neighbours ($\mathcal{R}(T) > 1$). In only 6% of the cells in total, $\mathcal{R}(V) > 1$ and $\mathcal{R}(T) < 1$ (**Figure 3.11**). Cells in this latter group, whose small apical size cannot be explained by a smaller general volume or a more elongated shape, generally are quite round under the apical surface; an example is shown in **Figure 3.2E** (top left cell in dark blue).

3.6 Discussion

In this study, we used a semi-automated segmentation tool to segment a wide stripe of approximately 1500 cells in the posterior notum at one time point of its early development (13 hAPF). We defined and extracted geometric features of interest from the resulting dataset and analysed the general 3D shape of cells. We found that cells are typically straight and not twisted, and get thinner towards their basal side. They also tend to be tilted and not orthogonal to their apical plane.

Interestingly, cell height and cell orientation are both locally homogeneous: cells in a same sub-region are approximately the same height and are tilted in the same direction. This could result from intercellular interactions between neighbouring cells. For instance, volume exclusion between adjacent cells could locally align them in similar directions. Epithelial cells form adherent bonds on their lateral surfaces which mediate mechanochemical signalling with their neighbours, and this signalling could contribute to regulating the height of their lateral sides in a self-organising manner. Alternatively, we saw in the Introduction of this thesis (Section 1.1.2) that cell geometry can be controlled by external cues. Here, the 3D environment of cells, such as the characteristics of the basal ECM or the apical cuticle, or the patterning at the tissue scale of molecular cues, could modulate the 3D shape of cells. In addition, we found that the patterns of cell area, volume, tubularity, height, length and orientation (**Figures 3.6 and 3.7**) are all symmetric with respect to the midline. This observation could support the idea of a regulation of cell geometry at the tissue

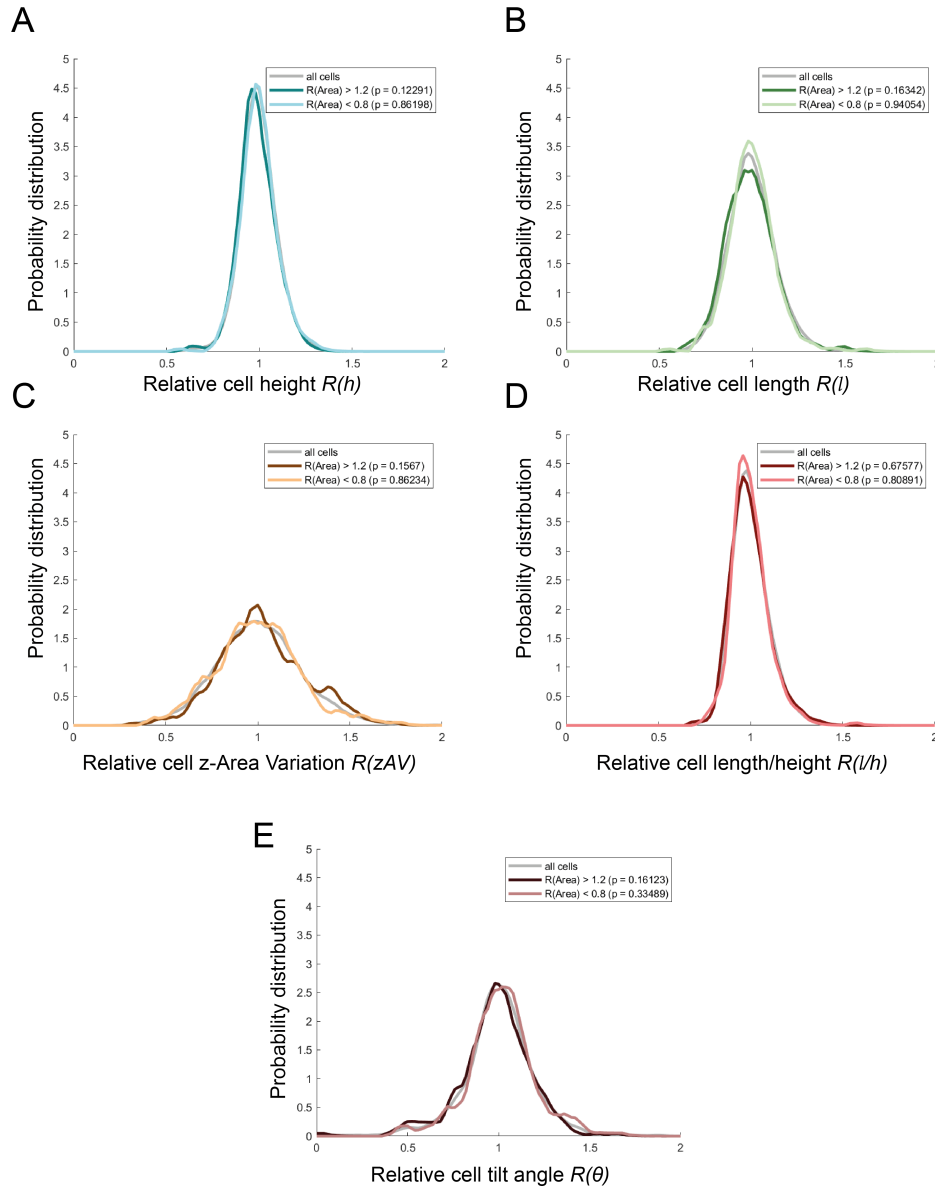


Figure 3.10 Probability distributions of $\mathcal{R}(h)$, $\mathcal{R}(l)$, $\mathcal{R}(zAV)$, $\mathcal{R}(l/h)$ and $\mathcal{R}(\theta)$ for cells with extreme relative areas. The grey curve indicates the probability distribution for all cells, independent of their relative areas. For cells apically smaller (light curve) or bigger (dark curve) than their neighbours, the legend indicates the p -value of a Student's t -test comparing the mean $\mathcal{R}(Q)$ in the cells in question with the mean $\mathcal{R}(Q)$ in all cells (grey curve). All p -values are greater than 0.1.

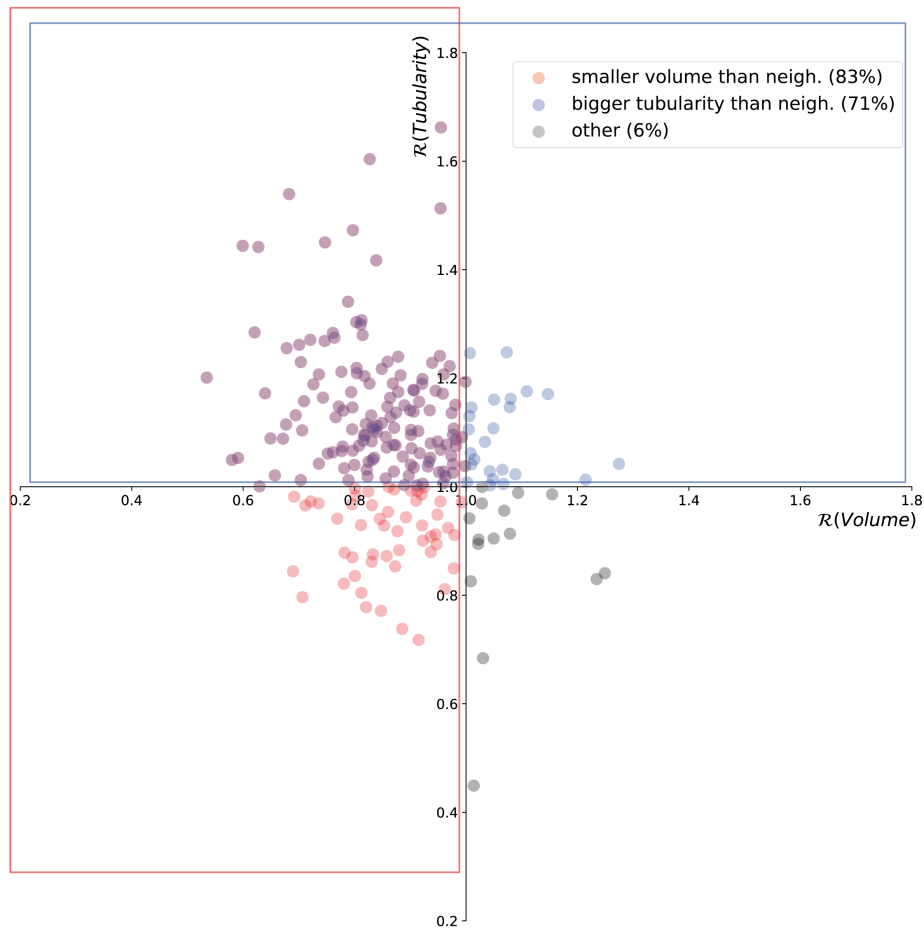


Figure 3.11 *Relative volume and tubularity of cells with small relative areas ($\mathcal{R}(A) < 0.8$). Red dots: $\mathcal{R}(V) < 1$; blue dots: $\mathcal{R}(T) > 1$; purple dots: both; grey dots: neither.*

level, although it is not incompatible with the emergence of self-organising processes in the inherently symmetric fly embryo.

We then turned our attention to the apical area and relative apical area of cells, as these two geometric features have been linked to apoptosis in Chapter 2. We found that the absolute apical area correlates with the absolute cell volume and tubularity (the ratio of their height to their average cross-sectional area), while the relative apical area correlates with relative volume and relative tubularity. In particular, we found that cells which are smaller in apical area than their neighbours, as apoptotic cells generally are, are also typically smaller in volume and greater in tubularity than their surroundings (while their other relative geometric features are not impacted).

As our analysis was conducted at a single time point of tissue development, it

would be necessary to segment the same regions at multiple time points to verify if our observations hold true later in the tissue. In particular, apoptotic cells generally appear later in the tissue, after the first division wave which starts around 16 hAPF. This means that most of the cells that we analysed here will not commit apoptosis. In order to characterise the 3D geometry of possible apoptotic cells, we would need to analyse 3D cell shape after 16 hAPF.

Could apoptotic cells have specific 3D characteristics, whose elucidation would improve our understanding of the role of cell geometry in the control of apoptosis? Providing a complete answer to this question would require to segment a tissue in 4D (space and time), to perform cell tracking and detect apoptotic cells, and to analyse their features in comparison with non-apoptotic cells, as we previously did in the apical plane. Moreover, segmenting a tissue in 4D would have a more general interest to the study of tissue morphogenesis. The stress inference technique (described in Section 1.2.3.2), which allows to infer the relative pressure and junctional forces in a tissue, can be applied to 3D cell configurations. Thus, provided that a segmentation is accurate enough to extract the cell curvatures and junction angles, we could analyse how the patterns of pressure and forces change over time. Moreover, we developed a pipeline which relates tissue deformations to cellular processes and which can be used to analyse 3D tissue dynamics (Guirao et al. 2015). Altogether, segmenting cells in 4D would give us access to their dynamics, to the mechanical constraints exerted on them, and would allow us to bridge this information with tissue morphogenesis.

Our current segmentation tool works on the basis of user-input clicks of the cell contours, which can become very time-consuming if done on a large number of cells or time points. Thus, developing a more automated segmentation method with minimal user input would be a crucial step towards the 3D study of apoptotic regulators. In parallel with the work described here, we have set the basis of a segmentation pipeline which would meet these requirements; further work will be needed to complete this pipeline and apply it to our tissue over time.

Chapter 4

Conclusion and Discussion

Contents

4.1	Biophysical regulation of apoptosis in the notum apical plane . .	110
4.1.1	Control of apoptosis by size factors	110
4.1.2	Generality of research findings	111
4.1.3	Molecular signalling: the role of Hippo and Notch	112
4.1.4	Coupling of cell division and cell death	114
4.1.5	A process of geometric cell competition?	115
4.2	Gaining deeper insight: the role of 3D geometry	115
4.2.1	Results	115
4.2.2	Possible regulations of apoptosis by 3D cell shape	116
4.2.3	Future work: going 4D	117
4.3	The role of apoptosis regulation	117

Cells have different geometries, and in particular different sizes, that affect their behaviours. Dynamic changes in cells' shape and size occur in response to internal and external controls (Section 1.1). These changes contribute to the biophysical regulation of the architecture and movements of epithelial tissues, in which forces can propagate over large scales through the tight coupling of epithelial cells. In particular, the morphogenetic movements of epithelial tissues emerge from coordinated cellular processes which often involve cell deformations (Section 1.2).

One of these cellular processes is apoptosis, a form of programmed cell death which plays a significant part in many morphogenetic events and whose molecular regulation has been extensively studied in several model organisms, including *Drosophila* (Section 1.3). Recent works investigating the biophysical control of apoptosis showed that several factors linked to tissue compaction, which impacts cell size, can influence apoptosis (Section 1.3.4.1). The emphasis now should be put on explaining the *in vivo* spatiotemporal patterning of apoptosis, as well as providing a clear picture of the interplay between genetic and mechanical inputs in the control of physiological apoptosis.

This thesis aimed at addressing these points. To do so, I used powerful quantitative methods to investigate the geometric regulation of apoptosis during epithelial development. The system we used is the fly notum, a tissue of several thousands of cells with a highly heterogeneous pattern of cell death. I conducted this work in close collaboration with biologists in the team, who acquired raw biological data and performed experiments to test our hypotheses.

4.1 Biophysical regulation of apoptosis in the notum apical plane

4.1.1 Control of apoptosis by size factors

To assess whether apoptosis could stem from normal tissue compaction, we studied the correlation between isotropic contractions of the notum and apoptosis. We found that physiological tissue compaction is neither necessary nor sufficient to trigger apoptosis in the notum. As such, compaction is unlikely to set the pattern of apoptosis. In accordance with this conclusion, when we homogeneously compressed developing pupae, apoptosis was not increased everywhere, but mainly in the apoptotic pattern. Therefore, our work provides the first direct evidence that tissue compaction can induce *in vivo* apoptosis. Furthermore, it establishes that compaction is not the main regulator of physiological apoptosis during notum development.

By contrast, we found that future apoptotic cells were characterised by two geometric factors related to their apical size: they have both a small apical area in the tissue, and a small relative area to their direct neighbours. These specific features are seen early in their lives, hours before any biological sign of apoptosis. Furthermore, the early absolute and relative apical areas of cells are predictive of

the global apoptotic pattern in the notum. By exerting uniaxial compaction on developing flies to reduce cell apical areas, we further verified that a small apical area influences apoptosis. Moreover, by generating clones of smaller *Tor^{RNAi}* cells, we found that their direct wild-type neighbours had a bigger relative area, and that this increase was associated with a stronger apoptosis rate. Overall, we propose two biophysical mechanisms that control the spatiotemporal regulation of notum apoptosis: a global, cell-autonomous one linked to apical area, and a local, non cell-autonomous one linked to relative apical area. To our knowledge, this constitutes one of the first early characterisations of physiological cell death *in vivo*, based on features seen hours before extrusion. Such an early prediction had been achieved *in vitro* by a deep learning model which could predict cell fate in co-cultures of MDCK wild-type and *scr^{KD}* cells up to 8 hours before apoptosis (non peer-reviewed work, [Soelistyo et al. 2021](#)).

4.1.2 Generality of research findings

Our prediction model, which uses the absolute and relative apical areas of cells to predict their survival, performs less well in the highly-apoptotic anterior midline where only few apoptoses are predicted. This lesser performance is likely to stem from the atypical geometry of early midline cells, which have large apical areas associated with a strong anisotropy in the antero-posterior direction. The fact that cells in the anterior midline are highly apoptotic although they have large apical areas indicates that their apoptosis might be regulated by different mechanisms than the rest of the tissue. Consistent with this idea, caspase 3 is ubiquitously expressed in midline cells throughout dorsal closure and the early notum development, while the rest of the notum does not display such a widespread apoptotic activity ([Fujisawa et al. 2019](#)). This suggests that midline cells could be programmed to undergo apoptosis during notum development, regardless of their apical geometry or other biophysical characteristics. This global apoptosis would contribute to the proper development of the notum which is formed by the fusion of the two wing discs along the midline, in accordance with the role of apoptosis in mediating the fusion of cell sheets (Section 1.3.3).

The midline is a well-defined region of the notum where many apoptoses take place, and as such, it has been useful to the study of the link between mechanical constraints and apoptosis ([Marinari et al. 2012](#); [Levayer et al. 2016](#); [Moreno et al. 2019](#)). However, our results suggest that conclusions made in the midline cannot be

readily generalised to the rest of the notum.

To assess the generality of our own results, future work should be directed towards the study of different tissues. A recent work which studied live-cell extrusion in the developing zebrafish heart is of particular interest (Priya et al. 2020). In this tissue, cardiomyocytes extrude to seed the basal trabecular layer. Priya et al. found that contractility, which is probably linked to cell size and morphology, controls cell delamination. Notably, proliferation-induced tissue crowding is required for delamination, similarly to what we observed in the notum. Finally, Priya et al. showed that Notch signalling correlates with cell apical area and modulates cell fate by impacting contractility. Thus, it would be especially interesting to verify if the Hippo pathway plays a role in the control of cardiomyocyte delamination, and to investigate the exact role of apical size factors in this system.

4.1.3 Molecular signalling: the role of Hippo and Notch

We investigated the mechanisms by which cell absolute and relative apical areas could influence apoptosis. We verified that the activity of the MAPK/ERK pathway, a known regulator of apoptosis which has been linked to tissue compaction (Moreno et al. 2019), does not correlate with cell apical size. In contrast, YAP/Yki, a component of the Hippo pathway, scales with cell apical area (López-Gay et al. 2020) while Notch activity correlates with relative cell sizes in the chick basilar papilla (Shaya et al. 2017). This led us to investigate the role of these pathways. We found that the control of apoptosis by apical area involves Hippo signalling, while the regulation of apoptosis by relative apical area requires Notch signalling. Thus, we identified molecular pathways involved in the geometric regulation of physiological apoptosis.

It remains to verify that the activity of these two pathways is indeed impacted in conditions that change the absolute or relative sizes of cells. For instance, we should test if the intensity of the *ban-nls:GFP* marker of *bantam* activity, a transcriptional reporter of YAP, is reduced in pupae that are uniaxially compressed. We would expect this reduction, as YAP is phosphorylated in densely packed mammalian cell cultures (Dupont et al. 2011; Nardone et al. 2017); *in vivo*, the *Drosophila* homologue of YAP, Yki, is activated by mechanical strain during the flattening of ovarian follicle cells (G. C. Fletcher et al. 2018). Moreover, using a fluorescent reporter of Notch activity, we should verify that Notch signalling correlates with relative cell areas in the *Drosophila* notum as is the case in the chick papilla. An absence of correlation would indicate that cell relative size requires Notch activity to mediate apoptosis,

but is sensed by another mechanism. Also, it would be important to analyse how Notch signalling is changed in the wild-type neighbours of *Tor^{RNAi}* clones, whose relative apical areas are increased.

One mode of action of Notch signalling in cell fate decision is the process of lateral inhibition, by which Notch activity leads to cell-autonomous transcriptional repression of Notch ligands, thereby inhibiting Notch signalling in the neighbour cells (Lai 2004; Artavanis-Tsakonas and Muskavitch 2010; Sjöqvist and Andersson 2019). This process promotes opposite cell fates between neighbours. Therefore, Notch-mediated lateral inhibition could at least partially explain how relative apical areas control apoptosis. The role of Notch could be to inhibit apoptosis in the bigger neighbours of a dying cell, consistent with the occurrence of apoptotic clusters when Notch is inhibited. To test this mechanism, we should verify if inducing apoptosis in a cell (for example, by selectively activating caspase) changes the Notch activity of its neighbours and is associated with a decrease in their probability to die. A classical model of Notch-mediated lateral inhibition involves the intercellular binding of Notch with its ligand Delta (Dl), whose activity is inhibited in Notch^{ON} cells. To verify if the geometric control of apoptosis is mediated by Notch binding with Delta, we could study how the apoptosis frequency of wild-type cells around clones of *Dl^{RNAi}* cells is impacted. An alternative Notch ligand in *Drosophila* is Serrate, a homologue of the mammalian Jagged family of Notch ligands.

Inhibiting Yki activity by inhibiting Ajuba or α -actinin changes but does not suppress the correlation between cell apical area and cell death. Therefore, the regulation of apoptosis by cell apical area likely involves other molecular mechanisms independent from Yki activity. Future work should aim at identifying these mechanisms in order to get a deeper understanding of the geometric control of cell death.

Recent reports highlighted crosstalks between the Notch and Hippo pathways in the control of cell fate decisions during development (reviewed in Totaro et al. 2018; Engel-Pizcueta and Pujades 2021). These reports paint a complex, context-dependent picture of the interactions between these two pathways. It suggests that the two mechanisms we found could be connected, instead of acting in a separate and parallel manner. To analyse the interplay of Notch and Hippo signalling in the developing notum, a first direction could be to investigate if, at a given apical area, *bantam* activity correlates with cell relative apical area; if this is the case, it would be interesting to verify if the relationship between relative apical size and cell survival

is impacted in *jub^{RNAi}* or *actn^{RNAi}* clones. Also, we could analyse *bantam* activity in the context of Notch inhibition, as well as Notch activity in tissues expressing clones of *jub^{RNAi}* cells.

Overall, we uncovered two biophysical factors of epithelial apoptosis whose action is linked to activity of Hippo and Notch. We propose the following model. After division, which plays a permissive role for apoptosis (see Section 4.1.4 below), YAP/Yki activity sets an apoptotic potential proportionally to cell apical area post-mitosis. Notch modulates binary survival decisions between neighbouring cells in a relative area-dependent manner, thereby tuning the local coordination of apoptosis.

4.1.4 Coupling of cell division and cell death

Studying the biophysical regulation of notum apoptosis led us to uncover a novel interplay between cell division and cell death. It had previously been shown that stress-induced apoptosis can promote the "compensatory proliferation" of neighbouring cells (Fan and Bergmann 2008); moreover, division defects can trigger cell death to eliminate unhealthy cells. However, the influence of normal cell division on apoptosis was not characterised. Here, we found that the probability of a cell to die increases with each round of division it goes through. Furthermore, inhibition of cell division by overexpression of *tribbles* blocks apoptosis, while upregulating division by overexpressing *cycE* enhances apoptosis. Thus, cell division seems to play a key role in the control of apoptosis in the developing notum. This process of "physiological compensatory apoptosis" could contribute to the regulation of cell number, and consequently, of epithelial architecture.

When studying how division impacts cell death in the region of the apoptotic pattern, we found that caspase activity peaks in offspring cells in the first hour after division. Although this peak of caspase activity is especially strong in future apoptotic cells, it is also seen in non-apoptotic cells. This led us to propose a model where division has a permissive role for apoptosis. Nonetheless, several hours can pass between division and the final burst of caspase activity that precedes apoptosis. It remains to clarify the dynamics of caspase activation during the entire life of an apoptotic cell, how the timing of caspase activation is linked to the timing of apoptosis (something we can study using time-lag cross-correlation), and if the coupling between these two timings involves thresholds of caspase activity that would trigger death decisions.

4.1.5 A process of geometric cell competition?

We uncovered a context-dependent modulation of apoptosis in the developing notum: cells that have a smaller apical area than their direct neighbours have a higher chance to be eliminated. This process may be reminiscent of cell competition, where loser cells are eliminated when mixed with another population of winner cells. In our case, the winning/losing characteristic would be cell apical area which informs the cell survival in comparison with adjacent cells, through a mechanism mediated by Notch.

We verified that the preferential elimination of cells smaller than their neighbours does not require *azot*, which has been linked to the determination of winner fate during competition in the *Drosophila* wing disc, pupal retina, adult brain and adult gut (Merino et al. 2015). In particular, activity of the *azot* pathway is required for the competition between wild-type and Myc or Minute cells. It should be noted that other pathways can mediate cell competition: in the *Drosophila* wing disc, Myc- and Minute-induced competition also requires components of the innate immunity responses, such as Toll-related receptors and NF- κ B activation in loser cells (Meyer et al. 2014). Moreover, Notch-deficient cells in squamous mouse epithelium display supercompetition behaviours and promote the elimination of neighbouring cells, and so far, this behaviour has not been associated with *azot* activity (Alcolea and Jones 2015).

Altogether, we identified a geometric feature of epithelial cells, namely their apical area, which confers them with differential chances to survive compared to their direct neighbours. In some ways, this process is akin to a form of geometric cell competition and requires Notch signalling. A novel characteristic of the mechanism we found is that it occurs in a wild-type cell population, unlike Myc-, Minute- or *scrb*-induced competition.

4.2 Gaining deeper insight: the role of 3D geometry

4.2.1 Results

Cells are 3D objects that communicate with each other and their environment below the apical plane, through mechanosensing structures the lateral and basal mem-

branes. Differences in relative apical areas could translate differences in relative volumes, or heights, or other geometric features. Therefore, we set out to analyse 3D cell shapes in the *Drosophila* notum and to investigate their link with the 2D characteristics of apoptotic cells.

To do so, we used a semi-automated segmentation tool which allowed us to achieve the 3D segmentation of a region of approximately 1500 cells in the posterior notum at 13 hAPF. We described the single-cell and tissue morphologies in this early developing notum, such as the narrowing of cells towards their basal side or the local homogeneity and global symmetry of cell height.

Furthermore, we studied the 3D geometric characteristics of cells which have small absolute or relative apical areas, and thus would have a higher risk to undergo apoptosis in our model. We found that a small absolute apical area correlates with a small volume, and a high tubularity; similarly, a small relative apical area correlates with a small relative volume and a high relative tubularity compared to the cell neighbours. In particular, 94% of the cells that are at least 20%-smaller in apical size compared to their neighbours are either smaller in volume or more tubular than their neighbours are.

4.2.2 Possible regulations of apoptosis by 3D cell shape

Ultimately, describing the early 3D features of future apoptotic cells, as we did for their 2D geometry, could improve our understanding of how cell geometry regulates apoptosis. For example, apoptotic cells could be characterised by a small volume, and/or a smaller volume than their neighbours. During *C. elegans* oogenesis, cell volume regulates apoptosis through a hydraulic process: mechanical instabilities caused by size differences amplify these differences, thus expanding bigger cells and deflating smaller cells whose shrinkage triggers their death (Chartier et al. 2021). This interesting hydraulic control of cell death relies on the specific mechanical organisation of the nematod gonad, where all germ cells directly communicate with a central pool of cytoplasm. Nevertheless, it provides an example of how heterogeneous cell volumes could mechanically influence apoptosis.

At a constant volume, cells would likely have constant nuclear sizes since nuclear volume generally scales with cell volume (Section 1.1.3). At the same time, a higher tubularity would result in a smaller cell width, or equivalently, a smaller apical radius. Thus, the more tubular the cell, the smaller its width and the higher the possibility that the nucleus is laterally compressed. Recent works suggest that the

nucleus could sense mechanical forces and adapt genetic activity in response to cell shape changes (Kirby and Lammerding 2018; Lomakin et al. 2020). Therefore, differences in cell tubularity could result in differences of cell behaviours mediated by nuclear mechanosensing. In the eventuality where cell tubularity would be found to predict cell survival or death, it would be interesting to test the role of this mechanism.

4.2.3 Future work: going 4D

To link 3D cell shape to apoptosis, further work would be needed in order to develop a 4D (3D space plus time) segmentation tool that would allow us to segment, track and analyse cell behaviours during the morphogenesis of the notum. Additionally, cell processes such as divisions and apoptoses should be detected so as to analyse the early behaviour and geometry of future apoptotic cells. Moreover, segmenting the cell nuclei would allow us to verify if they appear to be under stronger compression in apoptotic cells as compared to non-apoptotic cells.

Furthermore, since Notch and Hippo play a role in the geometric control of cell death, it would be interesting to investigate how their activities are impacted by 3D cell features. This would help indicate which geometric factor, among cell apical area, volume and tubularity, is more likely to regulate apoptosis.

4.3 The role of apoptosis regulation

The notum exhibits a highly heterogeneous and reproducible pattern of apoptosis, which we can globally predict using the information of cell absolute and relative apical areas. Cell size heterogeneity emerges from (i) an early pattern of cell areas that already displays some heterogeneity at the tissue scale (**Supplementary Figure 2.3**), and (ii) increased division waves at the posterior side of the tissue (**Figure 2.6A**). Thus, these two patterned cell characteristics (apical area and division rate) contribute to the regulation of apoptosis at the notum scale.

The reproducibility of the apoptosis pattern raises the following question: what is the role of apoptosis in the notum?

Since apoptosis primarily eliminates cells that are small in their local environment, it could contribute to decreasing cell size heterogeneity and maintaining size homeostasis. Cells only grow moderately in the developing notum, and as a re-

sult, reducing size heterogeneity would also require the shrinkage or elimination of cells that are bigger than their neighbours. These cells on the other side of the size spectrum do not appear to be eliminated by apoptosis, but could have a higher probability to divide. To test if apoptosis is a mechanism of size homeostasis, it would be interesting to study the time evolution of size heterogeneity (and in particular, if it decreases after apoptosis starts), and to compare the cell size heterogeneity in *miRHG* clones with respect to wild-type tissues.

Apoptosis drives a number of morphogenetic processes in epithelia, by promoting tissue fusion, causing folds and bending, and impacting the mechanical properties of a tissue (1.3.3). While the morphogenesis of the notum has been thoroughly investigated until 35-40 hAPF, in particular by our team (Bosveld, Bonnet, et al. 2012; Guirao et al. 2015), less is known about its late development whose imaging is rendered difficult by out-of-plane morphogenetic events such as the growth of sensory organ precursors. The precise patterning of apoptosis in the notum could regulate the formation of late morphogenetic folds which have not been described yet. Innovative microscopy techniques, which allow the multi-view imaging of developing organisms late in time (Leroy et al. 2022), would enable us to analyse the late morphogenesis of the notum and the role of apoptosis in its regulation.

Finally, apoptosis and proliferation drive the fluidisation of elastic tissues and the emergence of liquid-like behaviours (Ranft et al. 2010; see Section 1.3.3). This process comes naturally from the fact that both these cellular events trigger topology changes and cell rearrangements, which induce the dynamic reorganisation of tissues (Guirao et al. 2015). A tissue that is more fluid may be better able to adapt to internal or external perturbations through cell dynamics, a feature which can contribute to the robustness of morphogenesis. Hence, the heterogeneous patterns of apoptosis and proliferation may reflect spatial heterogeneity in the sources of morphogenesis variations, and a greater need to robustly adapt in some regions than others. To test this idea, we could quantify the morphogenetic defects and the variability of phenotypes in *trbl^{OE}* and *cycE^{OE}* flies compared to wild-type flies, when the pupae are subject to mechanical perturbations. We previously showed that suppressing divisions by overexpressing *trbl* impacts morphogenesis and other cell processes (Guirao et al. 2015). If proliferation and apoptosis were to work together to control the robustness of morphogenesis, we would also expect *trbl^{OE}* tissues to display a wider range of phenotypic defects than wild-type when perturbed. Conversely, *cycE^{OE}* nota could be more robust to developmental variations. However,

overexpression of *cyclin E* induces other defects, such as incomplete divisions, which could represent further obstacles to the robust development of the pupa.

References

- Abbott, M. K., & Lengyel, J. A. (1991). Embryonic head involution and rotation of male terminalia require the *Drosophila* locus head involution defective. *Genetics*, *129*(3), 783–789.
- Adelmann, J. A., Vetter, R., & Iber, D. (2022). Impact of cell size on morphogen gradient precision. *bioRxiv*. <https://doi.org/10.1101/2022.02.02.478800>
- Alcolea, M. P., & Jones, P. H. (2015). Cell competition: Winning out by losing notch. *Cell Cycle*, *14*(1), 9–17.
- Ambrosini, A., Rayer, M., Monier, B., & Suzanne, M. (2019). Mechanical function of the nucleus in force generation during epithelial morphogenesis. *Developmental Cell*, *50*(2), 197–211.
- Artavanis-Tsakonas, S., & Muskavitch, M. A. T. (2010). Notch: The past, the present, and the future. *Current Topics in Developmental Biology*, *92*, 1–29.
- Arya, R., & White, K. (2015). Cell death in development: Signaling pathways and core mechanisms. *Seminars in Cell & Developmental Biology*, *39*, 12–19.
- Baetcke, K. P., Sparrow, A. H., Nauman, C. H., & Schwemmer, S. S. (1967). The relationship of DNA content to nuclear and chromosome volumes and to radiosensitivity (ld50). *Proceedings of the National Academy of Sciences*, *58*(2), 533.
- Bardet, P.-L., Guirao, B., Paoletti, C., Serman, F., Léopold, V., Bosveld, F., Goya, Y., Mirouse, V., Graner, F., & Bellaïche, Y. (2013). PTEN controls junction lengthening and stability during cell rearrangement in epithelial tissue. *Developmental Cell*, *25*(5), 534–546.

- Basan, M., Risler, T., Joanny, J.-F., Sastre-Garau, X., & Prost, J. (2009). Homeostatic competition drives tumor growth and metastasis nucleation. *HFSP Journal*, 3(4), 265–272.
- Beadle, G. W., Tatum, E. L., & Clancy, C. W. (1938). Food level in relation to rate of development and eye pigmentation in *Drosophila melanogaster*. *Biological Bulletin*, 75(3), 447–462.
- Bergmann, A., Agapite, J., McCall, K., & Steller, H. (1998). The *Drosophila* gene *hid* is a direct molecular target of Ras-dependent survival signaling. *Cell*, 95(3), 331–341.
- Bergmann, A., Tugentman, M., Shilo, B.-Z., & Steller, H. (2002). Regulation of cell number by MAPK-dependent control of apoptosis: A mechanism for trophic survival signaling. *Developmental Cell*, 2(2), 159–170.
- Bertet, C., Li, X., Erclik, T., Cavey, M., Wells, B., & Desplan, C. (2014). Temporal patterning of neuroblasts controls notch-mediated cell survival through regulation of *hid* or *reaper*. *Cell*, 158(5), 1173–1186.
- Blanchard, G. B., Kabla, A. J., Schultz, N. L., Butler, L. C., Sanson, B., Gorfinkiel, N., Mahadevan, L., & Adams, R. J. (2009). Tissue tectonics: Morphogenetic strain rates, cell shape change and intercalation. *Nature Methods*, 6(6), 458–464.
- Boal, D. H. (2012). *Mechanics of the cell*. Cambridge University Press.
- Boehlke, C., Kotsis, F., Patel, V., Braeg, S., Voelker, H., Bredt, S., Beyer, T., Janusch, H., Hamann, C., Gödel, M., Müller, K., Herbst, M., Hornung, M., Doerken, M., Köttgen, M., Nitschke, R., Igarashi, P., Walz, G., & Kuehn, E. W. (2010). Primary cilia regulate mTORC1 activity and cell size through *Lkb1*. *Nature Cell Biology*, 12(11), 1115–1122.
- Böhni, R., Riesgo-Escovar, J., Oldham, S., Brogiolo, W., Stocker, H., Andruss, B. F., Beckingham, K., & Hafen, E. (1999). Autonomous control of cell and organ size by CHICO, a *Drosophila* homolog of vertebrate IRS1–4. *Cell*, 97(7), 865–875.
- Bosveld, F., Bonnet, I., Guirao, B., Tlili, S., Wang, Z., Petitalot, A., Marchand, R., Bardet, P.-L., Marcq, P., Graner, F., & Bellaïche, Y. (2012). Mechanical

- control of morphogenesis by Fat/Dachsous/Four-jointed planar cell polarity pathway. *Science*, 336(6082), 724–727.
- Bosveld, F., Markova, O., Guirao, B., Martin, C., Wang, Z., Pierre, A., Balakireva, M., Gaugue, I., Ainslie, A., Christophorou, N., Lubensky, D. K., Minc, N., & Bellaïche, Y. (2016). Epithelial tricellular junctions act as interphase cell shape sensors to orient mitosis. *Nature*, 530(7591), 495–498.
- Boulan, L., Andersen, D., Colombani, J., Boone, E., & Léopold, P. (2019). Inter-organ growth coordination is mediated by the Xrp1-Dilp8 axis in *Drosophila*. *Developmental Cell*, 49(5), 811–818.
- Bove, A., Gradeci, D., Fujita, Y., Banerjee, S., Charras, G., & Lowe, A. R. (2017). Local cellular neighborhood controls proliferation in cell competition. *Molecular Biology of the Cell*, 28(23), 3215–3228.
- Bowman, P., & McLaren, A. (1970). Viability and growth of mouse embryos after in vitro culture and fusion. *Development*, 23(3), 693–704.
- Brás-Pereira, C., & Moreno, E. (2018). Mechanical cell competition. *Current Opinion in Cell Biology*, 51, 15–21.
- Bryant, P. J., & Levinson, P. (1985). Intrinsic growth control in the imaginal primordia of *Drosophila*, and the autonomous action of a lethal mutation causing overgrowth. *Developmental Biology*, 107(2), 355–363.
- Buehr, M., & McLaren, A. (1974). Size regulation in chimaeric mouse embryos. *Development*, 31(1), 229–234.
- Butler, L. C., Blanchard, G. B., Kabla, A. J., Lawrence, N. J., Welchman, D. P., Mahadevan, L., Adams, R. J., & Sanson, B. (2009). Cell shape changes indicate a role for extrinsic tensile forces in *Drosophila* germ-band extension. *Nature Cell Biology*, 11(7), 859–864.
- Cadart, C. (2017). *Cell size homeostasis in animal cells* (Doctoral dissertation). Université Paris-Saclay.
- Chan, Y.-H. M., & Marshall, W. F. (2010). Scaling properties of cell and organelle size. *Organogenesis*, 6(2), 88–96.
- Chartier, N. T., Mukherjee, A., Pfanzelter, J., Fürthauer, S., Larson, B. T., Fritsch, A. W., Amini, R., Kreysing, M., Jülicher, F., & Grill, S. W. (2021). A hy-

- draulic instability drives the cell death decision in the nematode germline. *Nature Physics*, *17*(8), 920–925.
- Chen, C. S., Mrksich, M., Huang, S., Whitesides, G. M., & Ingber, D. E. (1997). Geometric control of cell life and death. *Science*, *276*(5317), 1425–1428.
- Chen, P., Tomschik, M., Nelson, K. M., Oakey, J., Gatlin, J. C., & Levy, D. L. (2019). Nucleoplasmin is a limiting component in the scaling of nuclear size with cytoplasmic volume. *Journal of Cell Biology*, *218*(12), 4063–4078.
- Chlasta, J., Milani, P., Runel, G., Duteyrat, J.-L., Arias, L., Lamiré, L.-A., Boudaoud, A., & Grammont, M. (2017). Variations in basement membrane mechanics are linked to epithelial morphogenesis. *Development*, *144*(23), 4350–4362.
- Clark, A. G., Wartlick, O., Salbreux, G., & Paluch, E. K. (2014). Stresses at the cell surface during animal cell morphogenesis. *Current Biology*, *24*(10), R484–R494.
- Classen, A.-K., Anderson, K. I., Marois, E., & Eaton, S. (2005). Hexagonal packing of *Drosophila* wing epithelial cells by the planar cell polarity pathway. *Developmental Cell*, *9*(6), 805–817.
- Colon-Plaza, S., & Su, T. T. (2022). Non-apoptotic role of apoptotic caspases in the *Drosophila* nervous system. *Frontiers in Cell and Developmental Biology*, *10*, 839358–839358.
- Conklin, E. G. (1912). Cell size and nuclear size. *Journal of Experimental Zoology*, *12*, 1–98.
- Conlon, I., & Raff, M. (1999). Size control in animal development. *Cell*, *96*(2), 235–244.
- Córdoba, S., & Estella, C. (2020). Role of Notch signaling in leg development in *Drosophila melanogaster*. In J. Reichrath & S. Reichrath (Editors), *Notch Signaling in Embryology and Cancer: Notch Signaling in Embryology* (Pages 103–127). Springer International Publishing.
- Coste, B., Mathur, J., Schmidt, M., Earley, T. J., Ranade, S., Petrus, M. J., Dubin, A. E., & Patapoutian, A. (2010). Piezo1 and Piezo2 are essential components of distinct mechanically activated cation channels. *Science*, *330*(6000), 55–60.

- Crino, P. B. (2011). Mtor: A pathogenic signaling pathway in developmental brain malformations. *Trends in Molecular Medicine*, *17*(12), 734–742.
- Cuervo, R., & Covarrubias, L. (2004). Death is the major fate of medial edge epithelial cells and the cause of basal lamina degradation during palatogenesis. *Development*, *131*(1), 15–24.
- Cuervo, R., Valencia, C., Chandraratna, R. A. S., & Covarrubias, L. (2002). Programmed cell death is required for palate shelf fusion and is regulated by retinoic acid. *Developmental Biology*, *245*(1), 145–156.
- da Silva, S. M., & Vincent, J.-P. (2007). Oriented cell divisions in the extending germband of *Drosophila*. *Development*, *134*(17), 3049–3054.
- Demidenko, Z. N., & Blagosklonny, M. V. (2008). Growth stimulation leads to cellular senescence when the cell cycle is blocked. *Cell Cycle*, *7*(21), 3355–3361.
- Diamantis, A., Beloukas, A. I., Kalogeraki, A. M., & Magiorkinis, E. (2013). A brief chronicle of cytology: From Janssen to Papanicolaou and beyond. *Diagnostic Cytopathology*, *41*(6), 555–564.
- Diaz-de-la-Loza, M.-d.-C., Ray, R. P., Ganguly, P. S., Alt, S., Davis, J. R., Hoppe, A., Tapon, N., Salbreux, G., & Thompson, B. J. (2018). Apical and basal matrix remodeling control epithelial morphogenesis. *Developmental Cell*, *46*(1), 23–39.
- Doxzen, K., Vedula, S. R. K., Leong, M. C., Hirata, H., Gov, N. S., Kabla, A. J., Ladoux, B., & Lim, C. T. (2013). Guidance of collective cell migration by substrate geometry. *Integrative Biology*, *5*(8), 1026–1035.
- Duda, M., Kirkland, N. J., Khalilgharibi, N., Tozluoğlu, M., Yuen, A. C., Carpi, N., Bove, A., Piel, M., Charras, G., Baum, B., & Mao, Y. (2019). Polarization of myosin II refines tissue material properties to buffer mechanical stress. *Developmental Cell*, *48*(2), 245–260.
- Dupont, S., Morsut, L., Aragona, M., Enzo, E., Giulitti, S., Cordenonsi, M., Zanconato, F., Le Digabel, J., Forcato, M., Bicciato, S., Elvassore, N., & Piccolo, S. (2011). Role of YAP/TAZ in mechanotransduction. *Nature*, *474*(7350), 179–183.

- Durand, M., Kraynik, A. M., Van Swol, F., Käfer, J., Quilliet, C., Cox, S., Talebi, S. A., & Graner, F. (2014). Statistical mechanics of two-dimensional shuffled foams: Geometry-topology correlation in small or large disorder limits. *Physical Review E*, *89*(6), 062309.
- Düvel, K., Yecies, J. L., Menon, S., Raman, P., Lipovsky, A. I., Souza, A. L., Triantafellow, E., Ma, Q., Gorski, R., Cleaver, S., Vander Heiden, M. G., MacKean, J. P., Finan, P. M., Clish, C. B., Murphy, L. O., & Manning, B. D. (2010). Activation of a metabolic gene regulatory network downstream of mTOR complex 1. *Molecular Cell*, *39*(2), 171–183.
- Eisenhoffer, G. T., Loftus, P. D., Yoshigi, M., Otsuna, H., Chien, C.-B., Morcos, P. A., & Rosenblatt, J. (2012). Crowding induces live cell extrusion to maintain homeostatic cell numbers in epithelia. *Nature*, *484*(7395), 546–549.
- Ellis, H. M., & Horvitz, H. R. (1986). Genetic control of programmed cell death in the nematode *C. elegans*. *Cell*, *44*(6), 817–829.
- Engel-Pizcueta, C., & Pujades, C. (2021). Interplay between Notch and YAP/TAZ pathways in the regulation of cell fate during embryo development. *Frontiers in Cell and Developmental Biology*, *9*, 2314.
- Etournay, R., Popović, M., Merkel, M., Nandi, A., Blasse, C., Aigouy, B., Brandl, H., Myers, G., Salbreux, G., Jülicher, F., & Eaton, S. (2015). Interplay of cell dynamics and epithelial tension during morphogenesis of the *Drosophila* pupal wing. *eLife*, *4*, e07090.
- Fan, Y., & Bergmann, A. (2008). Apoptosis-induced compensatory proliferation. The Cell is dead. Long live the Cell! *Trends in Cell Biology*, *18*(10), 467–473.
- Fankhauser, G. (1945). The effects of changes in chromosome number on amphibian development. *The Quarterly Review of Biology*, *20*(1), 20–78.
- Fankhauser, G., Vernon, J. A., Frank, W. H., & Slack, W. V. (1955). Effect of size and number of brain cells on learning in larvae of the salamander, *Triturus viridescens*. *Science*, *122*(3172), 692–693.
- Fantes, P., & Nurse, P. (1977). Control of cell size at division in fission yeast by a growth-modulated size control over nuclear division. *Experimental Cell Research*, *107*(2), 377–386.

- Farbman, A. I. (1968). Electron microscope study of palate fusion in mouse embryos. *Developmental Biology*, *18*(2), 93–116.
- Farge, E. (2011). Mechanotransduction in development. *Current Topics in Developmental Biology*, *95*, 243–265.
- Farhadifar, R., Röper, J.-C., Aigouy, B., Eaton, S., & Jülicher, F. (2007). The influence of cell mechanics, cell-cell interactions, and proliferation on epithelial packing. *Current Biology*, *17*(24), 2095–2104.
- Fingar, D. C., Salama, S., Tsou, C., Harlow, E. D., & Blenis, J. (2002). Mammalian cell size is controlled by mTOR and its downstream targets S6K1 and 4EBP1/eIF4E. *Genes & Development*, *16*(12), 1472–1487.
- Fletcher, D. A., & Mullins, R. D. (2010). Cell mechanics and the cytoskeleton. *Nature*, *463*(7280), 485–492.
- Fletcher, G. C., Diaz-de-la-Loza, M.-d.-C., Borreguero-Muñoz, N., Holder, M., Aguilar-Aragon, M., & Thompson, B. J. (2018). Mechanical strain regulates the Hippo pathway in Drosophila. *Development*, *145*(5), dev159467.
- Folkman, J., & Moscona, A. (1978). Role of cell shape in growth control. *Nature*, *273*(5661), 345–349.
- Fujisawa, Y., Kosakamoto, H., Chihara, T., & Miura, M. (2019). Non-apoptotic function of Drosophila caspase activation in epithelial thorax closure and wound healing. *Development*, *146*(4), dev169037.
- Gaffney, E. A., Gadêlha, H., Smith, D. J., Blake, J. R., & Kirkman-Brown, J. C. (2011). Mammalian sperm motility: Observation and theory. *Annual Review of Fluid Mechanics*, *43*, 501–528.
- Gagliardi, P. A., Dobrzyński, M., Jacques, M.-A., Dessauges, C., Ender, P., Blum, Y., Hughes, R. M., Cohen, A. R., & Pertz, O. (2021). Collective ERK/Akt activity waves orchestrate epithelial homeostasis by driving apoptosis-induced survival. *Developmental Cell*, *56*(12), 1712–1726.
- Gao, X., Zhang, Y., Arrazola, P., Hino, O., Kobayashi, T., Yeung, R. S., Ru, B., & Pan, D. (2002). Tsc tumour suppressor proteins antagonize amino-acid-TOR signalling. *Nature Cell Biology*, *4*(9), 699–704.

- Gibson, M. C., Patel, A. B., Nagpal, R., & Perrimon, N. (2006). The emergence of geometric order in proliferating metazoan epithelia. *Nature*, *442*(7106), 1038–1041.
- Ginzberg, M. B., Kafri, R., & Kirschner, M. (2015). On being the right (cell) size. *Science*, *348*(6236), 1245075.
- Glücksmann, A. (1951). Cell deaths in normal vertebrate ontogeny. *Biological Reviews*, *26*(1), 59–86.
- Gómez-Gálvez, P., Vicente-Munuera, P., Tagua, A., Forja, C., Castro, A. M., Letrán, M., Valencia-Expósito, A., Grima, C., Bermúdez-Gallardo, M., Serrano-Pérez-Higueras, Ó., Cavodeassi, F., Sotillos, S., Martín-Bermudo, M. D., Márquez, A., Buceta, J., & Escudero, L. M. (2018). Scutoids are a geometrical solution to three-dimensional packing of epithelia. *Nature Communications*, *9*(1), 1–14.
- Goyal, L., McCall, K., Agapite, J., Hartwig, E., & Steller, H. (2000). Induction of apoptosis by *Drosophila* reaper, hid and grim through inhibition of IAP function. *The EMBO journal*, *19*(4), 589–597.
- Gracia, M., Theis, S., Proag, A., Gay, G., Benassayag, C., & Suzanne, M. (2019). Mechanical impact of epithelial- mesenchymal transition on epithelial morphogenesis in *Drosophila*. *Nature Communications*, *10*(1), 1–17.
- Graner, F., & Glazier, J. A. (1992). Simulation of biological cell sorting using a two-dimensional extended Potts model. *Physical Review Letters*, *69*(13), 2031–2034.
- Graner, F., & Rivelino, D. (2017). ‘The Forms of Tissues, or Cell-aggregates’: D’Arcy Thompson’s influence and its limits. *Development*, *144*(23), 4226–4237.
- Grewal, S. S., Li, L., Orian, A., Eisenman, R. N., & Edgar, B. A. (2005). Myc-dependent regulation of ribosomal RNA synthesis during *Drosophila* development. *Nature Cell Biology*, *7*(3), 295–302.
- Gudipaty, S. A., Lindblom, J., Loftus, P. D., Redd, M. J., Edes, K., Davey, C. F., Krishnegowda, V., & Rosenblatt, J. (2017). Mechanical stretch triggers rapid epithelial cell division through Piezo1. *Nature*, *543*(7643), 118–121.

- Guirao, B., Rigaud, S. U., Bosveld, F., Bailles, A., López-Gay, J., Ishihara, S., Sugimura, K., Graner, F., & Bellaïche, Y. (2015). Unified quantitative characterization of epithelial tissue development. *eLife*, *4*, e08519.
- Hall, P. A., Coates, P. J., Ansari, B., & Hopwood, D. (1994). Regulation of cell number in the mammalian gastrointestinal tract: The importance of apoptosis. *Journal of Cell Science*, *107*(12), 3569–3577.
- Hara, Y., & Merten, C. A. (2015). Dynein-based accumulation of membranes regulates nuclear expansion in *Xenopus laevis* egg extracts. *Developmental Cell*, *33*(5), 562–575.
- Harris, H. (1967). The reactivation of the red cell nucleus. *Journal of Cell Science*, *2*(1), 23–28.
- Harrison, R. G. (1924). Some unexpected results of the heteroplastic transplantation of limbs. *Proceedings of the National Academy of Sciences*, *10*(2), 69.
- Harvey, K. F., Pflieger, C. M., & Hariharan, I. K. (2003). The *Drosophila* Mst ortholog, hippo, restricts growth and cell proliferation and promotes apoptosis. *Cell*, *114*(4), 457–467.
- Haupt, A., & Minc, N. (2018). How cells sense their own shape—mechanisms to probe cell geometry and their implications in cellular organization and function. *Journal of Cell Science*, *131*(6), jcs214015.
- Hay, B. A., Wassarman, D. A., & Rubin, G. M. (1995). *Drosophila* homologs of baculovirus inhibitor of apoptosis proteins function to block cell death. *Cell*, *83*(7), 1253–1262.
- Hermaniuk, A., Rybacki, M., & Taylor, J. R. E. (2017). Metabolic rate of diploid and triploid edible frog *Pelophylax esculentus* correlates inversely with cell size in tadpoles but not in frogs. *Physiological and Biochemical Zoology*, *90*(2), 230–239.
- Hernández-Martínez, R., & Covarrubias, L. (2011). Interdigital cell death function and regulation: New insights on an old programmed cell death model. *Development, Growth & Differentiation*, *53*(2), 245–258.

- Huang, J., Wu, S., Barrera, J., Matthews, K., & Pan, D. (2005). The Hippo signaling pathway coordinately regulates cell proliferation and apoptosis by inactivating Yorkie, the *Drosophila* homolog of YAP. *Cell*, *122*(3), 421–434.
- Huh, J. R., Foe, I., Muro, I., Chen, C. H., Seol, J. H., Yoo, S. J., Guo, M., Park, J. M., & Hay, B. A. (2007). The *Drosophila* inhibitor of apoptosis (IAP) DIAP2 is dispensable for cell survival, required for the innate immune response to gram-negative bacterial infection, and can be negatively regulated by the reaper/hid/grim family of IAP-binding apoptosis inducers. *Journal of Biological Chemistry*, *282*(3), 2056–2068.
- Inoki, K., Li, Y., Zhu, T., Wu, J., & Guan, K.-L. (2002). TSC2 is phosphorylated and inhibited by Akt and suppresses mTOR signalling. *Nature Cell Biology*, *4*(9), 648–657.
- Iritani, B. M., & Eisenman, R. N. (1999). C-Myc enhances protein synthesis and cell size during B lymphocyte development. *Proceedings of the National Academy of Sciences*, *96*(23), 13180–13185.
- Ishihara, S., & Sugimura, K. (2012). Bayesian inference of force dynamics during morphogenesis. *Journal of Theoretical Biology*, *313*, 201–211.
- Iskratsch, T., Wolfenson, H., & Sheetz, M. P. (2014). Appreciating force and shape — the rise of mechanotransduction in cell biology. *Nature Reviews Molecular Cell Biology*, *15*(12), 825–833.
- Izaguirre, J. A., Chaturvedi, R., Huang, C., Cickovski, T., Coffland, J., Thomas, G., Forgacs, G., Alber, M., Hentschel, G., Newman, S. A., & Glazier, J. A. (2004). CompuCell, a multi-model framework for simulation of morphogenesis. *Bioinformatics*, *20*(7), 1129–1137.
- Johnston, L. A., Prober, D. A., Edgar, B. A., Eisenman, R. N., & Gallant, P. (1999). *Drosophila* myc regulates cellular growth during development. *Cell*, *98*(6), 779–790.
- Kabla, A. J. (2012). Collective cell migration: Leadership, invasion and segregation. *Journal of The Royal Society Interface*, *9*(77), 3268–3278.
- Kerr, J. F. R. (1965). A histochemical study of hypertrophy and ischaemic injury of rat liver with special reference to changes in lysosomes. *The Journal of Pathology and Bacteriology*, *90*(2), 419–435.

- Kerr, J. F. R. (1971). Shrinkage necrosis: A distinct mode of cellular death. *The Journal of Pathology*, *105*(1), 13–20.
- Kerr, J. F. R., Wyllie, A. H., & Currie, A. R. (1972). Apoptosis: A basic biological phenomenon with wideranging implications in tissue kinetics. *British Journal of Cancer*, *26*(4), 239–257.
- Khait, I., Orsher, Y., Golan, O., Binshtok, U., Gordon-Bar, N., Amir-Zilberstein, L., & Sprinzak, D. (2016). Quantitative analysis of Delta-like 1 membrane dynamics elucidates the role of contact geometry on Notch signaling. *Cell Reports*, *14*(2), 225–233.
- Kieserman, E. K., & Heald, R. (2011). Mitotic chromosome size scaling in *Xenopus*. *Cell Cycle*, *10*(22), 3863–3870.
- Kilian, K. A., Bugarija, B., Lahn, B. T., & Mrksich, M. (2010). Geometric cues for directing the differentiation of mesenchymal stem cells. *Proceedings of the National Academy of Sciences*, *107*(11), 4872–4877.
- Kim, D.-H., Sarbassov, D. D., Ali, S. M., King, J. E., Latek, R. R., Erdjument-Bromage, H., Tempst, P., & Sabatini, D. M. (2002). mTOR interacts with raptor to form a nutrient-sensitive complex that signals to the cell growth machinery. *Cell*, *110*(2), 163–175.
- Kim, E., Goraksha-Hicks, P., Li, L., Neufeld, T. P., & Guan, K.-L. (2008). Regulation of TORC1 by Rag GTPases in nutrient response. *Nature Cell Biology*, *10*(8), 935–945.
- Kim, J., Kundu, M., Viollet, B., & Guan, K.-L. (2011). AMPK and mTOR regulate autophagy through direct phosphorylation of Ulk1. *Nature Cell Biology*, *13*(2), 132–141.
- Kirby, T. J., & Lammerding, J. (2018). Emerging views of the nucleus as a cellular mechanosensor. *Nature Cell Biology*, *20*(4), 373–381.
- Kleiber, M. (1932). Body size and metabolism. *Hilgardia*, *6*(11), 315–353.
- Kölsch, V., Seher, T., Fernandez-Ballester, G. J., Serrano, L., & Leptin, M. (2007). Control of *Drosophila* gastrulation by apical localization of adherens junctions and RhoGEF2. *Science*, *315*(5810), 384–386.

- Kuge, S., Jones, N., & Nomoto, A. (1997). Regulation of yAP-1 nuclear localization in response to oxidative stress. *The EMBO Journal*, *16*(7), 1710–1720.
- Kuipers, D., Mehonic, A., Kajita, M., Peter, L., Fujita, Y., Duke, T., Charras, G., & Gale, J. E. (2014). Epithelial repair is a two-stage process driven first by dying cells and then by their neighbours. *Journal of Cell Science*, *127*(6), 1229–1241.
- Kumar, S., Maxwell, I. Z., Heisterkamp, A., Polte, T. R., Lele, T. P., Salanga, M., Mazur, E., & Ingber, D. E. (2006). Viscoelastic retraction of single living stress fibers and its impact on cell shape, cytoskeletal organization, and extracellular matrix mechanics. *Biophysical Journal*, *90*(10), 3762–3773.
- Kurada, P., & White, K. (1998). Ras promotes cell survival in *Drosophila* by down-regulating hid expression. *Cell*, *95*(3), 319–329.
- Kuranaga, E., Matsunuma, T., Kanuka, H., Takemoto, K., Koto, A., Kimura, K., & Miura, M. (2011). Apoptosis controls the speed of looping morphogenesis in *Drosophila* male terminalia. *Development*, *138*(8), 1493–1499.
- Kyogoku, H., & Kitajima, T. S. (2017). Large cytoplasm is linked to the error-prone nature of oocytes. *Developmental Cell*, *41*(3), 287–298.
- Ladouceur, A.-M., Dorn, J. F., & Maddox, P. S. (2015). Mitotic chromosome length scales in response to both cell and nuclear size. *Journal of Cell Biology*, *209*(5), 645–652.
- Lai, E. C. (2004). Notch signaling: Control of cell communication and cell fate. *Development*, *131*(5), 965–973.
- Lam, M. S. Y., Lisica, A., Ramkumar, N., Hunter, G., Mao, Y., Charras, G., & Baum, B. (2020). Isotropic myosin-generated tissue tension is required for the dynamic orientation of the mitotic spindle. *Molecular Biology of the Cell*, *31*(13), 1370–1379.
- Laplane, M., & Sabatini, D. M. (2012). MTOR signaling in growth control and disease. *Cell*, *149*(2), 274–293.
- Leroy, O., Van Leen, E., Girard, P., Villedieu, A., Hubert, C., Bosveld, F., Bellaïche, Y., & Renaud, O. (2022). Multi-view confocal microscopy enables multiple organ and whole organism live-imaging. *Development*, *149*(4), dev199760.

- Levayer, R., Dupont, C., & Moreno, E. (2016). Tissue crowding induces caspase-dependent competition for space. *Current Biology*, *26*(5), 670–677.
- Levy, D. L., & Heald, R. (2010). Nuclear size is regulated by importin α and Ntf2 in *Xenopus*. *Cell*, *143*(2), 288–298.
- Lewis, F. T. (1928). The correlation between cell division and the shapes and sizes of prismatic cells in the epidermis of cucumis. *The Anatomical Record*, *38*(3), 341–376.
- Liang, X., Gomez, G. A., & Yap, A. (2015). Current perspectives on cadherin-cytoskeleton interactions and dynamics. *Cell Health and Cytoskeleton*, *7*, 11–24.
- Lisi, S., Mazzon, I., & White, K. (2000). Diverse domains of THREAD/DIAP1 are required to inhibit apoptosis induced by REAPER and HID in *Drosophila*. *Genetics*, *154*(2), 669–678.
- Lomakin, A. J., Cattin, C. J., Cuvelier, D., Alraies, Z., Molina, M., Nader, G. P. F., Srivastava, N., Sáez, P. J., Garcia-Arcos, J. M., Zhitnyak, I. Y., Bhargava, A., Driscoll, M. K., Welf, E. S., Fiolka, R., Petrie, R. J., De Silva, N. S., González-Granado, J. M., Manel, N., Lennon-Duménil, A. M., . . . Piel, M. (2020). The nucleus acts as a ruler tailoring cell responses to spatial constraints. *Science*, *370*(6514), eaba2894.
- López-Gay, J. M., Nunley, H., Spencer, M., Di Pietro, F., Guirao, B., Bosveld, F., Markova, O., Gague, I., Pelletier, S., Lubensky, D. K., & Bellaïche, Y. (2020). Apical stress fibers enable a scaling between cell mechanical response and area in epithelial tissue. *Science*, *370*(6514), eabb2169.
- Ma, D., Amonlirdviman, K., Raffard, R. L., Abate, A., Tomlin, C. J., & Axelrod, J. D. (2008). Cell packing influences planar cell polarity signaling. *Proceedings of the National Academy of Sciences*, *105*(48), 18800–18805.
- Madara, J. L., Stafford, J., Dharmasathaphorn, K., & Carlson, S. (1987). Structural analysis of a human intestinal epithelial cell line. *Gastroenterology*, *92*(5), 1133–1145.
- Manjón, C., Sánchez-Herrero, E., & Suzanne, M. (2007). Sharp boundaries of Dpp signalling trigger local cell death required for *Drosophila* leg morphogenesis. *Nature Cell Biology*, *9*(1), 57–63.

- Marinari, E., Mehonic, A., Curran, S., Gale, J., Duke, T., & Baum, B. (2012). Live-cell delamination counterbalances epithelial growth to limit tissue over-crowding. *Nature*, *484*(7395), 542–545.
- Martin, A. C., Gelbart, M., Fernandez-Gonzalez, R., Kaschube, M., & Wieschaus, E. F. (2010). Integration of contractile forces during tissue invagination. *Journal of Cell Biology*, *188*(5), 735–749.
- Martin, A. C., & Goldstein, B. (2014). Apical constriction: Themes and variations on a cellular mechanism driving morphogenesis. *Development*, *141*(10), 1987–1998.
- Martín, F. A., & Morata, G. (2006). Compartments and the control of growth in the *Drosophila* wing imaginal disc. *Development*, *133*(22), 4421–4426.
- Martino, F., Perestrelo, A. R., Vinarský, V., Pagliari, S., & Forte, G. (2018). Cellular mechanotransduction: From tension to function. *Frontiers in Physiology*, *9*, 824.
- Matamoro-Vidal, A., & Levayer, R. (2019). Multiple influences of mechanical forces on cell competition. *Current Biology*, *29*(15), R762–R774.
- McBeath, R., Pirone, D. M., Nelson, C. M., Bhadriraju, K., & Chen, C. S. (2004). Cell shape, cytoskeletal tension, and RhoA regulate stem cell lineage commitment. *Developmental Cell*, *6*(4), 483–495.
- Mendonsa, A. M., Na, T.-Y., & Gumbiner, B. M. (2018). E-cadherin in contact inhibition and cancer. *Oncogene*, *37*(35), 4769–4780.
- Merino, M. M., Rhiner, C., López-Gay, J. M., Buechel, D., Hauert, B., & Moreno, E. (2015). Elimination of unfit cells maintains tissue health and prolongs lifespan. *Cell*, *160*(3), 461–476.
- Messal, H. A., Alt, S., Ferreira, R. M. M., Gribben, C., Wang, V. M.-Y., Cotoi, C. G., Salbreux, G., & Behrens, A. (2019). Tissue curvature and apicobasal mechanical tension imbalance instruct cancer morphogenesis. *Nature*, *566*(7742), 126–130.
- Meyer, S. N., Amoyel, M., Bergantinos, C., De La Cova, C., Schertel, C., Basler, K., & Johnston, L. A. (2014). An ancient defense system eliminates unfit cells from developing tissues during cell competition. *Science*, *346*(6214), 1258236.

- Michailov, G. V., Sereda, M. W., Brinkmann, B. G., Fischer, T. M., Haug, B., Birchmeier, C., Role, L., Lai, C., Schwab, M. H., & Nave, K.-A. (2004). Axonal neuregulin-1 regulates myelin sheath thickness. *Science*, *304*(5671), 700–703.
- Miettinen, T. P., & Björklund, M. (2016). Cellular allometry of mitochondrial functionality establishes the optimal cell size. *Developmental Cell*, *39*(3), 370–382.
- Miettinen, T. P., Caldez, M. J., Kaldis, P., & Björklund, M. (2017). Cell size control – a mechanism for maintaining fitness and function. *Bioessays*, *39*(9), 1700058.
- Monier, B., Gettings, M., Gay, G., Mangeat, T., Schott, S., Guarner, A., & Suzanne, M. (2015). Apico-basal forces exerted by apoptotic cells drive epithelium folding. *Nature*, *518*(7538), 245–248.
- Moreno, E., Valon, L., Levillayer, F., & Levayer, R. (2019). Competition for space induces cell elimination through compaction-driven ERK downregulation. *Current Biology*, *29*(1), 23–34.
- Morin, X., & Bellaïche, Y. (2011). Mitotic spindle orientation in asymmetric and symmetric cell divisions during animal development. *Developmental Cell*, *21*(1), 102–119.
- Nakajima, Y., & Kuranaga, E. (2017). Caspase-dependent non-apoptotic processes in development. *Cell Death & Differentiation*, *24*(8), 1422–1430.
- Nardone, G., Vrbsky, J., Martini, C., Pribyl, J., Skládal, P., Pešl, M., Caluori, G., Pagliari, S., Martino, F., Maceckova, Z., Hajduch, M., Sanz-Garcia, A., Pugno, N. M., Stokin, G. B., & Forte, G. (2017). YAP regulates cell mechanics by controlling focal adhesion assembly. *Nature Communications*, *8*(1), 1–13.
- Nehls, S., Nöding, H., Karsch, S., Ries, F., & Janshoff, A. (2019). Stiffness of MDCK II cells depends on confluency and cell size. *Biophysical Journal*, *116*(11), 2204–2211.
- Nestor-Bergmann, A., Stooke-Vaughan, G. A., Goddard, G. K., Starborg, T., Jensen, O. E., & Woolner, S. (2019). Decoupling the roles of cell shape and mechanical stress in orienting and cueing epithelial mitosis. *Cell Reports*, *26*(8), 2088–2100.

- Neufeld, T. P., De La Cruz, A. F. A., Johnston, L. A., & Edgar, B. A. (1998). Coordination of growth and cell division in the *Drosophila* wing. *Cell*, *93*(7), 1183–1193.
- Neurohr, G. E., Terry, R. L., Lengefeld, J., Bonney, M., Brittingham, G. P., Moretto, F., Miettinen, T. P., Vaites, L. P., Soares, L. M., Paulo, J. A., Harper, J. W., Buratowski, S., Manalis, S., van Werven, F. J., Holt, L. J., & Amon, A. (2019). Excessive cell growth causes cytoplasm dilution and contributes to senescence. *Cell*, *176*(5), 1083–1097.
- Nolo, R., Morrison, C. M., Tao, C., Zhang, X., & Halder, G. (2006). The bantam microRNA is a target of the hippo tumor-suppressor pathway. *Current Biology*, *16*(19), 1895–1904.
- North, B. J., & Sinclair, D. A. (2012). The intersection between aging and cardiovascular disease. *Circulation Research*, *110*(8), 1097–1108.
- Okuda, S., Inoue, Y., & Adachi, T. (2015). Three-dimensional vertex model for simulating multicellular morphogenesis. *Biophysics and Physicobiology*, *12*, 13–20.
- Oldham, S., Montagne, J., Radimerski, T., Thomas, G., & Hafen, E. (2000). Genetic and biochemical characterization of dTOR, the *drosophila* homolog of the target of rapamycin. *Genes & Development*, *14*(21), 2689–2694.
- Pantalacci, S., Tapon, N., & Léopold, P. (2003). The Salvador partner Hippo promotes apoptosis and cell-cycle exit in *Drosophila*. *Nature Cell Biology*, *5*(10), 921–927.
- Pardee, A. B. (1974). A restriction point for control of normal animal cell proliferation. *Proceedings of the National Academy of Sciences*, *71*(4), 1286–1290.
- Pittenger, M. F., Mackay, A. M., Beck, S. C., Jaiswal, R. K., Douglas, R., Mosca, J. D., Moorman, M. A., Simonetti, D. W., Craig, S., & Marshak, D. R. (1999). Multilineage potential of adult human mesenchymal stem cells. *Science*, *284*(5411), 143–147.
- Plateau, J. A. F. (1873). *Statique expérimentale et théorique des liquides soumis aux seules forces moléculaires* (Volume 2). Gauthier-Villars.

- Potter, C. J., Huang, H., & Xu, T. (2001). Drosophila Tsc1 functions with Tsc2 to antagonize insulin signaling in regulating cell growth, cell proliferation, and organ size. *Cell*, *105*(3), 357–368.
- Prather, P., & de Vries, P. J. (2004). Behavioral and cognitive aspects of tuberous sclerosis complex. *Journal of Child Neurology*, *19*(9), 666–674.
- Priya, R., Allanki, S., Gentile, A., Mansingh, S., Uribe, V., Maischein, H.-M., & Stainier, D. Y. R. (2020). Tension heterogeneity directs form and fate to pattern the myocardial wall. *Nature*, *588*(7836), 130–134.
- Puliafito, A., Hufnagel, L., Neveu, P., Streichan, S., Sigal, A., Fygenson, D. K., & Shraiman, B. I. (2012). Collective and single cell behavior in epithelial contact inhibition. *Proceedings of the National Academy of Sciences*, *109*(3), 739–744.
- Ramanathan, S. P., Krajnc, M., & Gibson, M. C. (2019). Cell-size pleomorphism drives aberrant clone dispersal in proliferating epithelia. *Developmental Cell*, *51*(1), 49–61.
- Ranft, J., Basan, M., Elgeti, J., Joanny, J.-F., Prost, J., & Jülicher, F. (2010). Fluidization of tissues by cell division and apoptosis. *Proceedings of the National Academy of Sciences*, *107*(49), 20863–20868.
- Rens, E. G., & Merks, R. M. H. (2020). Cell shape and durotaxis explained from cell-extracellular matrix forces and focal adhesion dynamics. *iScience*, *23*(9), 101488.
- Ridley, A. J. (2011). Life at the leading edge. *Cell*, *145*(7), 1012–1022.
- Riga, A., Castiglioni, V. G., & Boxem, M. (2020). New insights into apical-basal polarization in epithelia. *Current Opinion in Cell Biology*, *62*, 1–8.
- Rivier, N., & Lissowski, A. (1982). On the correlation between sizes and shapes of cells in epithelial mosaics. *Journal of Physics A: Mathematical and General*, *15*(3), L143.
- Roca-Cusachs, P., Alcaraz, J., Sunyer, R., Samitier, J., Farré, R., & Navajas, D. (2008). Micropatterning of single endothelial cell shape reveals a tight coupling between nuclear volume in g1 and proliferation. *Biophysical Journal*, *94*(12), 4984–4995.

- Roca-Cusachs, P., Sunyer, R., & Trepats, X. (2013). Mechanical guidance of cell migration: Lessons from chemotaxis. *Current Opinion in Cell Biology*, *25*(5), 543–549.
- Roeder, A. H. K., Chickarmane, V., Cunha, A., Obara, B., Manjunath, B. S., & Meyerowitz, E. M. (2010). Variability in the control of cell division underlies sepal epidermal patterning in *Arabidopsis thaliana*. *PLoS Biology*, *8*(5), e1000367.
- Roeder, A. H. K., Cunha, A., Ohno, C. K., & Meyerowitz, E. M. (2012). Cell cycle regulates cell type in the *Arabidopsis* sepal. *Development*, *139*(23), 4416–4427.
- Roellig, D., Theis, S., Proag, A., Allio, G., Bénazéraf, B., Gros, J., & Suzanne, M. (2022). Force-generating apoptotic cells orchestrate avian neural tube bending. *Developmental Cell*, *57*(6), 707–718.
- Roffay, C., Chan, C. J., Guirao, B., Hiiragi, T., & Graner, F. (2021). Inferring cell junction tension and pressure from cell geometry. *Development*, *148*(18), dev192773.
- Rohde, J., Heitman, J., & Cardenas, M. E. (2001). The TOR kinases link nutrient sensing to cell growth. *Journal of Biological Chemistry*, *276*(13), 9583–9586.
- Roth, G., Blanke, J., & Wake, D. B. (1994). Cell size predicts morphological complexity in the brains of frogs and salamanders. *Proceedings of the National Academy of Sciences*, *91*(11), 4796–4800.
- Saw, T. B., Doostmohammadi, A., Nier, V., Kocgozlu, L., Thampi, S., Toyama, Y., Marcq, P., Lim, C. T., Yeomans, J. M., & Ladoux, B. (2017). Topological defects in epithelia govern cell death and extrusion. *Nature*, *544*(7649), 212–216.
- Scarpa, E., Finet, C., Blanchard, G. B., & Sanson, B. (2018). Actomyosin-driven tension at compartmental boundaries orients cell division independently of cell geometry in vivo. *Developmental Cell*, *47*(6), 727–740.
- Schleiden, M. J. (1838). Beiträge zur phytogenese. archiv für anatomie, physiologie und wissenschaftliche. *Medicin*, *5*, 136–176.

- Schuhmacher, M., Staeger, M. S., Pajic, A., Polack, A., Weidle, U. H., Bornkamm, G. W., Eick, D., & Kohlhuber, F. (1999). Control of cell growth by c-Myc in the absence of cell division. *Current Biology*, *9*(21), 1255–1258.
- Schwann, T. (1839). *Mikroskopische untersuchungen uber die uebereinstimmung in der struktur und dem wachsthum der thiere und pflanzen*. Verlag der Sander'schen Buchhandlung (GE Reimer).
- Shaya, O., Binshtok, U., Hersch, M., Rivkin, D., Weinreb, S., Amir-Zilberstein, L., Khamaisi, B., Oppenheim, O., Desai, R. A., Goodyear, R. J., Richardson, G. P., Chen, C. S., & Sprinzak, D. (2017). Cell-cell contact area affects Notch signaling and Notch-dependent patterning. *Developmental Cell*, *40*(5), 505–511.
- Shraiman, B. I. (2005). Mechanical feedback as a possible regulator of tissue growth. *Proceedings of the National Academy of Sciences*, *102*(9), 3318–3323.
- Sjöqvist, M., & Andersson, E. R. (2019). Do as i say, Not(ch) as i do: Lateral control of cell fate. *Developmental Biology*, *447*(1), 58–70.
- Soelistyo, C., Vallardi, G., Charras, G., & Lowe, A. R. (2021). Learning the rules of cell competition without prior scientific knowledge. *bioRxiv*. <https://doi.org/10.1101/2021.11.24.469554>
- Stevens, C. F. (1979). The neuron. *Scientific American*, *241*(3), 54–65.
- Stoker, M. G. P., & Rubin, H. (1967). Density dependent inhibition of cell growth in culture. *Nature*, *215*(5097), 171–172.
- Stroka, K. M., & Aranda-Espinoza, H. (2011). Effects of morphology vs. cell–cell interactions on endothelial cell stiffness. *Cellular and Molecular Bioengineering*, *4*(1), 9–27.
- Suzanne, M., Petzoldt, A. G., Spéder, P., Coutelis, J.-B., Steller, H., & Noselli, S. (2010). Coupling of apoptosis and L/R patterning controls stepwise organ looping. *Current Biology*, *20*(19), 1773–1778.
- Tapon, N., Ito, N., Dickson, B. J., Treisman, J. E., & Hariharan, I. K. (2001). The Drosophila tuberous sclerosis complex gene homologs restrict cell growth and cell proliferation. *Cell*, *105*(3), 345–355.

- Tee, A. R., Fingar, D. C., Manning, B. D., Kwiatkowski, D. J., Cantley, L. C., & Blenis, J. (2002). Tuberous sclerosis complex-1 and-2 gene products function together to inhibit mammalian target of rapamycin (mTOR)-mediated downstream signaling. *Proceedings of the National Academy of Sciences*, *99*(21), 13571–13576.
- Thompson, B. J., & Cohen, S. M. (2006). The Hippo pathway regulates the bantam microRNA to control cell proliferation and apoptosis in *Drosophila*. *Cell*, *126*(4), 767–774.
- Thompson, D. W. (1917). *On Growth and Form* (Volume 1). Cambridge University Press.
- Timmer, J. C., & Salvesen, G. S. (2007). Caspase substrates. *Cell Death & Differentiation*, *14*(1), 66–72.
- Totaro, A., Castellan, M., Di Biagio, D., & Piccolo, S. (2018). Crosstalk between YAP/TAZ and Notch signaling. *Trends in Cell Biology*, *28*(7), 560–573.
- Toyama, Y., Peralta, X. G., Wells, A. R., Kiehart, D. P., & Edwards, G. S. (2008). Apoptotic force and tissue dynamics during *Drosophila* embryogenesis. *Science*, *321*(5896), 1683–1686.
- Tozluoğlu, M., Duda, M., Kirkland, N. J., Barrientos, R., Burden, J. J., Muñoz, J. J., & Mao, Y. (2019). Planar differential growth rates initiate precise fold positions in complex epithelia. *Developmental Cell*, *51*(3), 299–312.
- Truman, J. W., Moats, W., Altman, J., Marin, E. C., & Williams, D. W. (2010). Role of Notch signaling in establishing the hemilineages of secondary neurons in *Drosophila melanogaster*. *Development*, *137*(1), 53–61.
- Tsuboi, A., Ohsawa, S., Umetsu, D., Sando, Y., Kuranaga, E., Igaki, T., & Fujimoto, K. (2018). Competition for space is controlled by apoptosis-induced change of local epithelial topology. *Current Biology*, *28*(13), 2115–2128.
- Tumaneng, K., Russell, R. C., & Guan, K.-L. (2012). Organ size control by Hippo and TOR pathways. *Current Biology*, *22*(9), R368–R379.
- Twitty, V. C., & Schwind, J. L. (1931). The growth of eyes and limbs transplanted heteroplastically between two species of *Amblystoma*. *Journal of Experimental Zoology*, *59*(1), 61–86.

- Udan, R. S., Kango-Singh, M., Nolo, R., Tao, C., & Halder, G. (2003). Hippo promotes proliferation arrest and apoptosis in the Salvador/Warts pathway. *Nature Cell Biology*, *5*(10), 914–920.
- Valon, L., Davidović, A., Levillayer, F., Villars, A., Chouly, M., Cerqueira-Campos, F., & Levayer, R. (2021). Robustness of epithelial sealing is an emerging property of local ERK feedback driven by cell elimination. *Developmental Cell*, *56*(12), 1700–1711.
- Vincent, J.-P., Fletcher, A. G., & Baena-Lopez, L. A. (2013). Mechanisms and mechanics of cell competition in epithelia. *Nature Reviews Molecular Cell Biology*, *14*(9), 581–591.
- Vogt, K. C. (1842). *Untersuchungen über die entwicklungsgeschichte der geburtshelferkröte (alytes obstetricans)*. Jent & Gassmann.
- Wagstaff, L., Goschorska, M., Kozyrska, K., Duclos, G., Kucinski, I., Chessel, A., Hampton-O’Neil, L., Bradshaw, C. R., Allen, G. E., Rawlins, E. L., Silberzan, P., Carazo Salas, R. E., & Piddini, E. (2016). Mechanical cell competition kills cells via induction of lethal p53 levels. *Nature Communications*, *7*(1), 1–14.
- Wang, S. L., Hawkins, C. J., Yoo, S. J., Müller, H.-A. J., & Hay, B. A. (1999). The drosophila caspase inhibitor DIAP1 is essential for cell survival and is negatively regulated by HID. *Cell*, *98*(4), 453–463.
- Wang, X., Merkel, M., Sutter, L. B., Erdemci-Tandogan, G., Manning, M. L., & Kasza, K. E. (2020). Anisotropy links cell shapes to tissue flow during convergent extension. *Proceedings of the National Academy of Sciences*, *117*(24), 13541–13551.
- Weaire, D., & Kermode, J. P. (1983). Computer simulation of a two-dimensional soap froth: I. method and motivation. *Philosophical Magazine B*, *48*(3), 245–259.
- Weinkove, D., Neufeld, T. P., Twardzik, T., Waterfield, M. D., & Leever, S. J. (1999). Regulation of imaginal disc cell size, cell number and organ size by Drosophila class IA phosphoinositide 3-kinase and its adaptor. *Current Biology*, *9*(18), 1019–1029.

- Wesley, C. C., Mishra, S., & Levy, D. L. (2020). Organelle size scaling over embryonic development. *Wiley Interdisciplinary Reviews: Developmental Biology*, *9*(5), e376.
- Wilson, E. B. (1925). *The cell in development and heredity*. Macmillan.
- Yan, G., Elbadawi, M., & Efferth, T. (2020). Multiple cell death modalities and their key features. *World Academy of Sciences Journal*, *2*(2), 39–48.
- Yang, Q., Xue, S.-L., Chan, C. J., Rempfler, M., Vischi, D., Maurer-Gutierrez, F., Hiiragi, T., Hannezo, E., & Liberali, P. (2021). Cell fate coordinates mechano-osmotic forces in intestinal crypt formation. *Nature Cell Biology*, *23*(7), 733–744.
- Yoo, S. J., Huh, J. R., Muro, I., Yu, H., Wang, L., Wang, S. L., Feldman, R. M., Clem, R. J., Müller, H.-A. J., & Hay, B. A. (2002). Hid, Rpr and Grim negatively regulate DIAP1 levels through distinct mechanisms. *Nature Cell Biology*, *4*(6), 416–424.
- Zhang, H., Stallock, J. P., Ng, J. C., Reinhard, C., & Neufeld, T. P. (2000). Regulation of cellular growth by the *Drosophila* target of rapamycin dTOR. *Genes & Development*, *14*(21), 2712–2724.
- Zhao, B., Wei, X., Li, W., Udan, R. S., Yang, Q., Kim, J., Xie, J., Ikenoue, T., Yu, J., Li, L., Zheng, P., Ye, K., Chinnaiyan, A., Halder, G., Lai, Z.-C., & Guan, K.-L. (2007). Inactivation of YAP oncoprotein by the Hippo pathway is involved in cell contact inhibition and tissue growth control. *Genes & Development*, *21*(21), 2747–2761.

RÉSUMÉ

L'apoptose est une forme de mort cellulaire programmée qui joue un rôle clé lors de la morphogenèse (acquisition de formes et structures pendant le développement), dans l'homéostasie des tissus adultes, ainsi que dans certaines maladies telles que les cancers. Alors que les signaux moléculaires responsables du déclenchement de l'apoptose ont été l'objet de multiples recherches, le rôle de facteurs biophysiques dans le contrôle de la mort cellulaire reste peu connu. Durant ma thèse qui avait pour modèle d'étude le thorax dorsal (ou notum) de la puppe de drosophile, j'ai développé des techniques d'analyse quantitative de données vidéo-microscopiques qui, combinées à l'utilisation d'outils génétiques de pointe, visaient à comprendre la régulation biophysique de l'apoptose. Tout d'abord, j'ai cherché à décrire les caractéristiques précoces des futures cellules apoptotiques et ai découvert deux caractéristiques géométriques prédictives de ces cellules : des petites aires apicales absolue et relative. Ensuite, j'ai étudié en détail ces deux facteurs géométriques et ai montré que leurs actions dans le contrôle de la mort faisaient intervenir deux voies de signalisation génétiques différentes, voies que j'ai identifiées. Ce faisant, j'ai également découvert une connexion inédite entre prolifération et mort cellulaire dans le contrôle du développement tissulaire. En conclusion, mon travail apporte un éclairage nouveau à notre compréhension de l'apoptose épithéliale en identifiant des facteurs géométriques impliqués de façon très précoce dans la régulation de la mort cellulaire.

MOTS CLÉS

Apoptose ; Géométrie cellulaire ; Aire apicale ; Morphogenèse ; Mécanobiologie ; Bioinformatique

ABSTRACT

Apoptosis is a form of programmed cell death which plays a key role in shaping multicellular organisms during development, in adult tissue homeostasis, as well as in pathological conditions such as cancer. While the molecular pathways triggering apoptosis have been extensively studied, the role of biophysical factors in driving cell death is far less understood. In particular, cell size and geometry impact a variety of cell processes, yet their possible interplay with apoptotic pathways remains unknown. Using the developing dorsal thorax (or notum) of the *Drosophila* as a model, I developed during my PhD advanced quantitative analyses of time-lapse microscopy data that, combined with the powerful genetic tools available in *Drosophila*, aimed at uncovering the biophysical mechanisms regulating apoptosis. First, I investigated the early characteristics of apoptotic cells and discovered two predictive geometrical features of these cells: small absolute and relative apical areas. Second, I studied in detail these two geometrical parameters and showed that their actions were linked to distinct genetic pathways, which I identified. By doing so, I also uncovered a novel coupling between cell proliferation and cell death in the control of tissue development. Overall, this work provides a new perspective to the understanding of epithelial apoptosis by identifying geometrical parameters that play an early role in the regulation of cell survival.

KEYWORDS

Apoptosis; Cell geometry; Apical area; Morphogenesis; Mecanobiology; Bioinformatics